Role of Interferon-stimulated gene 15 (ISG15) in replication fork progression and PARP inhibitor resistance in cancer

by

Yuri Seung

A thesis submitted for the degree of

Doctor of Philosophy



St Cross College, University of Oxford

Hilary Term 2024

Role of interferon-stimulated gene 15 (ISG15) in replication fork progression and PARP inhibitor resistance in cancer

A thesis submitted to the University of Oxford
for the degree of *Doctor of Philosophy*
Yuri Seung
St Cross College, Hilary Term 2024

Understanding PARP (Poly-ADP ribose polymerase) inhibitor resistance is crucial in cancer therapy, particularly in treating cancers associated with BRCA mutations. The role of ISG15 (Interferon-Stimulated Gene 15) in PARP inhibitor resistance adds a layer of complexity to this phenomenon. In this study, we have observed that ISG15 plays a crucial role in regulating the cell cycle, but it does not directly translate to lethality. However, in BRCA-deficient cells that acquired resistance against PARP inhibitor, we have documented that ISG15 and ISGylation are upregulated. The upregulated ISGylation correlates with the accelerated replication fork progression in BRCA1-deficient PARP inhibitor-resistant cells. Our research revealed that ISG15 can interact with Topoisomerase I (TOP1) and Dead-box helicase 5 (DDX5), and the interaction was explicitly enriched in BRCA1-deficient PARP inhibitor-resistant cells. Here, we showed that ISG15 and TOP1 epistatically regulate replication fork progression in BRCA1-deficient PARP inhibitor-resistant cells. Our results suggest that ISG15 and TOP1 may link R-loop homeostasis and replication speed regulation. A follow up investigation could explore the connection between PARP inhibitor resistance and R-loop regulation – for this purpose, a HeLa cell line with DOX-inducible FLAG-tagged RNAseH1 plasmid has been established.

Acknowledgements

I would like to thank my supervisor, Madalena Tarsounas, and my co-supervisors, Adan Pinto-Fernandez and Rebecca Dagg, for their supervision and support.

I want to acknowledge my colleagues, especially Ieuan and Birbal, who greatly supported me throughout my DPhil and gave me valuable advice until the end of my degree. Also, I would like to show appreciation for my colleagues: Giuliana, Rebecca, Anastasiya, Florian, Teressa, Birbal, Ieuan, Yanti, Alexa, Teofanija, Olivia, and Yifan. It was a great pleasure to be a part of an amazing team.

Thank you to my dearest friends, Jack, Hollie, Stef, Marek, and Fariha, for making my time in Oxford unforgettable. I would also like to thank my friends who supported me remotely: Eden, Yulania, Yuri Choi, Sooyeon, and Seong-ah. I want to thank my family, especially my parents and grandparents.

Finally, thank you, Sam, for supporting me through this unforgettable journey.

Declaration of authorship

I confirm that this thesis I am submitting is wholly my own work except where otherwise indicated.

Funding

The work presented here was performed at the Department of Oncology, University of Oxford.

Table of contents

Role of interferon-stimulated gene 15 (ISG15) in replication fork progression and PARP inhibitor resistance in cancer II

Acknowledgements III

Declaration of authorship IV

Funding IV

Table of contents V

List of tables X

List of figures XI

List of abbreviations XIV

Chapter 1 Introduction 18

1.1 DNA damage repair and maintenance of genome stability 19

1.1.1 DNA: molecular blueprint of genetic information 19

1.1.2 Response to DNA damage 20

1.1.3 Mechanisms of DNA single-strand break repair 20

1.1.1 Mechanisms of DNA double-strand break repair 22

1.2 Replication stress and genomic instability 28

1.2.1 Replication fork barriers 28

1.2.2 Consequences of replication stress 29

1.3 R-loops in genome instability 32

1.3.1 Sources of R-loops 32

1.3.2 Factors involved in R-loop formation 33
1.3.3 Regulation of R-loops 33
1.3.4 Physiological and pathological roles of R-loops 34
1.4 BRCA1/2 deficiency and cancer 35
1.4.1 BRCA1 and BRCA2 in maintaining genome integrity 35
1.4.2 Targeting BRCA1/2-mutated cancers 37
1.4.3 Mechanisms of PARPi treatment 38
1.4.4 Mechanisms of PARPi resistance 41
1.5 Innate immune response and cancer 45
1.5.1 Genome instability and cGAS-STING activation 45
1.5.2 Type I IFN signalling in cancer 47
1.5.3 ISG15: Type I IFN-stimulated protein with multi-faceted functions 48
1.6 Aim 53

Chapter 2 Material and methods 55

2.1 Cell lines and cell culture 56
2.2 Generation of knockout cell lines using CRISPR-Cas9 56
2.3 Resazurin-based cell viability assay 57
2.4 Resazurin-based cell proliferation assay 57
2.5 siRNA transfection 57
2.6 Immunoblotting 58
2.7 Cell cycle analysis 60
2.8 Bacterial transformation 61
2.9 Plasmid amplification and purification 61
2.10 Lentiviral transduction 61
2.11 Immunoprecipitation 62

2.12 ISG15 interactome immunoprecipitation LC-MS/MS analysis 63
2.13 LC-MS/MS data processing (PERSEUS) 64
2.14 DNA Fibre assays 64
2.15 Bulk RNA-seq data analysis 65
2.16 Differential expression analysis 66
2.17 Gene set enrichment analysis 66
2.18 DRIP-seq data analysis 66
2.19 ChIP-seq data analysis 66
2.20 Statistical analysis 67

Chapter 3 Experiment results I – Monitoring ISG expression in BRCA1/2-deficient cells and the effect of lacking ISG15 machinery proteins in the context of hIFNa2 treatment 68

3.1 ISG expression is induced by PARP inhibitor and hIFNa2 treatment 69
3.2 hIFNa2 treatment does not affect viability of BRCA-deficient cells 72
3.3 Generation of IFIT1, IFIT2 or ISG15 KO cell line in RPE1 hTERT *TP53*$^{-/-}$ Cas9 cells 73
3.4 Monitoring the effects of ISG15 loss in RPE1 hTERT *TP53*$^{-/-}$ Cas9 cells 76
3.5 Monitoring ISG expression upon hIFNa2 treatment in cells lacking components of ISG15 machinery 79
3.6 ISG15 loss results in alteration of cell cycle 83
3.7 ISG15 loss does not affect proliferation of BRCA1/2-proficient or deficient cells 86

Chapter 4 Experiment results II – Upregulated ISG15 expression in PARPi talazoparib-resistant cells and its role in replication fork progression..... 88

4.1 PARP inhibitors potentiate innate immune responses 89
4.2 Development of PARPi resistance alters transcriptome profile of BRCA-deficient cells 92
4.3 ISG15 plays a role in cell cycle progression and replication fork progression 99
4.4 ISG15 interacts with replication machinery proteins 103

Chapter 5 Experiment results III – R-loop regulating proteins does not directly affect survival of BRCA1-deficient talazoparib-resistant cells ... 113
5.1 Studying the role of proteins regulating R-loop homeostasis in the context of PARPi resistance 114

Chapter 6 Discussion and conclusion 121
6.1 Increased type I IFN protein expression in BRCA1/2-deficient cells and impact of ISG15 loss on cell cycle regulation 122
6.2 ISG15 deficiency and sensitivity to hIFNa2 treatment 123
6.3 Enhanced ISG15 expression and ISGylation in BRCA1-deficient TR cells 123
6.4 Role of ISG15 in replication fork machinery 125
6.5 Possible role of ISG15 in regulating R-loop levels 127
6.6 Studying the putative relationships between R-loop accumulation and PARPi resistance 128

Appendix 130

References 150

List of tables

Table 2.1 sgRNA used for knocking out target gene..... 57

Table 2.2 siRNAs used for knocking down target genes..... 58

Table 2.3 Primary antibodies used for immunoblotting..... 59

Table 2.4 Secondary antibodies used for immunoblotting..... 60

Table 2.5 Antibodies used for immunoprecipitation 62

List of figures

Figure 1.1 SSB sensing and PARylation cycle 21

Figure 1.2 SSB repair pathway 22

Figure 1.3 DSB repair by HR 26

Figure 1.4 DSB repair by NHEJ 27

Figure 1.5 Mechanisms to remodel or bypass the stalled replication fork 30

Figure 1.6 Illustration of synthetic lethality 37

Figure 1.7 Mechanism of action of PARP inhibitor 39

Figure 1.8 Mechanisms of PARPi resistance development 43

Figure 1.9 Type I IFN signalling is activated by DNA-damage induced cGAS-STING activation 46

Figure 1.10 Illustration of ISGylation cycle 49

Figure 1.11 Role of ISG15 in DNA damage response 51

Figure 3.1 Upregulated ISG expression PARPi and hIFNa2 treatment in H1299+shBRCA2^{DOX} and RPE1 hTERT *TP53*$^{-/-}$ Cas9 (*BRCA1*$^{-/-}$, *BRCA2*$^{-/-}$). 69

Figure 3.2 Sensitivity of BRCA-deficient cells to hIFNa2 and olaparib 72

Figure 3.3 Generation of IFIT1, IFIT2 and ISG15-KO RPE1 cell line 74

Figure 3.4 Sensitivity of ISG15-deficient cells to hIFNa2 and olaparib treatment 76

Figure 3.5 ISG expression monitored in ISG15 KO cells 77

Figure 3.6 Sensitivity of USP18-deficient cells to hIFNa2 and olaparib treatment 79

Figure 3.7 Generation of ISG15 and USP18 dKO in HAP1 cell line and studying the effect of double knockout upon hIFNa2 treatment 81

Figure 3.8 Effect of ISG15 loss in cell cycle progression 83

Figure 3.9 Effect of silencing ISG15 in BRCA1/2-proficient and deficient cells 86

Figure 4.1 Upregulated ISG expression PARPi treatment in H1299+shBRCA2^{DOX} and RPE1 hTERT *TP53*$^{-/-}$ Cas9 (*BRCA1*$^{-/-}$, *BRCA2*$^{-/-}$). 89

Figure 4.2 Upregulation of innate immune response genes in BRCA-deficient cells that have developed PARPi resistance 93

Figure 4.3 Interferon-stimulated gene 15 (ISG15) expression in BRCA1-deficient PARPi-naïve and resistant cells 95

Figure 4.4 Monitoring ISGylation level in BRCA1-deficient talazoparib-naïve and resistant cells 97

Figure 4.5 Effect of silencing ISG15 in cell cycle progression 99

Figure 4.6 Effects of ISG15 in replication fork progression 101

Figure 4.7 ISG15 interacts with replication machinery proteins and its interaction with RNA metabolism proteins are upregulated in PARPi-resistant cells 103

Figure 3.8 ISG15 interacts with TOP1, DDX5 and Ku70 106

Figure 4.9 TOP1 depletion in HCT116 cells results in decrease of fork speed 107

Figure 4.10 ISG15 and TOP1 regulates replication fork progression in the same pathway in BRCA1-deficient talazoparib resistant cells 109

Figure 4.11 TOP1 can bind to the R-loop forming sites 110

Figure 5.1 Silencing USP11 does not affect cell viability of RPE1 hTERT *TP53*$^{-/-}$ Cas9 cells upon talazoparib treatment 114

Figure 5.2 SETX depletion does not affect cell survival of RPE1 hTERT *TP53*$^{-/-}$ Cas9 cells 116

Figure 5.3 SETX depletion does not affect cell proliferation of RPE1 hTERT *TP53*$^{-/-}$ Cas9 cells 117

Figure 5.4 Establishing HeLa cell line carrying DOX-inducible FLAG-tagged RNaseH cassette 119

Supplemental Figure 1. Model of RPE1 hTERT *TP53*$^{-/-}$ Cas9 cell line developed resistance against PARPi talazoparib 131

Supplemental Figure 2. Detection of IFIT2 in immunoprecipitated samples upon hIFNa2 treatment 132

Supplemental Figure 3. Detection of ISG15-conjugated substrates from immunoprecipitated samples 133

List of abbreviations

%	Percent
ºC	Celsius degree
DNA	Deoxyribonucleic acid
A	Adenosine
Alt-NHEJ	Alternative non-homologous end joining
BARD1	BRCA1-associated ring domain
BER	Base-excision repair
BIR	Break-induced repair
BRCA1	Breast cancer susceptibility gene 1
BRCA2	Breast cancer susceptibility gene 2
C	Cytosine
cDNA	Complementary DNA
CldU	5'-chloro-2'-deoxyuridine
CtIP	CtBP-interacting protein
ChIP	Chromatin immunoprecipitation
ChIP-seq	ChIP-sequencing
D-loop	Displacement loop
Da	Dalton(s)
DDR	DNA damage response
dHJ	Double Holliday junction
DMEM	Dulbecco's Modified Eagle's Medium
DMSO	Dimethyl sulfoxide
DOX	Doxycycline
DRIP	DNA-RNA immunoprecipitation

DRIP-seq	DRIP-sequencing
DSB	Double-strand break
DSBR	Double-strand break repair
DTT	Dithiothreitol
EDTA	Ethylenediaminetetraacetic acid
EdU	5-Ethynyl-2´-deoxyuridine
FBS	Foetal bovine serum
FDR	False discovery rate
Fig.	Figure
G	Guanine
GSEA	Gene Set enrichment Analysis
h	Hour(s)
HR	Homologous recombination
HRP	Horseradish peroxidase
IdU	5'-Iodo-2'-deoxyuridine
IFN	Interferon
IFIT1	Interferon-induced protein with tetratricopeptide repeats 1
IFIT2	Interferon-induced protein with tetratricopeptide repeats 2
IR	Ionising radiation
ISG	Interferon-stimulated gene
ISG15	Interferon-stimulated gene 15
ISRE	IFN-stimulated response elements
KO	Knockout
LC-MS/MS	Liquid Chromatography with tandem mass spectrometry
M	Molar

min	Minute(s)
MMR	Mismatch repair
mtDNA	Mitochondrial DNA
NER	Nucleotide excision repair
NHEJ	Non-homologous end joining
PAR	Poly [ADP-ribose]
PARG	PAR glycohydrolase
PARP	PAR polymerase
PARP1	PAR polymerase 1
PARPi	PARP inhibitors
PBS	Phosphate saline buffer
PBST	0.05% Tween 20 in PBS
PCR	Polymerase chain reaction
PCNA	Proliferating cell nuclear antigen
RNA	Ribonucleic acid
RNA-seq	RNA-sequencing
ROS	Reactive oxygen species
RT-qPCR	Quantitative reverse transcription PCR
R-loop	Three-stranded nucleic acid structure comprised of a DNA:RNA hybrid and a displaced strand of DNA
RPA	Replication protein A
SDS	Dodecyl sulphate-polyacrylamide
SDSA	Synthesis-dependent strand annealing
SETX	Senataxin
SUMO	Small ubiquitin-like modifier

sgRNA	Single guide RNA
shRNA	Short hairpin RNA
siRNA	Small interfering RNA
SSA	Single-strand annealing
SSB	Single-strand break
ssDNA	Single-stranded DNA
T	Thymidine
TOP1	DNA topoisomerase 1
TN	Talazoparib-naïve
TR	Talazoparib-resistant
USP11	Ubiquitin specific peptidase 11
USP18	Ubiquitin specific peptidase 18
UV	Ultra-violet
V	Volt
WT	Wild-type
XRCC1	X-ray repair cross complementing protein 1
53BP1	p53-binding protein 1

Chapter 1

Introduction

1.1 DNA damage repair and maintenance of genome stability

1.1.1 DNA: molecular blueprint of genetic information

The human body is comprised of approximately 10^{13} cells [1, 2] that operate in varying levels of organisation. The genetic instructions encoded in DNA dictate each cell's structure, behaviour, and function. The complete set of DNA is called the genome, characterised by linear arrays of double-stranded DNA molecules [3]. This structure is then further arranged into 23 pairs of chromosomes in the cell nucleus [4]. Additionally, a fraction of the genetic information is stored within circular mitochondrial DNA (mtDNA) [5]. Notably, the human genome exhibits a high degree of conservation among the population, with genetic variations uniformly distributed across the entire genome.

While semi-conservative DNA replication is generally rapid and accurate, the process is not entirely failproof [6]. DNA polymerases can cause replication errors, which, if not corrected, have the potential to cause spontaneous mutations [7].

DNA damage can be induced by exogenous (ionising radiation (IR), chemotherapeutic drugs) or endogenous (aldehydes and reactive oxygen species) sources [8, 9]. Some of these treatments can inflict various DNA lesions, including impediments to replication fork progression, potentially resulting in replication fork collapse. This, in turn, triggers formation of DNA single strand breaks (SSBs) [8], which can exacerbate into DNA double strand breaks (DSBs) if remain unrepaired [10]. Briefly, unrepaired SSBs disrupt the progression of DNA replication fork. It leads to the collision of replication fork with the breakage site, creating a single-ended DSB [11].

1.1.2 Response to DNA damage

Since maintaining genomic integrity is vital for cell survival, cells have evolved effective mechanisms for DNA damage repair. The process exists in both prokaryotic and eukaryotic organisms [12].

Since the cells are exposed to the constant threat of endogenous or exogenous DNA-damaging agents, they have evolved a plethora of DNA damage response mechanisms. The coordinated DNA damage surveillance network is referred to as DNA damage response (DDR) [13, 14].

DDR responds to various types of DNA damages, including SSBs, DSBs, base damage, bulky DNA adducts, cross-linked DNA, and replication stress [15]. The DDR process leads to the activation of cell cycle checkpoints to determine whether or not to proceed, ensuring that DNA damage is repaired before the cell enters next phase of the cell cycle. However, if the damage is too severe to repair, the cells undergo programmed cell death, or apoptosis [16].

1.1.3 Mechanisms of DNA single-strand break repair

SSBs are one of the most frequent DNA lesions found in cells [17]. SSBs are primarily detected by PARP enzymes (Fig.1.1) Among the PARP enzymes, it is PARP1 that predominantly conducts the majority of Poly-(ADP-ribosyl)ation (PARylation) activity [18]. Upon SSB detection via PARP1, an ADP-ribose unit is transferred from PARP1 to its substrate or itself by utilising nicotinamide adenine dinucleotide (NAD+) as a co-substrate [19, 20]. This process is called PARylation, and PAR chains have rapid turnover due to the enzymatic activity of PARG, which hydrolyses the molecules [21].

PARylation facilitates the recruitment of X-ray repair cross-complementing protein, or XRCC1 to the damaged site. XRCC1 functions as a scaffolding protein that recruits required DNA repair proteins for SSB repair [22].

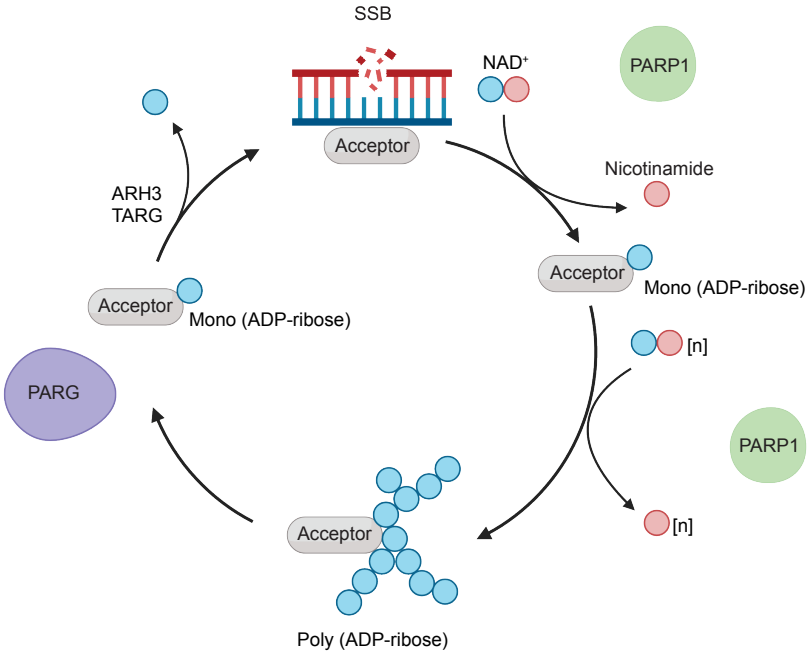


Figure 1.1 SSB sensing and PARylation cycle

PARP1 is activated upon detecting DNA damage. By using NAD+ as substrate for PAR chain formation, PARP1 can PARylate itself or its substrates. PAR chain is rapidly degraded by Poly(ADP-ribose) glycohydrolase (PARG). The remaining mono (ADP-ribose) is removed by ADP-ribosylhydrolase 3 (ARH3) or terminal ADP-ribose glycohydrolase (TARG).

SSB repair proteins such as APE1, LIG3 or FEN1 are recruited by XRCC1. Damaged DNA ends are removed by APE1 or FEN1. Following the process, DNA Pol β and LIG3 mediates DNA gap filling and ligation, respectively (Fig.1.2) [23, 24].

1.1.1 Mechanisms of DNA double-strand break repair

The repair of DSBs is preferentially performed by non-homologous end joining (NHEJ) or homologous recombination (HR), although other pathways such as alternative end joining (alt-EJ), and single-strand annealing (SSA) can also be utilised [10, 25, 26].

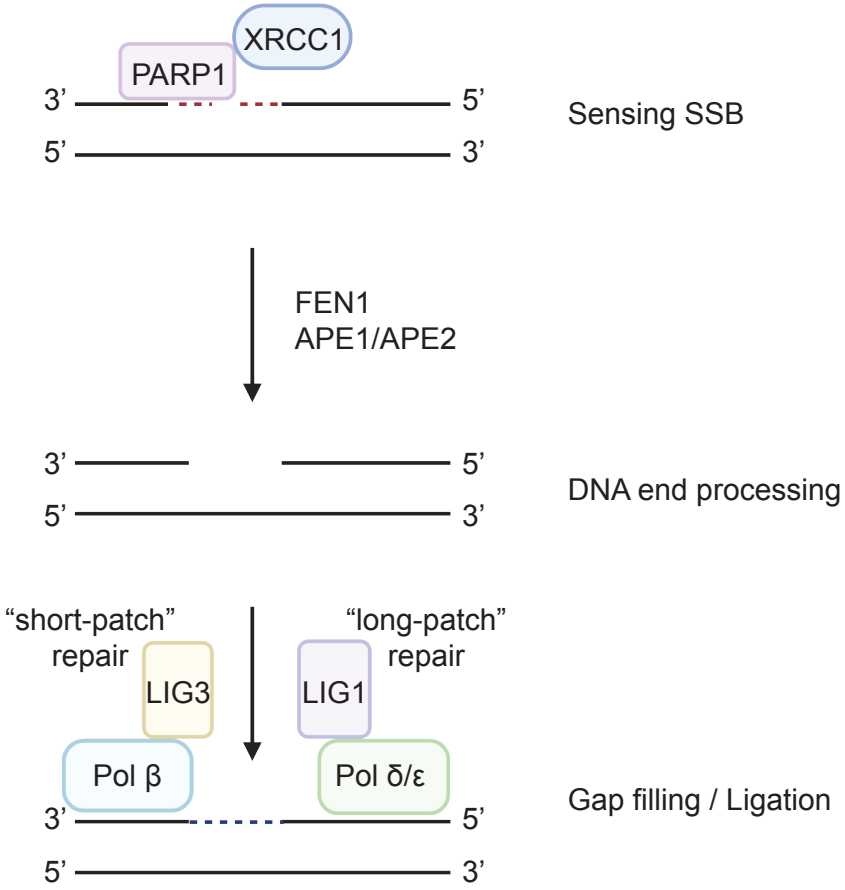


Figure 1.2 SSB repair pathway

Upon SSB detection by PARP1, XRCC1 is recruited to the damaged site. XRCC1 then signals the downstream DNA repair proteins, such as FEN1, DNA Pol β, and APE1. During short-patch repair, APE1 or APE2 excise the damaged DNA. Following the excision, DNA Pol β fills in the gap and LIG3 seals the end. For long-patch repair, FEN1 carries out removal of

damaged nucleotides. DNA Pol δ or Pol ε then synthesises the DNA and LIG1 seals the gap.

HR is an error-free repair pathway of repairing DSBs (Fig. 1.3). For a DSB to be repaired by HR, it is necessary that the BRCA1-BARD1 complex acts to remove the 53BP1-RIF1 complex from the breakage sites, thereby allowing nucleases to resect the DNA ends. When the broken DNA end is processed by CtIP and the Mre11-Rad50-Nbs1 (MRN) complex, a 3'-ssDNA overhang is generated, which is bound by phosphorylated RPA. BRCA1 then interacts with PALB2, which enables the localisation of BRCA2 to the damage site [27]. BRCA2 then promotes loading of the RAD51 recombinase on the ssDNA, which replaces RPA to generate the RAD51 nucleoprotein filament [28]. The RAD51-nucleoprotein filament promotes homology search and catalyses strand invasion of the sister chromatid [26]. The invading ssDNA anneals with one DNA strand within the template dsDNA, resulting in formation of a DNA joint called a D-loop, facilitated also by the BRCA1-BARD1 complex [29]. This DNA intermediate undergoes synthesis-dependent strand annealing (SDSA) or formation of double Holliday junction (dHJ). The dHJ is then processed by helicases and nucleases, including the Bloom Syndrome RecQ-like helicase (BLM) and MUS81 endonuclease [30]. The dHJ can be processed by three ways, including dissolution, crossover resolution and non-crossover resolution. Dissolution is conducted via the BLM-TopIIIα complex, producing only non-crossover products. Crossover and non-crossover resolutions are mediate via SLX1-SLX4 and MUS81-EME1 complexes, and GEN1. The process yields both crossover and non-crossover products [31-34].

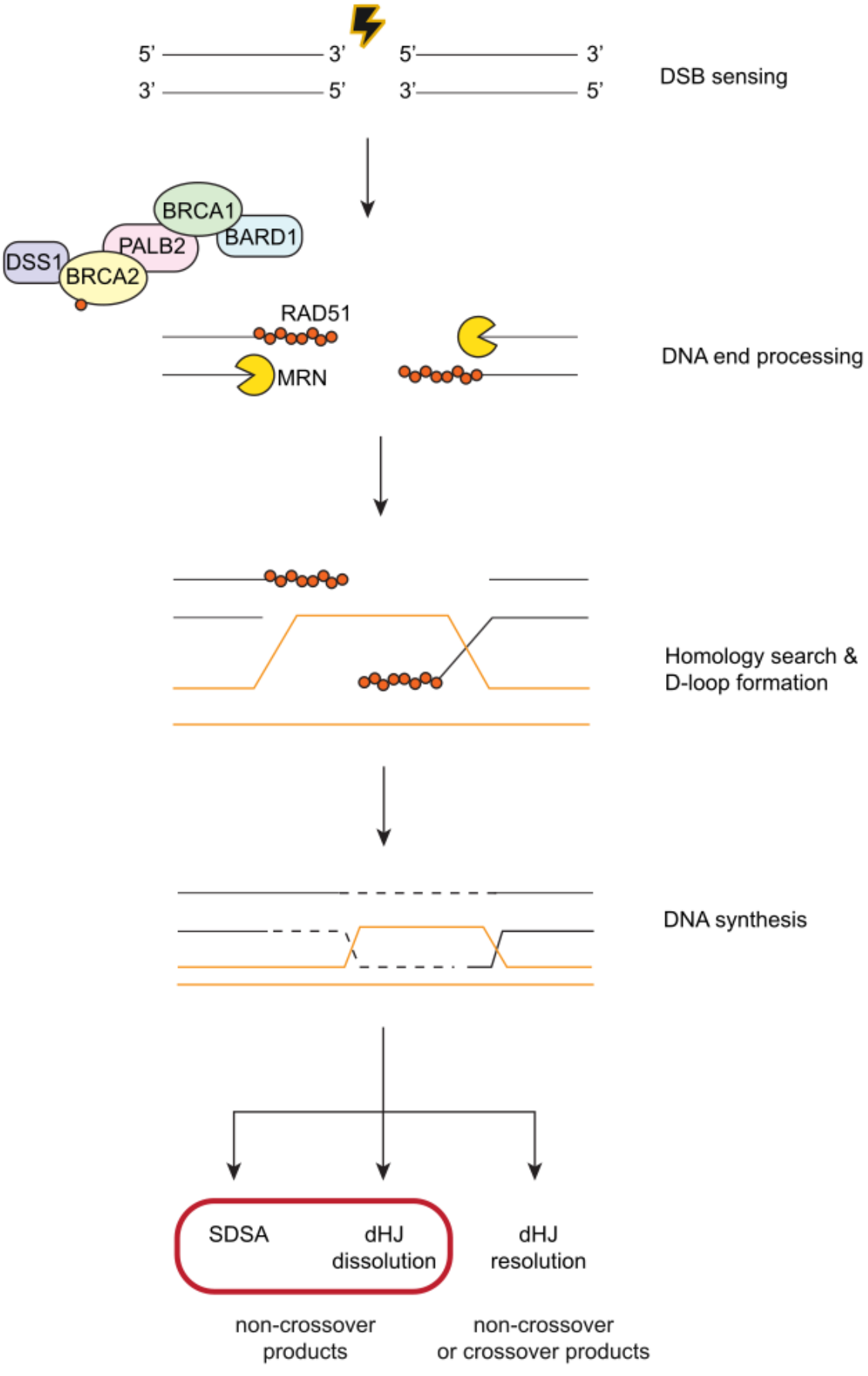

5'
3'
3'
5'
5'
3'
3'
5'
DSB sensing
BRCA1
BARD1
PALB2
DSS1
BRCA2
RAD51
MRN
DNA end processing
Homology search &
D-loop formation
DNA synthesis
SDSA
dHJ
dissolution
dHJ
resolution
non-crossover
products
non-crossover
or crossover products

Figure 1.3 DSB repair by HR

Upon DSB detection by MRN complex, ATM is recruited to the damage site (figure not shown). ATM then phosphorylates serine residue of H2AX, which recruits downstream proteins for DSB repair. BRCA1-BARD1 complex mediates ubiquitination of CtIP, which enables MRN complex to carry out DNA end resection. The newly generated 3'-overhang is rapidly coated by RPA (figure not shown). BRCA1-BARD1 complex, with the help from PALB2, recruits BRCA2-DSS1 complex, which displaces RPA and loads RAD51 to the ssDNA. The RAD51-coated nucleofilament invades sister chromatid for searching homologous sequences. This strand invasion results in Dissociation loop (D-loop) formation. D-loop is then resolved by SDSA or undergoes dHJ formation. SDSA results in non-crossover products. dHJ resolution can either yield non-crossover and crossover products. However, if dHJ is dissolved, the end product is always non-crossover.

HR pathway is error-free but is restricted to S and G2 phase since the pathway relies on a sister chromatid to use it as a template for DNA repair [35]. In contrast, NHEJ occurs throughout the cell cycle, making it primary pathway for the DSBs (Fig. 1.4). First, Ku70-Ku80 heterodimer (Ku) recognises DSB and functions as a scaffolding protein to recruit downstream proteins involved in NHEJ [26]. Amongst them is DNA-dependent protein kinase catalytic subunit (DNA-PKcs kinase), which forms a DNA-dependent protein kinase (DNA-PK) complex with the Ku-bound DNA ends. The process ensures to protect the broken DNA ends and recruit other repair factors. If the broken DNA ends are not compatible, Artemis processes the ends to make it compatible for ligation. Finally, DNA ligase IV (LIG4) and X-ray repair cross-complementing protein 4 (XRCC4) facilitates the ligation of processed DNA ends [36, 37].

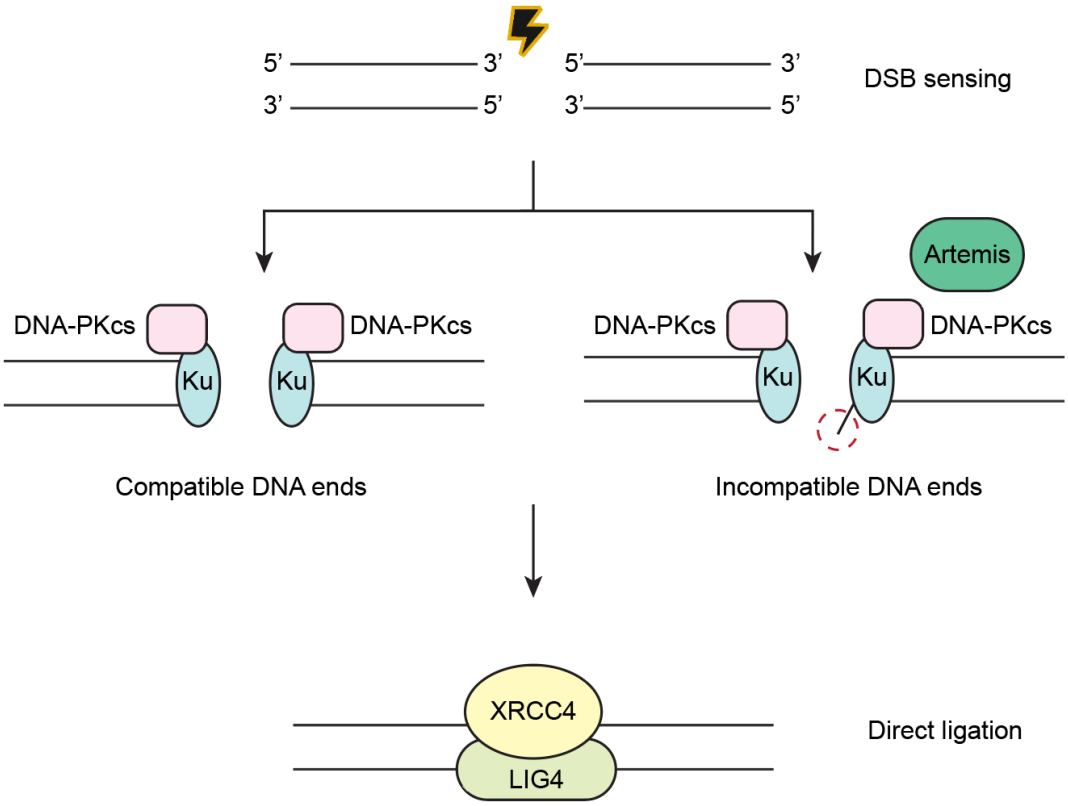


Figure 1.4 DSB repair by NHEJ

Upon DSB detection by MRN complex, ATM is recruited to the damage site (figure not shown). ATM then phosphorylates serine residue of H2AX, which recruits downstream proteins for DSB repair. Ku70 and Ku80 binds to the DNA ends, protecting the DNA ends from nucleolytic degradation and functioning as a scaffolding protein. DNA-PKcs is further recruited for the process. If the DNA ends are compatible to each other, XRCC4 and LIG4 process and ligate both ends of the DNA. However, if the DNA ends are incompatible to each other, DNA-PKcs recruits Artemis for DNA end processing. Then XRCC4 and LIG4 joins both ends to complete the repair.

Other DSB repair pathways include alt-NHEJ and SSA, which are beyond the scope of this thesis.

1.2 Replication stress and genomic instability

1.2.1 Replication fork barriers

The progression of replication fork can be impeded by many obstacles, including DNA secondary structures (e.g. G4 quadruplex), DNA-protein crosslinks, and R-loops [38, 39].

G-quadruplex (G4) is a non-canonical DNA secondary structure formed in Guanine-rich sequences [40]. Four Guanines interact through Hoogsteen base pairing, a variation of base pairing in which the nucleobases held together by hydrogen bonds, to form structure known as G-quartet, or G-tetrad [41]. Two or more G-quartets stack on top of each other to form a G4. Unresolved G4 can act as a replication roadblock and induce the ssDNA gap formation in front of the G4-containing strand [42].

The interaction between DNA and proteins plays a crucial role in various cellular processes, including cell division, replication, and transcription [43, 44]. The processes are mostly transient and tightly regulated. However, endogenous stress or exogenous DNA damaging agent can inadvertently promote the covalent, irreversible binding between protein and DNA [45]. The covalent linkage of proteins with a DNA strand, or DNA-protein crosslinks (DPCs) can pose a physical barrier to replication fork progression.

R-loops are three-stranded nucleic acid structures, composed of a DNA:RNA hybrid and the displaced ssDNA strand from transcription [46]. R-loop arises from transcription-replication collisions (TRCs). It is established that TRCs can occur in two orientations: head-on (HO), in which transcription machinery and replication fork are moving towards each other, and co-directional (CD), in which transcription machinery and replication fork move in the same direction [47].

In heads-on TRC, the replisome moves towards the transcription machinery, which leads to the increased positive supercoiling or direct collision with the transcription unit. RNA Polymerase is stalled upon the collision, and the nascent RNA strand invades DNA duplex, forming an RNA:DNA hybrid with displaced ssDNA, or R-loop [46-50]. The structure itself, or its association with a paused RNA polymerase, impedes the replication fork progression [51].

In co-directional TRC, the replisome and the transcription machinery move in the same direction, causing “traffic jam” that may impede each other’s progress [52]. While they can still induce DNA damage, CD collisions are known to be less harmful to cells compared to HO collisions [52].

1.2.2 Consequences of replication stress

As described above, various types of replication fork barriers challenge accurate DNA replication. Replication barriers interfering with the replication progression, along with dysregulated origin firing, are often collectively termed “replication stress” [53]. Transient replication stress is mostly tolerated, but prolonged replication stress can threaten genome stability.

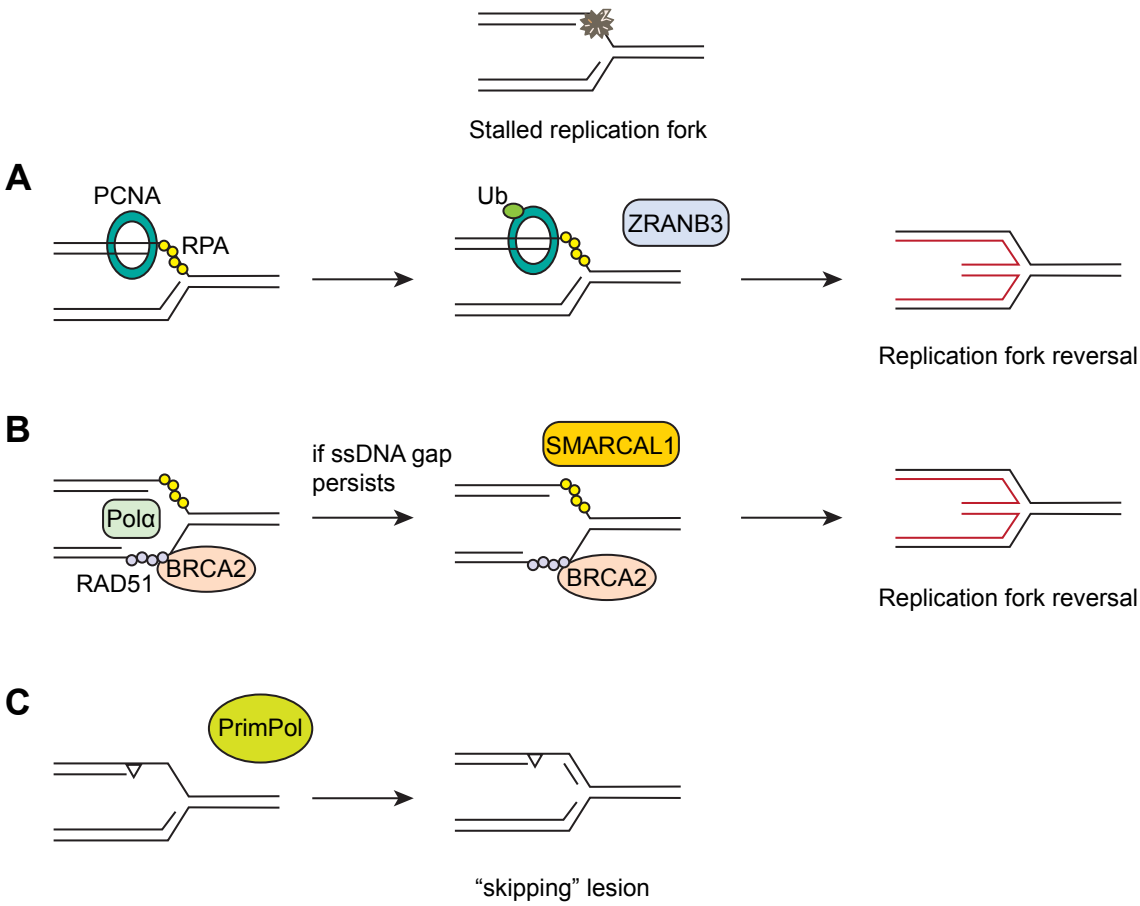


Figure 1.5 Mechanisms to remodel or bypass the stalled replication fork

(A) Upon replication fork stalling, RPA rapidly binds to the exposed ssDNA. RPA recruits E2 and E3 enzyme of ubiquitin, and subsequent modification by ubiquitylation recruits ZRANB3, a DNA-annealing helicase and endonuclease, to the stalled replication fork. ZRANB3 unwinds the DNA strands at stalled replication fork, which then facilitates the exposure of ssDNA regions, promoting the annealing of nascent DNA strands for formation of “reversed fork”. (B) BRCA2 mediates RAD51 loading onto the replication fork under stress. RAD51 directly interacts with DNA Pol α, stabilising the binding of the DNA polymerases to the replication fork. The stabilisation facilitates the nascent DNA synthesis, preventing the junction gap formation. In case of persisting ssDNA gap, SMARCAL1, DNA translocase, is recruited to the site to facilitate the regression of replication fork. (C) Upon the replication fork stalling,

PrimPol reprimes the downstream of replication roadblocks, enabling the replication to proceed. The “skipping” of roadblocks results in ssDNA gaps.

Unresolved replication stress can lead to replication fork stalling. Stalled replication forks activate DNA damage tolerance pathways, to alleviate stress [54]. One of the most well-known responses is fork reversal. When the replication fork is stalled, the helicase is uncoupled from the DNA. This leads to the generation of ssDNA stretches on the leading strand [55]. RPA rapidly binds to the exposed ssDNA stretch, and it triggers activation of ATR to phosphorylate itself and ssDNA-bound RPA, protecting the DNA strand from degradation [56, 57]. The pRPA-coated ssDNA then recruits the downstream proteins responsible for fork reversal and remodelling. One of the most well-known processes is ZRANB3-mediated fork reversal (Fig.1.5A). pRPA recruits E2 and E3 enzyme of ubiquitin to the site, and modification of PCNA via ubiquitylation facilitates the interaction between PCNA and recruited ZRANB3, a DNA translocase [58], which starts fork reversal.

Alternatively, BRCA2 can mediate RAD51 loading onto the exposed ssDNA of the stalled replication fork to mitigate replication stress (Fig. 1.5B). RAD51 then interacts with DNA Pol α, stabilising the polymerase to promote DNA synthesis to prevent ssDNA gap formation [59]. However, the process is not always failproof. Therefore, the generated ssDNA gaps are remodelled by DNA translocase SMARCAL1, leaving the structure vulnerable to MRE11-dependent degradation [59, 60]. Recent studies have suggested that cells utilising different types of fork remodelling proteins depending on the types of replication intermediates [60-63]. Another mechanism to mitigate the damage from a stalled replication fork is repriming (Fig. 1.5C). Repriming is mediated by PrimPol, which has both DNA

polymerase and DNA primase activity [64, 65]. PrimPol reprimes downstream of the DNA lesions or bulky adducts. This enables the restart of the replication but leaves a ssDNA gap. The resulting gap is then filled by translesion synthesis (TLS) or template switching (TS) [66]. TLS is mediated by specialised TLS polymerases, the DNA polymerases that lack 3'-5' proofreading domain [67]. In TS, the cells use newly synthesised DNA as a template to fill in the gap. However, the detailed mechanism of TS still remains elusive [67].

1.3 R-loops in genome instability

1.3.1 Sources of R-loops

As described in section 1.2.1, R-loop is a three-stranded nucleic acid structure composed of a DNA:RNA hybrid and the displaced ssDNA strand from transcription [46]. They form when nascent RNA transcript hybridises with the complementary DNA strand of the DNA-RNA duplex, displacing the other DNA strand.

R-loops can form in various genomic contexts. Co-transcriptional R-loops can be formed throughout the transcription. During transcription, nascent RNA can hybridise with the template DNA strand behind the RNA polymerases, forming an R-loop. The process is more likely to take place in highly transcribed GC-rich regions, in which sequences RNA-DNA hybrids are more stable than the DNA-DNA duplex [51, 68].

R-loops can also arise at telomeres and centromeres. Telomeric repeat-containing RNA (TERRA) is a long non-coding RNA (lncRNA) transcribed by RNA Polymerase II (RNAPII) [69, 70].

1.3.2 Factors involved in R-loop formation

There are various factors can influence the R-loop formation [71, 72]. Firstly, sequence composition can play a role in R-loop synthesis. GC-rich regions are more prone to R-loop formation due to the higher stability of GC pairs in RNA-DNA hybrids [73].

Secondly, transcriptional activity can contribute to R-loop formation. A high transcription rate can increase the likelihood of RNA re-annealing with the DNA template, leading to R-loop formation [73, 74].

Last but not least, the RNA processing and export process can also affect the R-loop formation. For instance, the capping enzyme, which plays a major role in pre-mRNA processing, can promote R-loop formation when the enzyme is bound to phosphorylated RNAPII [75]. Moreover, deficiencies in splicing of pre-mRNA and export of messenger ribonucleoprotein (mRNP; mRNA with bound proteins) can lead to the accumulation of R-loops [76-78].

1.3.3 Regulation of R-loops

Since RNA:DNA hybrids play a multifaceted role in the cell, such as chromosome separation during mitosis, DNA replication, immunoglobulin (Ig) switching and transcription regulation, maintaining the homeostasis of R-loop level is crucial in maintaining genome stability [71].

R-loop is regulated by a number of different proteins: ribonucleases, helicases, RNA-binding proteins, topoisomerases and chromatin remodelling factors [79]. RNaseH1 and RNaseH2 ribonucleases remove RNA:DNA hybrids through the endonucleolytic cleavage, resolving R-loops [80]. The enzymatic activity of RNaseH2 is restricted for G2/M, whereas RNaseH1 functions independently of cell cycle [81].

Helicases capable of unwinding RNA:DNA hybrids are known to resolve R-loops. A number of helicases are reported to resolve R-loops: SETX, AQR, WRN, BLM, RTEL1, PIF1, FANCM, ATRX, CasDinG, and several DEAD/H-box helicases [82]. Among the RNA-binding proteins, THO complex, a multi-protein complex bridging between transcription and mRNA processing, negatively regulates R-loop formation [83, 84]. Furthermore, nuclear RNA exosomes are reported to play a role in modulating R-loops [85].

Topoisomerase I and II alleviate torsional stress generated during transcription and DNA replication, which can contribute to R-loop formation. By resolving these supercoils, they prevent the formation of R-loops [86].

Recent studies have shown that chromatin remodelling factors are involved in R-loop regulation as well. Facilitates Chromatin Transcription (FACT) complex is reported to mediate the R-loop mediated TRCs [87]. Moreover, Switch/Sucrose non-fermentable (SWI/SNF) complex helps in maintaining chromatin structure and resolving R-loop mediated TRCs [88].

1.3.4 Physiological and pathological roles of R-loops

R-loops play significant roles in maintaining normal cellular physiology. With the help of RNaseH1, the processed 3'-ends of R-loops serve as a primer for mitochondrial replication [89]. The RNA:DNA hybrid also promotes a class-switching recombination process [90]. R-loops can function as a gene regulator since they are enriched at gene promoters and gene 3'-ends [91-95]. For instance, R-loops can facilitate the termination of transcription in certain genes. Moreover, they can epigenetically regulate transcription by protecting CpG islands in promoters from methylation [96].

Recent studies also suggest that R-loop is involved in DNA repair. Several studies showed that R-loop level correlates with efficiency of homologous recombination and non-homologous end joining repair [97-99], but the mechanism remains elusive.

Although R-loops serve crucial regulatory roles in normal cellular physiology, including gene regulation, replication, and telomere maintenance, they can also contribute to genomic instability and neurologic diseases [100]. Aberrant R-loop formation can lead to genomic instability through replication fork stalling and transcription-replication collision [101]. Moreover, cancer cells are more prone to R-loop accumulation due to nucleotide depletion or TRCs [74]. In addition to this, cells deficient in members of Fanconi Anaemia pathway, such as BRCA1, FANCA and FANCD2 showed higher level of R-loops [102-104].

R-loops are also strongly linked to neurodegenerative diseases as well. Mutations in SETX, a helicase that resolves R-loops, are linked to amyotrophic lateral sclerosis (ALS) and ataxia with oculomotor apraxia 2 (AOA2) [47]. Moreover, R-loop formation at FXN and FMR1 gene promotes the silencing of these genes, leading to fragile X syndrome [105]. Furthermore, elevation of R-loop level is reported in patients with Aicardi-Goutières syndrome [106].

1.4 BRCA1/2 deficiency and cancer

1.4.1 BRCA1 and BRCA2 in maintaining genome integrity

BRCA1 and BRCA2 act as safeguard against genome instability. As described in section 1.1.1, BRCA1 and BRCA2 play essential roles in DNA repair via HR. However, their roles are not limited to DNA repair [107-109]. Both BRCA1 and BRCA2 are involved in cell cycle regulation and checkpoint control. Multiple

studies have shown that protein and mRNA levels of BRCA1 change throughout the cell cycle, with the highest expression levels in the late G1 and S phases [110, 111]. Moreover, in HCC1937 cell line, it is observed that BRCA1 deficiency results in failed G1/S, intra-S and G2/M checkpoint activation [112, 113].

BRCA1 regulates G1/S checkpoint by interacting with hypo-phosphorylated Rb, which interacts with E2F to suppress the transcription of its downstream targets and cell proliferation [114]. The intra-S-phase checkpoint activation is mediated by phosphorylation of Ser1387 of BRCA1 via ATM [115, 116]. ATM also mediates phosphorylation of Ser1423 of BRCA1, which enables the protein to activate Chk1 that regulates G2/M checkpoint [117, 118].

Similar to BRCA1, expression of BRCA2 is tightly regulated in a cell cycle-specific manner [119]. Moreover, formation of BRCA2-PALB2 complex is crucial for maintaining G2/M checkpoint [120]. This process ensures that cells with DNA damage do not progress through the cell cycle until the damage is repaired. This process ensures daughter cells to inherit error-free DNA and helps to maintain genomic integrity.

Moreover, BRCA1 and BRCA2 are also involved in maintaining telomere stability. Telomeres are regions containing repetitive nucleotide sequences, serving as protective caps at the ends of chromosome. Previous studies have established that maintaining telomeres is essential for genome stability [121-126]. BRCA1 ensures the stability of telomeres by regulating telomere length and removing pathogenic telomeres with the help of CtIP [127-129].

Last but not least, BRCA1 and BRCA2 act at stalled replication forks. Formation of BRCA1-BARD1 complex enhances the interaction between BRCA1-BARD1 complex and RAD51, which increases the presence of RAD51 at stalled

replication fork [130]. Similarly, when replication fork is stalled, BRCA2 is relocated to the stalled replication fork to promote the stable RAD51 nucleofilament formation. And as previously mentioned, the structure protects the stalled replication fork from MRE11-mediated nucleolytic degradation [131, 132]. Moreover, BRCA2 mediates replication fork restart by promoting the template switching of impeded nascent DNA with an intact sister chromatid [133].

1.4.2 Targeting BRCA1/2-mutated cancers

Since BRCA1 and BRCA2 play major roles in maintaining genome integrity, mutations in these genes can result in increased risk of tumour development [134]. It is well established that in familial breast and ovarian cancers, BRCA1 and BRCA2 genes are mutated in approximately 25% of tumours [135].

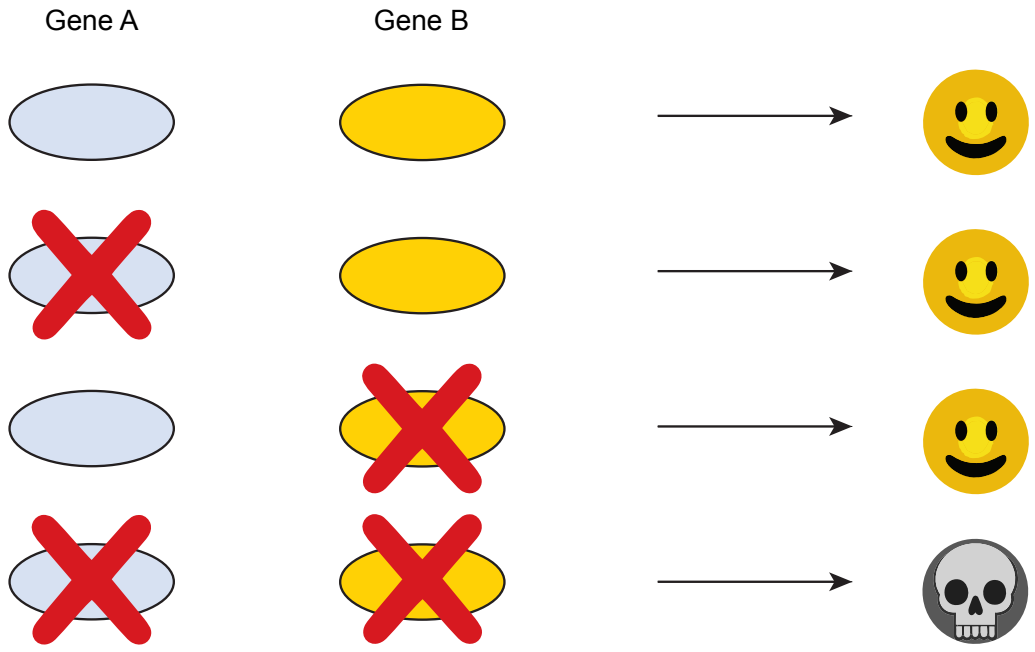


Figure 1.6 Illustration of synthetic lethality

Basic principles of synthetic lethality. The alteration of single gene is viable, whereas the simultaneous mutations of two genes leads to the cell death.

Moreover, BRCA1 and BRCA2 mutations are commonly found in sporadic cancers, ranging from skin cancers to pancreatic cancers [136].

Since BRCA1 and BRCA2 are mutated in a large number of cancer patients, specific therapies targeting BRCA1/2 deficiency have been developed, and patients with a range of cancer types are expected to be benefit from these targeted therapies.

One of the most well-known strategies to target the BRCA1/2 deficiency in cancer is using PARP inhibitors, which was the first clinical approach based on exploiting synthetic lethality (Fig.1.6) [137].

1.4.3 Mechanisms of PARPi treatment

Poly [ADP-ribose] polymerase 1, or PARP1 was the first PARP family enzyme purified and cloned in humans [138]. As briefly described in section 1.1.3, PARP1 utilises NAD+ as a co-factor to form a poly-ADP-ribose (PAR) chains on itself and other target proteins [139]. PARP1 acts as a first responder to the DNA damage; the PAR chains serve as a scaffold to recruit DNA repair proteins to the damaged sites [139-141]. The process facilitates the DDR to SSBs and subsequent repair of DNA breaks [142].

As briefly mentioned above, PARP inhibitors were the first clinically translated strategies based on synthetic lethality. Initially, it was suggested that PARP1 inhibition results in unrepaired SSB, which can lead to replication fork collapse and ultimately DSBs [143]. Therefore, BRCA1/2-deficient cells, which cannot carry out faithful DNA repair through HR and relies heavily on more error-prone repair pathways, end up accumulating DSBs, ultimately resulting in cell death (Fig.1.7A, B). However, more recent studies have suggested different mechanisms of action of PARP inhibitors in HR-deficient cells (Fig. 1.7B) [144].

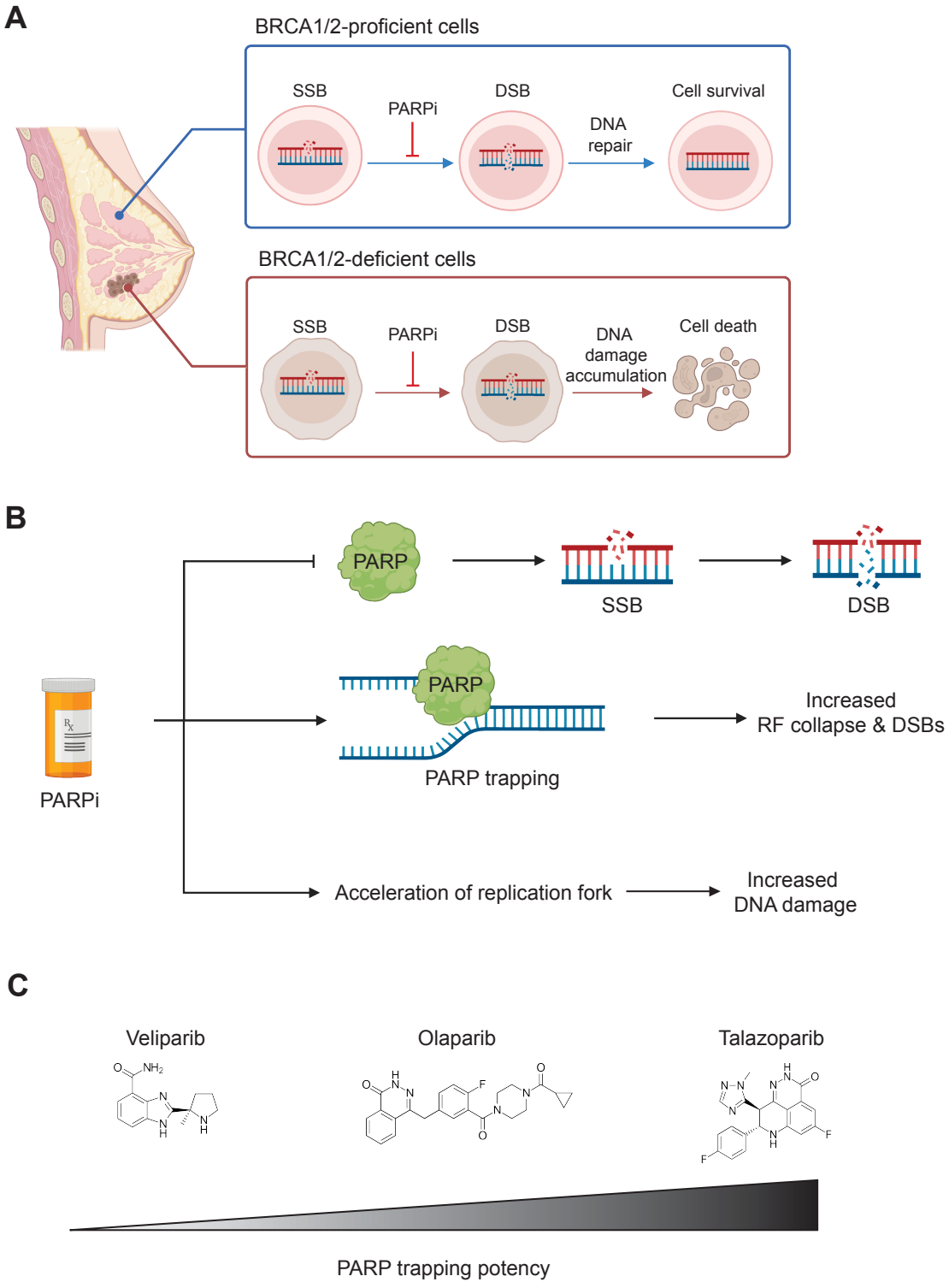


Figure 1.7 Mechanism of action of PARP inhibitor

(A) Schematic of synthetic lethal relationship between PARP inhibition and repair of SSBs, which can be converted into DSBs in HR-deficient cells. The cells lack the ability to perform HR result into accumulation of harmful DSBs, and ultimately cell death. (B) Proposed mechanisms of action of PARP inhibitors. (Top) Inhibition of enzymatic activity of PARP1

prevents the protein from PARylating its substrates. As a result, PARP1 can no more mediate the SSB repair. The unrepaired SSBs then results into DSB, increasing genomic instability. (Middle) Trapping of PARP1 on nascent DNA functions as a replication barrier. Prolonged replication stress results in replication fork collapse, which can be exacerbated into DSBs. (Bottom) Inhibition of PARP1 increases replication fork progression, inducing DNA damage responses. (C) Molecular structures of three PARP inhibitors used in clinic (Veliparib, olaparib, talazoparib). The PARP inhibitors differ in PARP trapping potency: talazoparib is the most potent PARP trapper, followed by olaparib, and veliparib being the least efficient PARP trapper.

More recently, it has been established that PARP inhibitors directly trap PARP onto DNA, forming DNA-protein crosslinks, the complications of which have been described above [145]. PARP inhibitors induce the formation of toxic PARP-DNA complexes by trapping PARP1 onto the damaged chromatin. The process prevents auto-PARylation and release of PARP1 from the DNA, ultimately leading to defects in replication fork progression (Fig.1.7B) [146-148]. Additionally, it can further lead to the replication fork stalling, and eventually replication fork collapse and DSB formation. Supporting this theory, PARP1-defective and depleted cells show resistance to PARP inhibitors [146, 149]. Moreover, several studies have established the correlation between the PARP inhibitor's PARP-trapping potency and cytotoxicity [146, 148-151]. In summary, the correlation between PARP trapping potency and cytotoxicity lies in the ability of PARP inhibitors to cause persistent DNA damage by both inhibiting enzymatic activity and trapping PARP on DNA. The dual mechanism enhances therapeutic efficacy of these inhibitors in cells with underlying HR defects [148].

Furthermore, it has been shown that inhibition of PARP1 induces acceleration of replication fork progression, which can result in replication stress (Fig.1.7B). This

study shows that PARP inhibitor treatment increased the replication fork speed by 1.4-fold [152], resulting in increased replication stress. The dysregulated replication fork progression can dampen the fidelity of DNA polymerase, contributing to the increased genomic instability [153].

1.4.4 Mechanisms of PARPi resistance

Initially, HR-deficient tumours respond well to PARP inhibitor treatment. However, much like other anti-cancer treatments, PARP inhibitor treatment shows poor long-term sensitivity due to the development of resistance [144]. One of the most well-established resistance mechanisms against PARP inhibitor is restoration of HR capacity. Through functioning HR, cells can correct PARP inhibitor-induced DNA lesions, therefore survive the treatment.

The most frequent mechanism of resistance seen in the patients is the re-expression of BRCA1/2 by restoration of open reading frame [154]. Additionally, recent study shows that demethylation of BRCA1 promoter restores the expression of the protein, reactivating HR pathway [155] (Fig.1.8A).

In addition to reversion mutations of BRCA1/2, loss of 53BP1 and its interacting proteins can lead to partial restoration of HR. 53BP1, which plays a major role in DSB repair pathway choice, interacts with RIF1, REV7 and Shieldin to protect the DNA ends from being resected [156-158]. However, if 53BP1 is lost and the DNA end resection is no longer repressed, then cells partially restore HR, rendering cells resistant to PARP inhibitors (Fig.1.8B).

Another mechanism of resistance is stabilisation of replication fork. In BRCA-deficient cells, the stalled fork cannot be protected upon fork reversal. The regressed arms become exposed to nucleases, such as MRE11, EXO1, and MUS81 [159, 160]. The recruitment of the nucleases is mediated by fork

remodelling proteins, such as SMARCAL1, ZRANB3, or HLTF [60, 161]. Excessive fork degradation leads to fork collapse, potentiating harmful genomic rearrangements and possible cell death. Loss of these proteins results in protection of replication fork, conferring resistance to the PARP inhibitors (Fig.1.8C).

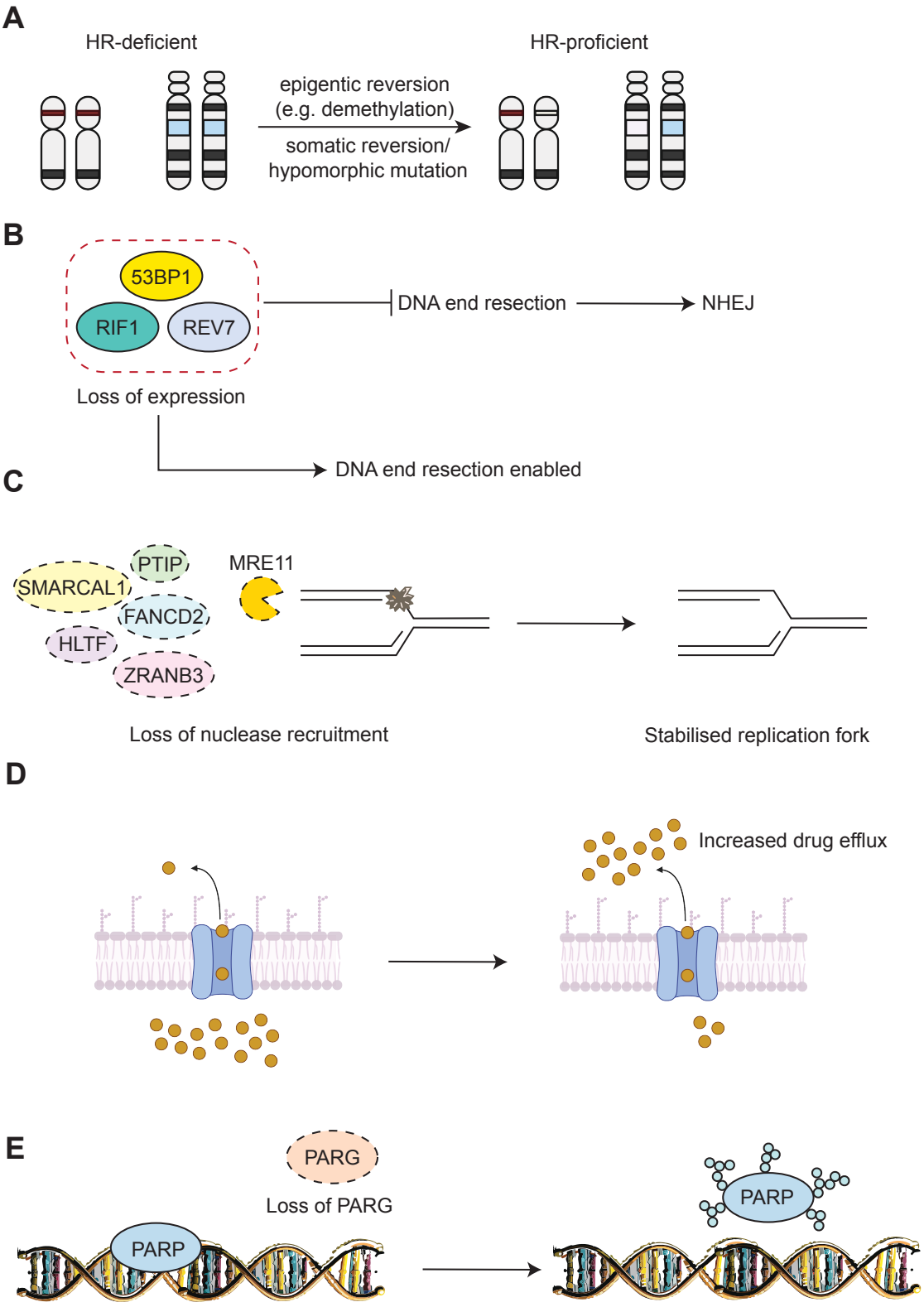


Figure 1.8 Mechanisms of PARPi resistance development

(A) Restoration of BRCA1/2 function is often mediated by frameshift mutation resulting in restoration of open reading frame (ORF). It leads to

the expression of functional BRCA1/2. Alternatively, hypomorphic mutations of BRCA1/2 can restore partially functional BRCA1/2, conferring to PARP inhibitor resistance. (B) Loss of 53BP1 and its downstream proteins results in promoting DNA end resection, which enables RAD51 recruitment and subsequent HR pathway. (C) Reduced recruitment of proteins involved in fork remodelling, which often recruits nucleases, prevents excessive nucleolytic degradation of stalled replication forks in BRCA1/2-deficient environment, therefore stabilising the fork. (D) Overexpression of drug-efflux transporter genes, *ABCB1*, which is known as *MDR1,* increases drug efflux. The process limits cellular availability of PARP inhibitor, therefore decreases the effectivity of the drug. (E) PARG hydrolyses ribose-ribose bonds in PAR chains to release mono (ADP-ribose) and oligo (ADP-ribose). In terms of preventing PAR accumulation, PARG works in the same direction as PARP inhibitor does. Since PARP inhibitor cannot fully block PARP activity, PARG activity is essential for the effective treatment response. Therefore, loss of PARG confers resistance to PARP inhibitor.

Acquiring PARP inhibitor resistance can be mediated by pharmacological response as well (Fig. 1.8D). Overexpression of *ABCB1* genes, or multi-drug resistance (*MDR1)*, which encodes p-glycoprotein pump, is known to be an adaptive response to remove introduced chemical or drug from cells [162]. The upregulated expression of p-glycoprotein efflux pump reduces the PARP inhibitor concentration in cells, dampening the efficacy of the drug.

Most recently, studies suggest that loss of PARG, the hydrolase that degrades PAR chain, also contributes to the development of PARP inhibitor resistance by partial restoration of PARP1's PARylating capacity [163, 164]. PARG hydrolases α(1"-2') or α(1"'-2") glycosidic linkage of PAR chain to release mono(ADP-ribose) and oligo(ADP-ribose) [165]. In the aspect of antagonising the activity of PARP, PARG works in the same way as PARP inhibitors; both prevents PAR

accumulation [166]. Since PARP inhibitors inhibit catalytic activity of PARP through its competitive binding to the NAD+ binding domain [167], it cannot fully block the activity of PARP. Therefore, the activity of PARG is crucial for PARP inhibitor response. If PARG is lost, the residual activity of PARP1 upon PARP inhibitor treatment can restore the PAR chain formation and rescue the downstream signalling [163], lowering the efficiency of the treatment.

1.5 Innate immune response and cancer

1.5.1 Genome instability and cGAS-STING activation

Previous studies have shown that genomic instability can trigger innate immune response via cGAS-STING activation [168-171]. As previously described, the instability can arise from exposure to exogenous or endogenous stressors, prolonged DNA replication stress, or deficiencies in DNA repair mechanisms.

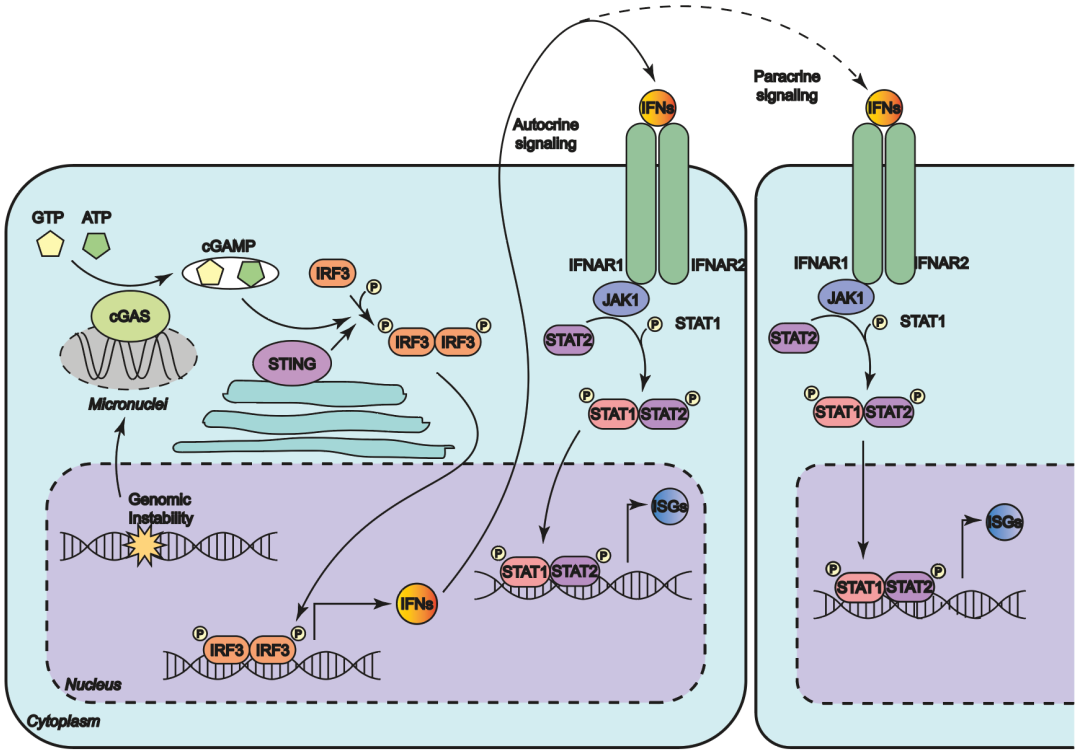


Figure 1.9 Type I IFN signalling is activated by DNA-damage induced cGAS-STING activation

Chromosomal fragments are recognized by the nucleic acid sensor cyclic GMP-AMP synthase, or cGAS. When DNA is bound to cGAS, it triggers conformation change in cGAS to enable cGAMP synthesis. cGAMP activates stimulator of interferon genes, or STING. The activated STING is then re-localized to the Golgi. STING triggers phosphorylation of interferon regulatory factor, IRF3. This mediates expression and secretion of proinflammatory cytokines. Among them, there is type I interferon (IFN-I). When IFN-I (for example, IFN-α) binds to the heterodimeric IFN receptor (IFNAR1/IFNAR2), the receptor activates JAK-STAT pathway to induce expression of IFN-stimulated genes (ISGs). IFN-α can bind to the IFN receptors on the same cells or neighbouring cells, inducing autocrine or paracrine IFN-responses.

Defective DNA replication, DNA damage repair or aberrant mitosis result in micronuclei formation. When ruptured, micronuclei either expose or release nuclear DNA, which then re-localises cytosolic GMP-AMP synthase (cGAS) to micronuclear chromatin to activate the pathway [172-175]. However, the detailed mechanism of how cellular, membrane-enclosed DNA is released into cytoplasm following DNA damage remains elusive.

The cGAS detects self-DNA fragments released into cytoplasm (Fig. 1.9). When cGAS recognises the DNA fragment, it leads to synthesis of 2'3' cyclic GMP-AMP (cGAMP), which then binds to Stimulator of Interferon Genes (STING) [176-180]. STING then triggers phosphorylation of Interferon regulatory factor 3 (IRF3) via TANK-binding kinase 1 (TBK1). Phosphorylated IRF3 undergoes dimerization, which enables nuclear translocation of the protein and trigger transcription of type I IFN response genes [181]. The subsequent production, secretion, and binding to the Interferon-α/β receptor (IFNAR) of IFN-I induces the expression of

interferon-stimulated genes and cellular responses, including enhanced antigen presentation by major histocompatibility complex class 1 (MHC1), which in turn leads to the activation of CD8+ T cells, priming the CD8+ T cells against the tumour-derived antigens [182, 183].

1.5.2 Type I IFN signalling in cancer

Type I IFNs bind to type I IFN receptor formed by IFNAR1 and IFNAR2 on the cell surface and lead to a sequence of signalling events involving the kinases JAK1 and TYK1 and transcription factors STAT2 and STAT1, leading to the expression of a subset of genes called interferon-stimulated genes (ISGs). Antiviral, antiproliferative and immunomodulatory responses are subsequently elicited by the different ISGs. Consequently, the cells become more antigenic and produce more pro-inflammatory cytokines. The IFN-I response, therefore, acts as a bridge between innate immunity and adaptive immunity, by promoting antigen presentation, chemokine production and indirectly facilitating antibody production of B cells by activating effector T cell responses [184, 185]. Cytotoxic T lymphocytes (CTLs), or CD8+ effector T cells, are able to recognise tumour antigens. They eliminate tumour cells by triggering death ligand/death receptor (Fas by Fas ligand (FasL))-mediated apoptosis and/or releasing cytolytic enzymes such as granzyme B or Perforin [186]. Therefore, type I IFN response is often recognised as essential driver of antitumour immunity [187]. For instance, recombinant forms of IFN-I have been approved as anti-cancer forms of therapy for several cancer types, showing positive responses [188, 189].

However, chronic IFN stimulation can lead to immune exhaustion, which leads to induction of immunosuppressive pathways and inhibition of T cell and Antigen-presenting cells (APCs), resulting in tumour-favouring conditions [187]. Several

studies have shown that type I IFN signalling is elevated in metastatic cancer cells [190, 191]. Moreover, it can promote production of the pro-inflammatory cytokine, IL-6, which is known to contribute to a tumour-favouring microenvironment [192-194]. Therefore, it is critical to fully understand how IFN-I responses affect cellular functions and how to tightly control their treatment effects.

1.5.3 ISG15: Type I IFN-stimulated protein with multi-faceted functions

Interferon-stimulated gene 15 (ISG15) is one of the most strongly induced genes by type I IFN signalling [195]. ISG15 consists of two ubiquitin-like domains and shares structural similarities with ubiquitin and other ubiquitin-like proteins, such as Small ubiquitin-like modifier (SUMO) proteins, NEDD8 and FAT10 [196-198]. Similar to Ubiquitin, ISG15 can covalently conjugate to lysine residues of its target proteins. The process is known as ISGylation, and involves sequential activities of E1 activating enzyme (UBE1L), E2 conjugating enzyme (UBCH8), and E3 ligases (HERC5, TRIM25, EFP) [199-201]. ISGylation can be reversed by the Ubiquitin-specific peptidase 18 (USP18), which removes ISG15 from its targets [202] (Fig. 1.10).

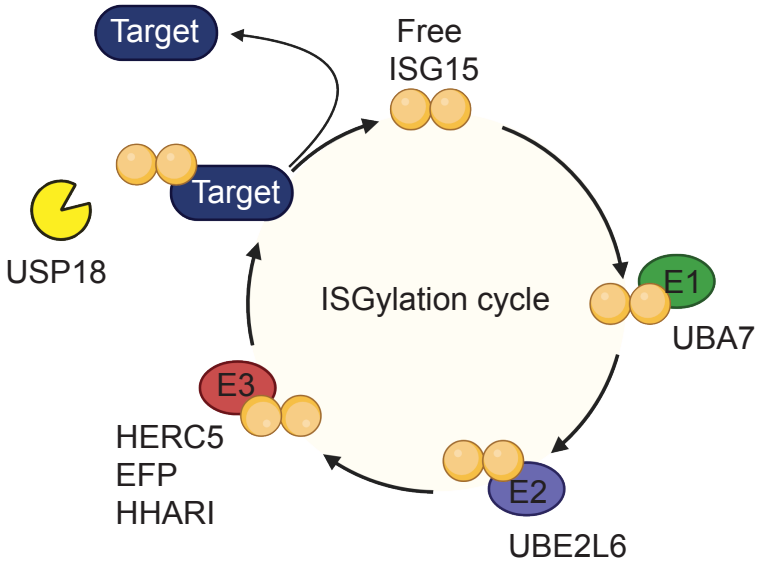


Figure 1.10 Illustration of ISGylation cycle

Activation of ISG15 mediated by the formation of high-energy thioester bond between C-terminal Glycine residue of ISG15 and the catalytic cysteine residue of Ubiquitin-like modifier-activating enzyme 7 (UBA7), which is specific for ISG15 [203]. Activated ISG15 is transferred to ubiquitin-conjugating enzyme E2L6 (UBE2L6), which helps to bind active ISG15 on their cysteine residues. Finally, one of the E3 ligases (HERC5. EFP, HHARI) conjugates ISG15 to its target protein.

One of the primary functions of ISG15 is its involvement in the antiviral defence mechanism. ISG15 can be conjugated to viral proteins, marking them for degradation, or inactivation and inhibiting viral replication [204]. This modification interferes with the ability of viruses to evade the host immune system [205-208]. Moreover, a recent study also showed that ISG15 can directly bind to STING and facilitate its oligomerisation to initiate signalling and IFN-I production [209].

ISG15 also plays a role in regulating type I IFN production and response signalling. For instance, ISG15 can bind to Retinoic acid-inducible gene 1 (RIG-1), a cytosolic pattern recognition receptor (PRR) that can trigger type I IFN production, and signal for autophagic degradation [210, 211]. Moreover, unlike

ubiquitin and other Ubiquitin-like proteins (UBLs), free ISG15 shows cytokine-like characteristic; it can bind to Lymphocyte function-associated antigen 1 (LFA-1) on lymphocytes and leukocytes, inducing secretion of IFN-ɣ [212, 213].

As well as playing a pivotal role in innate immune response, recent studies show that ISG15 plays a role in broader spectrum of cellular processes. ISG15 can modulate protein synthesis by modifying RNA-binding partners via ISGylation [200, 214-216].

ISG15 and ISGylation are also involved in tissue differentiation, especially in murine foetal cells [217]. In mice, the vast majority of proteins present at endometrium undergo ISGylation in the initial stages of pregnancy. Free ISG15 and ISGylated substrates are detected at implantation sites from the middle to late stages of gestation. Moreover, dysregulation of ISGylation via USP18 deletion resulted in foetal death [217, 218].

Most interestingly, recent findings illustrate that ISG15 has been implicated in DNA repair mechanisms, contributing to the maintenance of genomic stability. One of the most well-known functions of ISG15 in DNA damage response is its involvement in p53 regulation [219, 220]. Briefly, p53 activity is increased upon DNA damage as the DNA mismatch proteins hMutL and PMS1/2 are stabilised by ATM, which phosphorylates and activates p53 [221, 222]. ISG15, which has p53-responsive elements and induced in a p53-depedent manner under DNA damage, conjugates to p53 to enhance the binding of p53 to the promoters of target genes, such as CDKN1 or BAX. This ISG15-mediated p53 regulation establishes positive feedback loop of p53 activity upon DNA damage [223]. EFP-mediated ISGylation of p53 on its two lysine residues, K291 and K292, facilitates acetylation and phosphorylation of p53 (Fig.1.11A). This process increases p53

binding to p53 response elements (p53RE) to enhance the expression of target genes, suggesting the positive feedback regulation between ISG15 and p53 [223]. Furthermore, HERC5-mediated ISGylation of misfolded p53 leads to its proteasomal degradation, indirectly promoting the function of correctly-folded p53 (Fig.1.11B) [219].

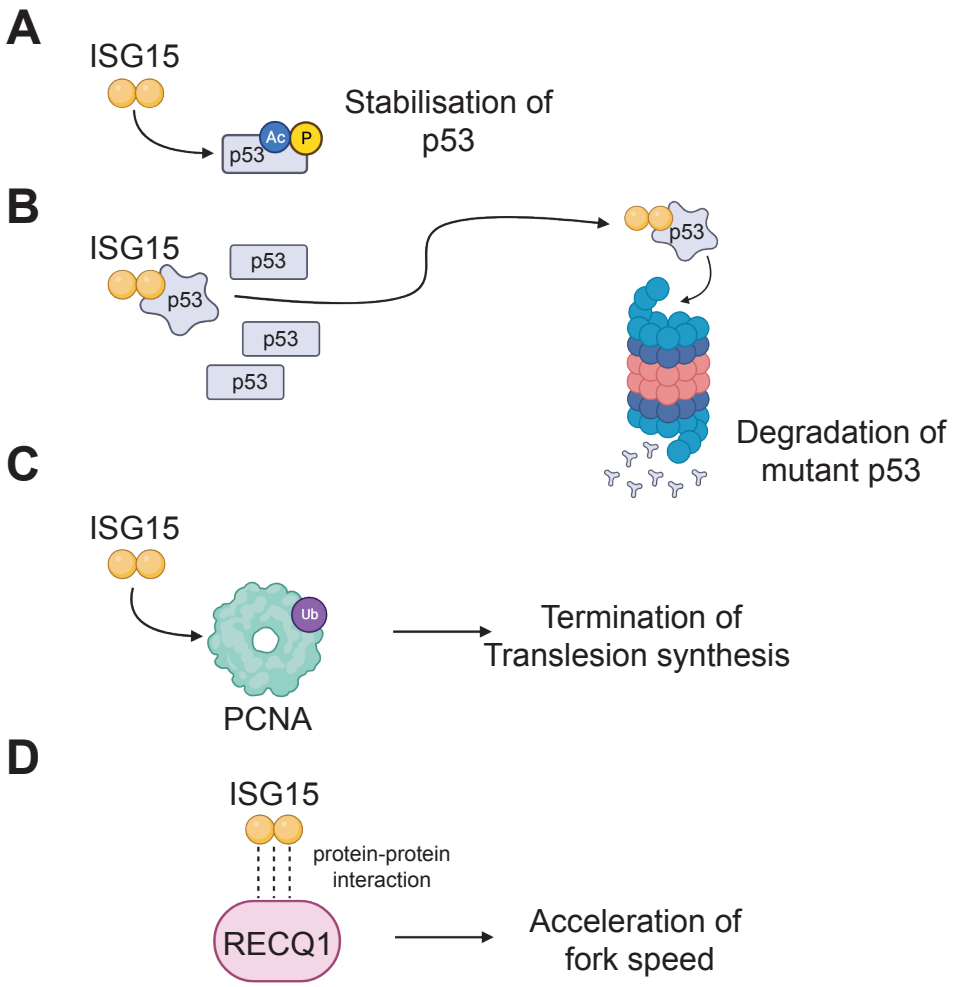


Figure 1.11 Role of ISG15 in DNA damage response

(A) DNA-damage induces ISGylation of p53. ISGylation amplifies both acetylation and phosphorylation of p53, subsequently elevating its affinity for p53 response elements (p53RE). This heightened binding capability then triggers the activation of its target genes. (B) Misfolded or aberrant

p53 are ISGylated via HERC5, which results in proteasomal degradation. (C) ISGylation of mono-ubiquitinated PCNA tethers the protein for increased affinity to Ubiquitin specific peptidase 10, USP10 (figure not shown). The process leads to deubiquitination of PCNA and release of DNA Pol-η from PCNA, terminating the TLS. (D) ISG15 can non-covalently interact with RECQ1 to accelerate the fork speed.

ISG15 is also involved in termination of translesion synthesis (TLS) (Fig. 1.11C). Upon the DNA damage, PCNA undergoes post-translational modifications, such as ubiquitination and SUMOylation to orchestrate DNA damage tolerance response [224-227]. The mono-ubiquitination of PCNA at K164 by Rad6-Rad18 enables the recruitment of error-prone TLS polymerase, DNA Pol η [54, 228, 229]. ISG15 can detect mono-ubiquitinated PCNA and conjugate to the substrate via EFP. The ISGylation of PCNA tethers the protein for increased affinity towards Ubiquitin-specific peptidase 10 (USP10), which de-ubiquitinates PCNA. The process allows PCNA to release the TLS Pol and to re-engage with replicative DNA polymerases [230].

Moreover, recent findings suggest that ISG15 is playing a role in replication machinery (Fig. 1.11D). A study showed that upregulated ISG15 expression resulted in accelerated replication fork progression and reduced sensitivity towards CPT-induced fork slowing, which is primarily dependent on non-covalent interaction between ISG15 and RECQ1 [231]. In addition to this, recent study shows that USP18 deficiency in cells results in increase of ISG15-conjugates and increased sensitivity towards ionising radiation, highlighting the putative role of ISG15 and ISGylation in DDR [232].

1.6 Aim

As previously stated [170], our lab has characterised the biphasic transcriptional changes of human cells upon loss of BRCA2. During this study, the team has utilised human non-small cell lung carcinoma H1299 cells carrying a doxycycline (DOX)-inducible short hairpin RNA (shRNA) against BRCA2. The cells were cultured in the presence or absence of DOX for 28 days and collected at two different time points (day 4, day 28) and subjected to RNA-seq analysis to assess transcriptional changes upon acute and chronic BRCA2 loss.

From the RNA-seq data, it was observed that acute BRCA2 loss resulted in dysregulation of genes involved in cell cycle regulation, chromosome segregation, DNA replication and DNA repair.

Interestingly, the chronic loss of BRCA2 led to increased expression of innate immune response genes, especially those associated with type I Interferon (IFN) response. Previous studies [168, 233] have shown that micronuclei formation can induce type I IFN responses as previously stated. The lab has confirmed that loss of BRCA2 induces increase of cGAS-positive micronuclei formation.

Furthermore, we then treated the cells with PARP inhibitor to study whether the treatment on BRCA2-deficient cells could also impact on interferon responses. We observed that PARP inhibitor treatment elicits an innate immune response in vitro and in vivo. Therefore, we have hypothesised that type I IFN genes may play a physiological role in survival of BRCA-deficient cells, especially in the context of PARPi treatment.

In this study, we aimed to understand whether developing resistance against PARP inhibitor alters the transcriptional profile of BRCA-deficient cells and tumours. The characterisation of the transcriptomes from PARPi-naïve and

resistant cells may reveal crucial differences, which could allow us to identify the detailed mechanism of PARPi resistance and combat the rapidly occurring resistance observed in clinics.

From the transcriptomics data, we have found out that ISG15 is upregulated in BRCA-deficient cells and tumours that have developed PARPi resistance. Therefore, we aimed to elucidate the role of ISG15 in PARPi resistance in the context of BRCA deficiency.

Previous studies suggest that ISG15 is involved in the replication machinery, potentially by modifying key proteins involved in DNA replication and repair processes. This involvement could help stabilize replication forks, prevent collapse, and mitigate replication stress.

We have hypothesised that ISG15 may be conjugating to key proteins involved in DNA replication and repair, modulating their activity, localization, or stability. This post-translational modification could help maintain replication fork integrity, facilitate timely repair of damaged DNA, or activate cell cycle checkpoints to allow more time for repair.

By investigating these aspects, we would expect to gain a deeper understanding of how ISG15 contributes to PARPi resistance and potentially identify new therapeutic targets to overcome resistance in BRCA-deficient cancers.

Chapter 2

Material and methods

2.1 Cell lines and cell culture

Human non-small cell lung carcinoma H1299 cells were cultivated in monolayers in Dulbecco's Modified Eagle Medium (DMEM) (Sigma-Aldrich, D5796) supplemented with 10% tetracycline-free foetal bovine serum (Scientific Laboratories Supplies limited, 35-075-CV). Human non-small cell lung carcinoma H1299 cells carrying doxycycline (DOX)-inducible shRNA against BRCA2 was cultured in the same condition. For inducing shBRCA2 in H1299 cells, 2 μg/mL DOX (Sigma-Aldrich, D9891) was added in the growth medium. *BRCA1/2*$^{+/+}$, *BRCA1*$^{-/-}$ (a gift from Dr Daniel Durocher, University of Toronto, Canada) and *BRCA2*$^{-/-}$ human retinal epithelial pigment epithelial-1 (RPE1) cells, transduced with hTERT and TP53-deletion, were cultivated in monolayers in DMEM (Sigma-Aldrich, D5796) supplemented with 10% foetal bovine serum (Merck Life Science UK, F7524) and 2μg/mL blasticidin (Life Technologies, A1113903). Human colorectal carcinoma HCT116 cells carrying auxin-inducible degron against Topoisomerase I (HCT116mAID-TOP1, a gift from Dr Laura Baranello, Karolinska Institutet, Sweden) were cultivated in monolayers in DMEM (Sigma-Aldrich, D9891) supplemented with 10% foetal bovine serum (Merck Life Science UK, F7524), 1 mg/mL puromycin (Thermo Fisher, A11138-03) and 125 mg/ml hygromycin B (Thermo Fisher, 10687010).

2.2 Generation of knockout cell lines using CRISPR-Cas9

Briefly, 2.0-5.0 x10^4 cells were co-transfected with Cas9 protein and sgRNA, using Dharmafect 1 (Dharmacon, Cat #T-2001-03). Forty-eight hours after transfection, cells were seeded in 96-well plates to obtain single cell clones. After single cell clones were obtained, individual cultures were subjected to IFN

treatment for 24 hr to induce ISG15 expression, followed by immunoblotting to screen for deletion of the protein of interest.

Table 2.1 sgRNA used for knocking out target gene

Name of construct	Sequences (5'-3')	Provider	Catalogue Number
ISG15	CTGCGTCAGCCGTACCTCGT	Dharmacon	CM-004235-01-0002

2.3 Resazurin-based cell viability assay

Between 300 cells/well and 1000 cells/well were grown in 96-well plates and treated with indicated doses of drugs for 6 days. To determine viability, cells were incubated with 10 μg/mL resazurin (Sigma-Aldrich, R7017) in growth medium at 37˚C for 2 hours. Fluorescence was measured (excitation: 544 nm, emission: 590 nm) using POLARstar Omega plate reader (BMG Labtech).

2.4 Resazurin-based cell proliferation assay

Cells were seeded (1000-2000 cells per well) in triplicate in a 96-well-plate to reach 70-80% confluency after 8 days. Cells were then incubated at the 37˚C and 5% CO2. Proliferation of cells was measured every 2 days. To quantify the proliferation rate, cells were incubated at 37˚C for 2 hours with 10 μg/mL of resazurin (Sigma, R7017) in growth medium at 37˚C for 2 hours. Fluorescence was measured (excitation: 544nm, emission: 590nm) using POLARstar Omega plate reader (BMG Labtech).

2.5 siRNA transfection

Cells were transfected with siRNA using Dharmafect 1 (Dharmacon, Cat #T-2001-03) or RNAiMAX (Invitrogen, 13778075). Briefly, 0.4-1.0 x10^6 cells were

transfected with 80 nM siRNA by reverse transfection. After 48 hr of transfection, cells were harvested, and the target gene depletion was determined by immunoblotting. The non-targeting AllStars Negative control siRNA (Qiagen, 1027281) was included in all experiments that utilised siRNA transfection.

Table 2.2 siRNAs used for knocking down target genes

Name of construct	Sequences (5'-3')	Provider	Catalogue Number
BRCA1	CAGCAGTTTATTACTCACTAA	Qiagen	S102654575
53BP1	CAGGACAGTCTTTCCACGAAT	Qiagen	SI02663731
ISG15	GCGCAGAUCACCCAGAAGA, GCAACGAAUUCCAGGUGUC, GGCUGACCUUCGAGGGGAA, AAAGGCUGUUGUAAAGAGA	Dharmacon	L-004235-03-0010
HERC5	GCAAGAAUGUAUAGAAG, AAUAGAACAGGCAUCAUUA, UCAAAUCCCUUCCGCUAUA, AAAGAAAUCUGACGUCAAU	Dharamacon	L-005174-00-0005
USP18	UUUUUGAUGUGGACUCAAAUU, UUUGAGUCCACAAUCAAAAAGA	Thermo Fisher	AM16704, ID: 105194
UBA7	CAUCUUUGCUAGUAAUCUA, CGAAUUGUGGGCCAGAUUA, AUAGAGCGCUCCAUCUCA, GCAUGGAGUUUCUG	Dharmacon	L-019759-00-0005
USP11	GCGCACAFCUGCAUGUACAU, GAGAAGCACUGGUAUAAGC, GGACCGUGAUGAUAUCUUC, GAAGAAGCGUUACUAUGAC	Dharmacon	L-006063-00-0005
SETX	GCACGUCAGUCAUGCGUAA, UAGCACAGGUUGUUAAUCA, AAAGAGUACUUCACGAAUU, GGACAAAGAGUUCGAUAGA	Dharmacon	L-021420-00-0005
TOP1	GAAAAUGGCUUCUCUAGUC, GAUUUCCGAUUGAAUGAUU, GCACAUCAAUCUACACCCA, CGAAGAAGGUAGUAGAGUC	Dharmacon	L-005278-00-0005

2.6 Immunoblotting

To prepare the whole cell extract, cells were washed with 1x PBS, followed by trypsinisation for harvest. Pelleted cells are then washed with 1x PBS and

resuspended in SDS-PAGE loading buffer (0.16 M Tris-HCl pH 6.8, 4% SDS, 20% glycerol, 0.01% bromophenol blue, 100 mM DTT), supplemented with protease inhibitor (Roche, 4693159001) and phosphatase inhibitor (Roche, 4906845001) cocktails. Samples were briefly sonicated, heated at 70℃ for 10 min and centrifuged at 13,000rpm for 7 min. Protein concentration was quantified using a Nanodrop spectrophotometer. Equal amounts of protein (50-150 µg) were loaded on NuPAGE-Novex 4-12% Bis-Tris or 12% Bis-Tris gel and run in MOPS buffer (Life Technologies, NP0001) or 3-8% Tris-acetate gels and run in TA buffer (Life Technologies, LA0041). Proteins were transferred onto 0.2 µM nitrocellulose membranes (GE Healthcare) using semi-dry transfer in transfer buffer (Life Technologies, NP00061) with 10% methanol. Membranes were blocked in 5% skimmed milk in PBS-Tween (PBST; 0.05% Tween 20 [Sigma-Aldrich, P7949] in PBS) or 3% Bovine Serum Albumin (BSA; Sigma-Aldrich, A7906) in PBST. Membranes were incubated overnight at 4°C with primary antibodies, washed with PBST, followed by Horseradish peroxidase (HRP)-conjugated secondary antibodies diluted in 5% skimmed milk in PBST at room temperature for 1 hour. Membranes are then washed with PBST and developed by Enhanced Chemi-Luminescence (ECL; Millipore and GE Healthcare) detection on X-ray films (Life Technologies, 34089).

Table 2.3 Primary antibodies used for immunoblotting

Specificity	Host	Provider	Catalogue Number	Dilution
BRCA1	Mouse	Calbiochem	OP92	1:1’000
BRCA2	Mouse	Calbiochem	OP95	1:1’000
GAPDH	Mouse	Novus Biologicals	6C5	1:30’000
RPA (Ser33)	Rabbit	Abcam	ab211877	1:500
RPA	Mouse	Abcam	ab2175	1:1’000
Chk1 (Ser345)	Rabbit	Cell Signalling	2348S	1:500

Chk1	Mouse	Santa Cruz Biotechnology	sc-8408	1:1’000
ISG15	Rabbit	Cell Signalling	2743	1:400
SMC1	Rabbit	Bethyl Laboratories	A300-055A	1:10’000
UBA7	Rabbit	Cell Signalling	4813S	1:1’000
IRF3 (Ser386)	Rabbit	Abcam	ab76493	1:1’000
IRF3	Mouse	Santa Cruz Biotechnology	sc-33641	1:1’000
IFIT1	Rabbit	Cell Signalling	14769S	1:1’000
IFIT2	Rabbit	Proteintech	23604-1-AP	1:1’000
IFIT2 (F-12)	Mouse	Santa Cruz Biotech	SC-390724	1:1’000
USP18	Rabbit	Cell Signalling	4813S	1:1’000
DDX5	Mouse	R&D Systems	MAB6370	1:500
Ku70	Mouse	Abcam	ab3114	1:1’000
TOP1	Mouse	Santa Cruz Biotechnology	sc-271285	1:1’000
SETX	Rabbit	Bethyl Lab	A301-104A	1:1’000
USP11	Rabbit	Bethyl Lab	A301-613A	1:1’000
α-Tubulin	Rabbit	Abcam	ab4074	1:2’000

Table 2.4 Secondary antibodies used for immunoblotting

Specificity	Host	Provider	Catalogue Number	Dilution
Mouse	Goat	Dako	P0447	1:5’000
Rabbit	Goat	Dako	P0448	1:5’000

2.7 Cell cycle analysis

Asynchronous cells were labelled with 25μM EdU for 30 min. Cells were then trypsinised and processed using Click-iT EdU Alexa Fluor 647 flow cytometry assay kit (Thermo Fisher Scientific, C10419) according to manufacturer’s instructions. The cells are further stained with 20μg/mL propidium iodide (Sigma Aldrich, P4864) and 10μg/mL RNase A (Thermo Fisher Scientific, 12901) in PBS for 30 min, protected from light. A total of 10,000 events per conditions were recorded using CytoFLEX Flow Cytometer. Flow cytometry data were analysed with FlowJo software.

2.8 Bacterial transformation

DH5α competent cells (Thermo Fisher Scientific, 18265017) were used for bacterial transformation. Briefly, 100ng/μL plasmid DNA was delivered through giving heat shock to the competent cells at 42°C. Competent cells transformed with plasmid of interest were then incubated at 37°C shaking incubator for 45-60 minutes. Following the incubation, 50-100μL of the transformation mixture was seeded on LB agar (Sigma Aldrich, L3147-1KG) plate using a bacterial spreader. Cells were incubated at 37°C overnight.

2.9 Plasmid amplification and purification

Following the bacterial transformation, single colony was selected from the plate and then inoculated in 100-500mL LB (Gibco™, 10855001) for overnight growth at 37°C shaking incubator. The overnight bacterial culture was harvested by centrifugation at 6000g for 15 min at 4°C. QIAGEN Plasmid Maxi Kit (QIAGEN, 12162) was used for the purification of the plasmid, and the procedure followed the manufacturer's protocol. DNA concentration was measured by using a Nanodrop spectrophotometer.

2.10 Lentiviral transduction

Briefly, 7.0μg of plasmid DNA was added to Lenti-X packaing single shots (TakaraBio, 631275), which then delivered to the recipient 293T cells. Transfected cells were incubated at 37°C, 5% CO_2 for 4 hours. After 4 hours, fresh growth medium was added. The cells were incubated for an additional 24-48 hours. Lentiviral particles were collected by filtering through a 0.45μm filter (VWR, 514-4127). The filtered viral supernatant was diluted to a MOI of 1-10 and mixed with 4μg/mL polybrene. The mixture was added to the target cells and

incubated at 37°C, 5% CO_2 for overnight. Post-transduction, cells were removed from viral supernatant and washed with 1X PBS for 10 times. Cells were then transferred to new flask and cultured for further selection.

2.11 Immunoprecipitation

Cells were harvested and lysed in lysis buffer (20mM HEPES pH 8.0, 150mM NaCl, 0.2% NP-40. 10% Glycerol, 5mM NEM, protease inhibitor (Roche, 4693159001), phosphatase inhibitor (Roche, 4906945001)) on ice. Lysates were first centrifuged at 600g for 5 min at 4°C, supernatants are transferred to clean tubes and the remaining lysates are centrifuged at 14,000g for 10 min at 4°C and transferred into the new tubes, followed by quantifying protein concentration using a Nanodrop spectrophotometer. Only the samples above concentration of 2mg/mL proceeded for immunoprecipitation. Protein A or G dynabeads were incubated with 5µg of antibodies with rotation at room temperature for 10 min. Lysates were then added to beads-antibody mix and incubated at 4°C overnight. Beads are then washed with lysis buffer for 3 times and transferred into clean tubes. Beads are then added with 80µL of SDS-PAGE loading buffer (0.16 M Tris-HCl pH 6.8, 4% SDS, 20% glycerol, 0.01% bromophenol blue, 100 mM DTT) and heated at 90℃ for 5 min. Supernatants are then transferred into clean tubes. For the remaining beads, 50µL of SDS-PAGE loading buffer is added and heated at 90℃ for 5 min. Supernatants are then transferred into the new tubes. Samples are then analysed with Immunoblotting.

Table 2.5 Antibodies used for immunoprecipitation

Specificity	Host	Provider	Catalogue Number
ISG15	Rabbit	Invitrogen	703131
TOP1	Rabbit	Invitrogen	MA5-38376

DDX5	Rabbit	Abcam	ab126730
Ku70	Rabbit	Abcam	ab83501

2.12 ISG15 interactome immunoprecipitation LC-MS/MS analysis

RPE1 cells were lysed with Co-IP lysis buffer (20 mM Hepes pH 8.0, 150 mM NaCl, 0.2% NP-40, 10% glycerol, 5 mM NEM, phosphatase and protease inhibitor cocktails) and proceeded for immunoprecipitation using 5 µg of ISG15 antibody (Santa Cruz #sc-166755) with 25 µL of protein G Sepharose slurry (Invitrogen; #15920-10) for 16 h at 4 °C. Beads were washed 4 times with Co-IP lysis buffer and immunocomplexes were eluted with 2X Laemmli buffer. The samples were then prepared for MS analysis as previously described [232]. Briefly, proteins were reduced with reducing buffer (200mM DTT in 0.1 M Tris pH 7.8), followed by alkylation with 200 mM iodoacetamide in 0.1 M Tris pH 7.8, protected from light. Samples were acidified by adding of 12% phosphoric acid and processed on S-TrapTM mini columns (C02-mini-80, ProtiFi). Columns were washed with 90 % methanol in 100 mM triethylammonium bicarbonate (TEAB). The suspension is then centrifuged at 4000 g. Proteins were digested with trypsin (1:100 w/w) in 1 mM HCl overnight at RT. Peptides were eluted and dried in a vacuum concentrator. Dried peptides were dissolved in Buffer A (98 % MilliQ-H20, 2 % CH3CN and 0.1 % TFA) and 2.2% of the tryptic peptides were analysed by LC-MS/MS using a U3000 HPLC connected to an Orbitrap Ascend tribrid instrument (Thermo Scientific). The tryptic peptides were loaded onto a PepMapC18 trap column (300µm x 5mm, 5µm particle size, ThermoFisher) and separated on a 50cm EasySpray column (ES803, ThermoFisher) using a 60 min linear gradient from 2 to 35% acetonitrile, 0.1% formic acid and at 250nl/min flow rate. MS data were acquired in data-independent mode (DIA) with minor changes

from previously described method [234], [235]. Briefly, MS1 scans were acquired in the Orbitrap over the mass range of 350 – 1650m/z, with a 45k resolution, maximum injection time of 91 ms, an AGC set to 125% and a RF lens at 30%. MS2 scans were then collected using the tMSn scan function, with 40 variable width DIA scan windows at 30K orbitrap resolution, normalized AGC target of 1000%, maximum injection time set to auto and a 30 % collision energy.

2.13 LC-MS/MS data processing (PERSEUS)

Raw mass spectrometry files were label free quantified using the default settings on DIA-NN (version 1.8; library-free mode) and the Uniprot reference proteome UP000005640 (2022) as FASTA file. Data were further processed in Perseus (version 1.6.2.3). The mass spectrometry proteomics data will be made available via the ProteomeXchange Consortium via the PRIDE partner repository [236].

2.14 DNA Fibre assays

Cells were sequentially pulse-labelled by two different nucleoside analogues, 25μM of 5'-chloro-2'-deoxyuridine thymidine (CldU) and 250μM of 5'-iodo-2'-deoxyuridine (IdU) for exactly 30 min each. Cells were washed with 1X PBS for 3 times between the pulses. After labelling, cells were washed with ice-cold 1X PBS for 3 times and collected. Cells were spotted (2μL of $5x10^5$ cells/mL PBS cell suspension), and lysed on positively charged microscope slides (VWR, 631-0146), by 7μL spreading buffer (200mM Tris-HCl pH 7.4, 50mM EDTA, 0.5% SDS) for 2 min at room temperature. Individual DNA fibres were spread by tilting the slides at 35 degrees. After air-drying, the fibres were fixed with 3:1 Methanol/Acetic acid fixative at room temperature for 10 minutes. The fibres then stored at 4 degrees overnight. Next day, fibres were rehydrated in deionized

water, followed by denaturing in 2.5M HCl for 1 hr. Fibres then washed with 1X PBS and blocked with blocking solution (2% BSA and 0.1% Tween 20 in PBS) for 40 min. Next, fibres were incubated for 3 hr with primary antibodies, (CldU: 1:500, rat monoclonal anti-BrdU (Abcam, ab6326), IdU: 1:100, mouse monoclonal anti-BrdU (Becton Dickinson, 347580)), diluted in blocking solution. The fibres are washed with PBST (0.2% Tween 20 in 1X PBS) for five times, then incubated 1 hr with secondary antibodies (CldU: 1:300, Goat anti-rat Alexa Fluor 555 (Invitrogen, A21434), IdU: 1:300, Goat anti-mouse Alexa Fluor 488 (Invitrogen, A11001)), diluted in blocking solution. After washing with PBST for five times, slides were mounted with Prolong Gold Antifade mounting medium (Invitrogen, P36930). Images were acquired with a Leica DMI6000B inverted microscope and fluorescence imaging workstation equipped with HCX PL APO x100/1.4-0.7 oil objective, and then analysed with ImageJ software.

2.15 Bulk RNA-seq data analysis

Paired-end reads in FASTQ files were assessed for sequencing quality and adapters using FastQC (v0.11.9). After initial quality control, paired-end reads were aligned to the human reference genome (GRCh38/hg38) and coordinate sorted using STAR (v2.7.10b) and Samtools (v1.19) respectively. Aligned BAM files were checked for mapping quality using Samtools and samples with at least 90% primary alignments were retained to ensure a high mapping quality. Properly paired reads with mapping quality greater than 30 were summarized using featureCounts (v2.0.3). The raw gene count matrix was further processed using custom R script and genes with low read counts (less than ~ 2.5 counts per million in more than 3 samples) were filtered out.

2.16 Differential expression analysis

The analyses were carried out using R package edgeR (v3.36.0). Filtered counts were Trimmed mean of M-value (TMM) normalized and common and tag-wise dispersion were estimated with option “robust = TRUE”. Quasi-likelihood negative binomial generalized log-linear model was fit to counts data and gene-wise empirical Bayes quasi-likelihood F-tests for a given contrast was performed to test for differential expression. Unless stated otherwise, differentially expressed genes (DEGs) were identified based on $|Log_2(\text{Fold change})| > 0.5$ and False Discovery Rate (FDR) using Benjamini-Hochberg adjusted p-values < 0.05.

2.17 Gene set enrichment analysis

Gene set enrichment analysis (GSEA) was performed to assess the enrichment of genes in gene sets from the Reactome database. A threshold of $p < 0.05$ was used to identify significant pathways where genes were enriched.

2.18 DRIP-seq data analysis

The Paired-end DRIP-seq data for human HeLa cells were downloaded from Sequence Read Archive, SRA (SRR15663580, SRR15663581). Raw data was aligned to the human reference genome (GRCh38/hg38) using BWA-MEM. Properly paired reads with mapping quality greater than 28 were kept, coordinate sorted using Samtools and duplicate reads marked with Picard. Input subtracted bigwig files were obtained using “bamCompare” function in deepTools (v3.5.1).

2.19 ChIP-seq data analysis

The data for chromatin immunoprecipitation sequencing (ChIP-seq) of native TOP1 in human HCT116 cells were downloaded from Gene Expression Omnibus

(GEO, accession number: GSE57628), and aligned to the human reference genome (GRCh38/hg38) using BWA-MEM. Aligned BAM files were coordinate sorted and reads with mapping quality of less than 20 were filered out using Samtools. Duplicate reads were marked with Picard and input subtracted bigwig files were generated using “bamCompare” function in deepTools.

2.20 Statistical analysis

All statistical analyses were performed using the GraphPad Prism 8.0 software. The data are presented as the mean ±SEM from individual experiments, which have been biologically repeated at least two times. Student’s t-test (two-tailed) was applied to compare differences between two groups and following abbreviations are used to present statistical significance: ns as non-significant (P>0.05), *P<0.05, **P<0.01, ***P<0.001, ****P<0.0001

Chapter 3

Experiment results I – Monitoring ISG expression in BRCA1/2-deficient cells and the effect of lacking ISG15 machinery proteins in the context of hIFNa2 treatment

3.1 ISG expression is induced by PARP inhibitor and hIFNa2 treatment

From the previous study published by the lab, the loss of BRCA2 is shown to be associated with distinct alterations in cell physiology [170]: the early, acute phase is characterised by decreased transcription of genes involved in cell cycle progression, chromosome segregation, DNA repair and replication. In contrast, the late, chronic phase is defined by elevation of IFN-regulated innate immune response of genes. Interestingly, loss of RAD51 is known to result in upregulation of ISGs as well [237]. Regarding that the loss of proteins involved in homologous recombination results in upregulated innate immune response, we were determined to study whether the expression of ISGs plays a role in survival of HR-deficient cells.

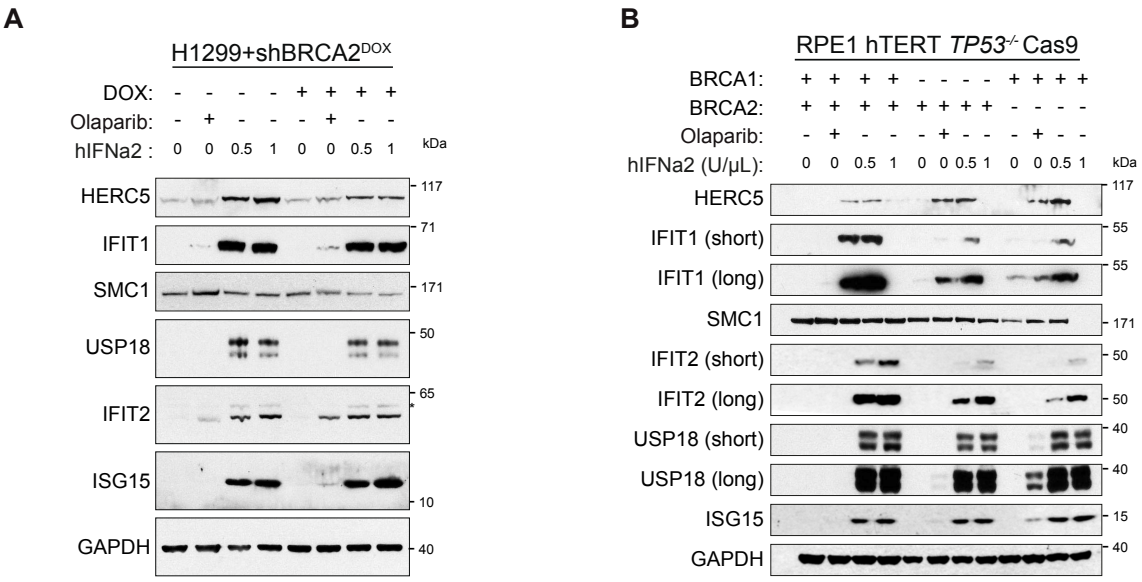


Figure 3.1 Upregulated ISG expression PARPi and hIFNa2 treatment in H1299+shBRCA2^{DOX} and RPE1 hTERT *TP53*$^{-/-}$ Cas9 (*BRCA1*$^{-/-}$, *BRCA2*$^{-/-}$)

(A) Human H1299 cells carrying a doxycycline (DOX)-inducible shRNA against BRCA2 were grown in the presence or absence of 2 µg/mL DOX and treated with olaparib (10µM) for 3 days or hIFNa2 (500U/mL,

1,000U/mL) for 1 day. Whole-cell extracts were prepared and immunoblotted as shown. SMC1 and GAPDH were used as loading controls. (B) Human *BRCA1/2*$^{+/+}$, *BRCA1*$^{-/-}$, and *BRCA2*$^{-/-}$ RPE1 hTERT *TP53*$^{-/-}$ Cas9 cells were treated with olaparib (10μM) for 5 days or hIFNa2 (500U/mL, 1,000U/mL) for 1 day. Whole-cell extracts were prepared and immunoblotted as shown. SMC1 and GAPDH were used as loading controls. The data are representative of at least 2 independent experiments.

Given that the previous study suggests that PARPi treatment on HR-deficient cells can induce premature ISG expression and upregulated innate immune response in chronic BRCA-loss cells, we wanted to study whether PARPi treatment leads to increase expression of ISGs in protein level and whether BRCA deficiency affects the cells' sensitivity towards hIFNa2 treatment.

In human H1299 cells containing a DOX-inducible shRNA against BRCA2, we have observed that IFIT1 and IFIT2 expression is potentiated by olaparib treatment (Fig. 3.1A). The induction of these proteins could be observed in both BRCA2-proficient and BRCA2-deficient cells, but BRCA2-deficient cells show slightly stronger induction upon olaparib treatment. IFIT1 and IFIT2 are induced upon hIFNa2 treatment, but there was no observable expression difference between two doses. However, ISG15 was only induced upon olaparib treatment in BRCA2-deficient cells. Interestingly, expression of HERC5, the E3 ligase of ISG15, seems to be less potentiated by hIFNa2 treatment in BRCA2-deficient cells than in BRCA2-proficient cells. Olaparib treatment seems to increase the expression of the protein, regardless of the BRCA2 status. Interestingly, USP18, the antagonist of ISG15, does not seem to be upregulated upon olaparib treatment.

Intrigued by these results, we repeated the experiment on human RPE1 cells in which BRCA1 and BRCA2 are deleted with CRISPR/Cas9. This was to confirm that the observed phenotype is not a cell-type specific event.

In RPE1 cells, IFIT1, USP18 and ISG15 are induced upon olaparib treatment in both BRCA1-and BRCA2-deficient cells, whereas BRCA1/2-proficient cells exhibit no difference upon the treatment (Fig. 3.1B). Interestingly, IFIT1 expression seems to be downregulated in BRCA1-and BRCA2-deficient cells. Moreover, the IFIT1 expression in BRCA1/2-deficient cells seem to be induced less when treated with lower dose of hIFNa2 (500U/mL). In contrast, USP18 expression upon hIFNa2 treatment was not affected by BRCA status.

HERC5 is induced slightly stronger upon hIFNa2 treatment in BRCA1-and BRCA2-deficient RPE1 cells compared to wild-type cells, but there was no noticeable expression difference between two doses.

Unlike H1299 cells, IFIT2 was not induced upon olaparib treatment in RPE1 cells. Moreover, we could observe that the protein expression is lower in BRCA1-and BRCA2-deficient cells and the protein induction upon hIFNa2 treatment is weaker in those cells when compared to BRCA1/2-proficient cells.

The results indicate that there is a trend of ISG upregulation upon PARPi treatment in BRCA1/2-deficient cells, but the individual ISG expression is affected by intrinsic difference between BRCA1 and BRCA2 deficiency.

3.2 hIFNa2 treatment does not affect viability of BRCA-deficient cells

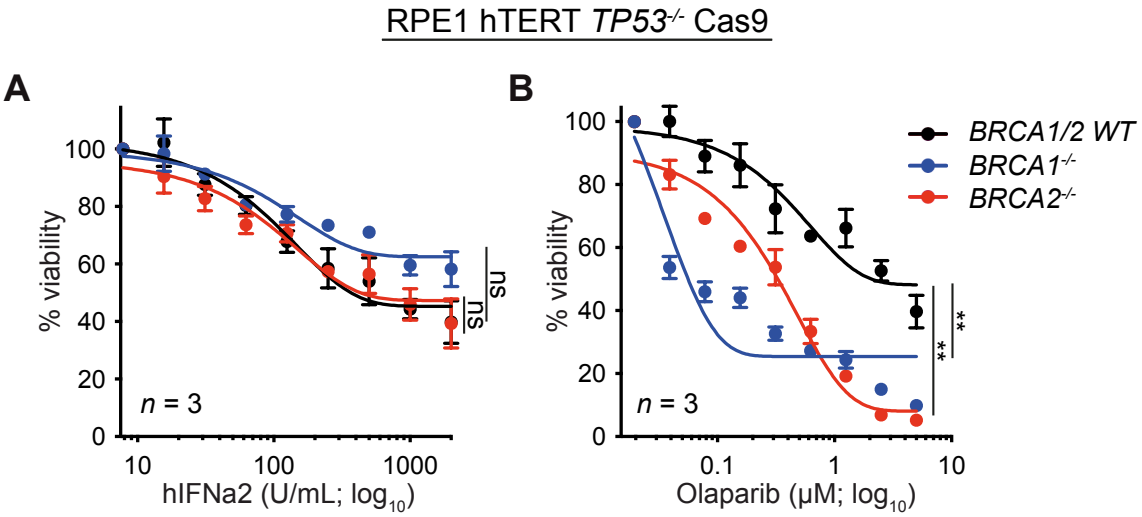


Figure 3.2 Sensitivity of BRCA-deficient cells to hIFNa2 and olaparib
(A, B) Human RPE1 cells expressing Cas9, immortalised by hTERT overexpression and TP53 deletion (RPE1 hTERT *TP53*$^{-/-}$ Cas9) with or without BRCA1/2 expression were treated with hIFNa2 (A) or olaparib (B) at the indicated doses. Six days after, cell viability was measured using resazurin-based assay. Error bars represent standard error of the mean (SEM) of n = 3 biologically independent experiments, each performed in triplicate. Statistical significance was determined by an unpaired two-tailed t-test.

Since we had observed the tendency that ISG expression is upregulated upon PARPi treatment in BRCA1/2-deficient cells, and these ISGs are also induced by type I IFN [232], we determined to the effect of hIFNa2 on BRCA1/2-deficient cells. As a control, we used olaparib treatment, which we know has a strong effect on HR-deficient cells [238].

The viability of RPE1 cells lacking BRCA1 or BRCA2 was not altered by treatment with hIFNa2 treatment (Fig. 3.2A) in contrast to the sensitivity of these cells to PARPi olaparib treatment (Fig. 3.2B). The results imply that hIFNa2 treatment itself does not affect the survival of BRCA1/2-deficient cells.

3.3 Generation of IFIT1, IFIT2 or ISG15 KO cell line in RPE1 hTERT *TP53*$^{-/-}$ Cas9 cells

As we observed an upregulation of ISG expression upon PARPi treatment, especially in BRCA1/2-deficient cells, we determined to study if these genes had a role in BRCA1/2-deficient cells' response to PARPi. To address the question, we began by generating knockout cell lines using RPE1 hTERT *TP53*$^{-/-}$ Cas9 cells (Fig. 3.3A).

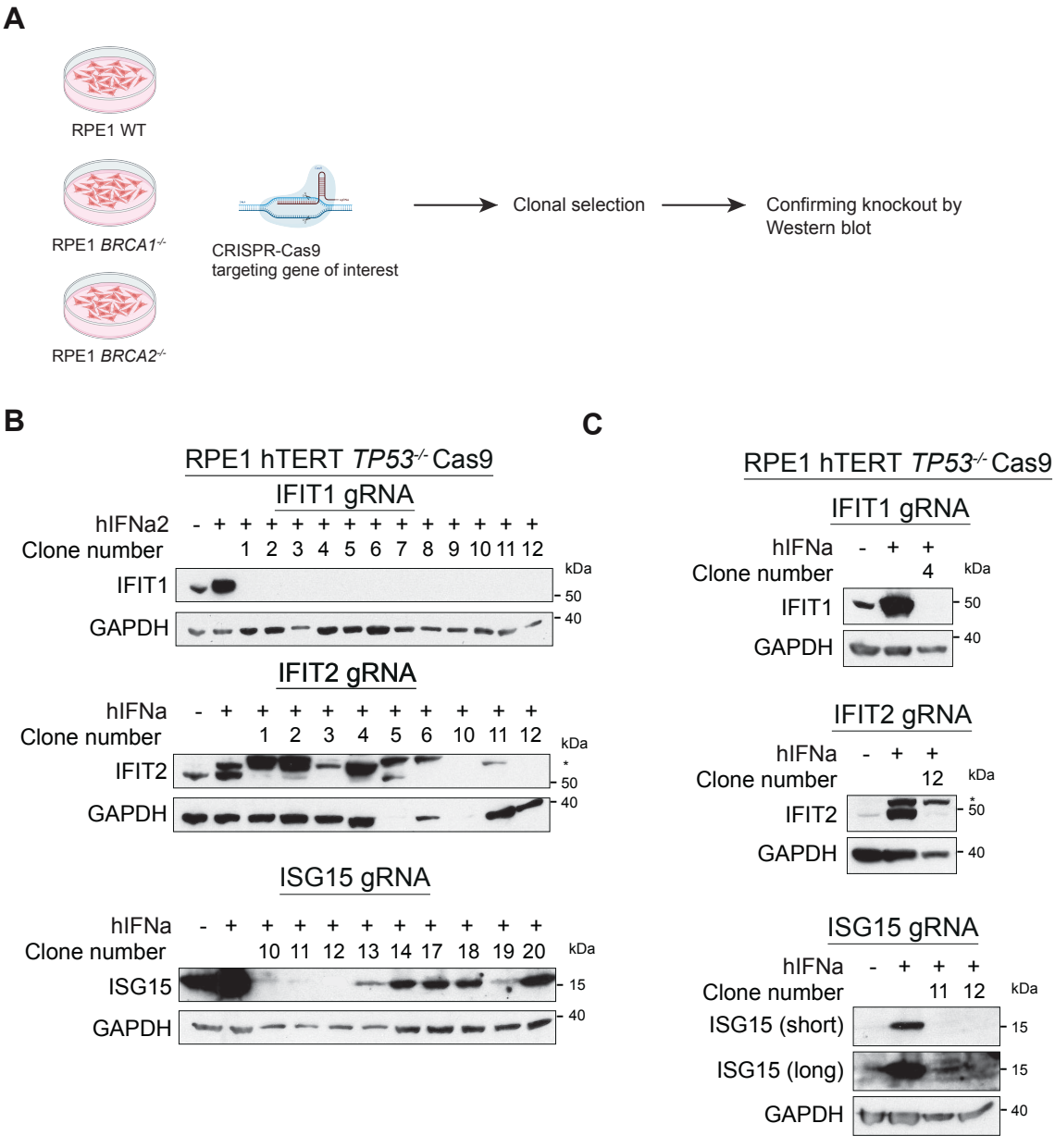


Figure 3.3 Generation of IFIT1, IFIT2 and ISG15-KO RPE1 cell line

(A) Schematic representation of IFIT1, IFIT2 and ISG15 KO-RPE1 cell lines. (B) Initial test to shortlist the single cell clones. Human RPE1 hTERT *TP53*$^{-/-}$ Cas9 cells were transfected with single guide RNA (sgRNA) targeting *IFIT1*, *IFIT2* or *ISG15* as indicated to generate the knockouts of the desired genes. Each sample is treated with 500U/mL hIFNa2 for 24 hours to induce ISG expression. Whole-cell extracts were prepared and immunoblotted as shown. GAPDH was used as a loading control. (C) Candidate clones shortlisted from (B) are treated with 500U/mL hIFNa2 for 24 hours to induce ISG expression. Whole-cell extracts were prepared and immunoblotted as shown.

Initially, we have utilised three cell lines: RPE1 hTERT *TP53*$^{-/-}$ Cas9 *BRCA1*$^{+/+}$ *BRCA2*$^{+/+}$, RPE1 hTERT *TP53*$^{-/-}$ Cas9 *BRCA1*$^{-/-}$, RPE1 hTERT *TP53*$^{-/-}$ Cas9 *BRCA2*$^{-/-}$. Briefly, cells were seeded at 10,000 cells per in a 96-well plate. Then crRNA of target gene is transfected with tracrRNA for 24 hours. Two days after, (72 hours after initial transfection) the transfected cells are proceeded with single-cell cloning. Cells were then incubated at 37°C with 5% CO_2 and 3% O_2 until the wells reach confluency. Once the cells reach the confluency, they are then transferred into 24-well plate; the process is repeated until they transferred into 6-well plate.

From this experiment, only RPE1 hTERT *TP53*$^{-/-}$ Cas9 *BRCA1*$^{+/+}$ *BRCA2*$^{+/+}$ cells tolerated transfection. Since the lack of BRCA1 or BRCA2 can make cells more susceptible to stressors and less viable under transfection of CRISPR/Cas9, this result was not surprising.

In RPE1 hTERT *TP53*$^{-/-}$ Cas9 *BRCA1*$^{+/+}$ *BRCA2*$^{+/+}$ cells, 33 of IFIT1 KO clone candidates, 22 of IFIT2 KO clone candidate and 36 of ISG15 KO clone candidates survived to reach the confluency of 6-well plate. These candidates are treated with 500U/mL of hIFNa2 for 24 hours to induce ISG expression, which is then

followed by whole cell extraction and immunoblotting (Fig. 3.3B). Candidate clones were shortlisted through this process. Among the shortlisted candidates, IFIT1 #4, IFIT2 #12, ISG15 #12 are confirmed (Fig. 3.3C). The successive testing of candidate clones has ensured the robustness of establishing knockout cell line, by eliminating the false positive candidates (Fig 3.3C).

Among these knockout cell lines, we were particularly interested in ISG15 KO cells because ISG15 is the only protein that has upregulated upon PARPi treatment in different cell lines lacking BRCA (Fig. 3.1A, B). We have speculated that ISG15 may play a role in cells' response to PARPi.

3.4 Monitoring the effects of ISG15 loss in RPE1 hTERT *TP53*$^{-/-}$ Cas9 cells

To interrogate the role of ISG15 in response to PARPi treatment, we have utilised RPE1 hTERT *TP53*$^{-/-}$ Cas9 and newly generated RPE1 hTERT *TP53*$^{-/-}$ Cas9 *ISG15*$^{-/-}$ cell line (Fig. 3.3C). We were curious whether loss of ISG15 gene affect the sensitivity to PARPi or hIFNa2 treatment.

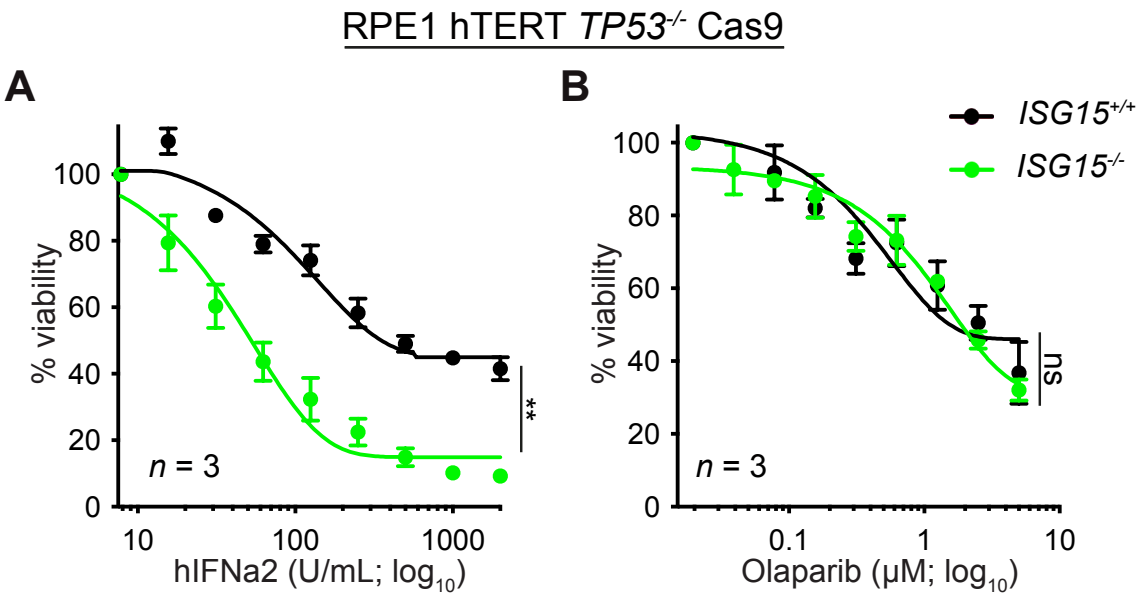


Figure 3.4 Sensitivity of ISG15-deficient cells to hIFNa2 and olaparib treatment

(A, B) Human RPE1 hTERT *TP53*$^{-/-}$ Cas9 cells with or without ISG15 expression were treated with hIFNa2 (A) or olaparib (B) at the indicated doses. Six days after, cell viability was measured using resazurin-based assay. Error bars represent standard error of the mean (SEM) of n = 3 biologically independent experiments, each performed in triplicate. Statistical significance was determined by an unpaired two-tailed t test.

The viability of ISG15-deficient RPE1 cells was decreased upon hIFNa2 treatment ISG15-proficient cells (Fig. 3.4A). However, ISG15 status did not have an impact on sensitivity of the cells to olaparib (Fig. 3.4B). From this experiment, we have concluded that ISG15 status does not affect the sensitivity to PARPi.

Given that the role of ISG15 in DNA repair is not as pivotal as BRCA1 or BRCA2 and the cell line used in the experiment is capable to carry out HR, loss of ISG15 may have resulted in marginal effect on cells' sensitivity to PARPi treatment.

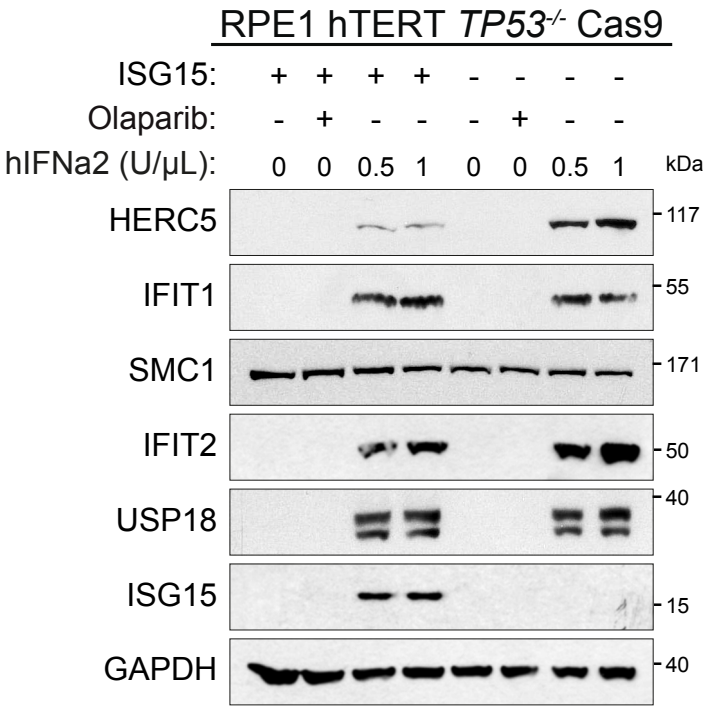


Figure 3.5 ISG expression monitored in ISG15 KO cells

ISG expression of human RPE1 hTERT *TP53*$^{-/-}$ Cas9 *ISG15*$^{+/+}$ and *ISG15*$^{-/-}$ cells. Cells were treated with olaparib (10μM) for 5 days or hIFNa2 (500U/mL, 1,000U/mL) for 24 hours. Whole-cell extracts are prepared and immunoblotted as shown. SMC1 and GAPDH were used as loading control. The data represents 3 independent biological experiments.

As we observed increased sensitivity to hIFNa2 treatment in ISG15 KO cells, we then determined to study whether the ISG15 KO cells show change in ISG expression upon drug treatment when compared to WT cells. To interrogate this, we have treated cells with olaparib and hIFNa2, respectively (Fig. 3.5). As we have expected, the basal level expression of ISGs remained unchanged between both WT and ISG15 KO cells. Olaparib treatment did not induce ISG expression in both cell lines; given that the ISG15 KO cell line did not show sensitivity towards

olaparib treatment (Fig. 3.4B), this was not surprising. IFIT1 and USP18 expression was not altered upon ISG15 status. However, HERC5 and IFIT2 seems to have increased induction level upon hIFNa2 treatment. Given that HERC5 serves as an E3 ligase of ISG15, and ISGylation is stimulated by hIFNa2 treatment, the higher induction of HERC5 upon treatment in ISG15 KO cells may be due to the increased availability of HERC5 protein. We speculated that unaltered expression of USP18 between WT and ISG15 KO may be due to the role of USP18 in type I IFN signalling, in which the protein acts as a scaffold to the type I IFN receptor subunit IFNAR2 to mediate suppression of type I IFN signalling [239]. From this experiment, we concluded that ISGs are differentially regulated or stabilised upon hIFNa2 treatment under the context of ISG15 deficiency. Intrigued by this result, we then determined to study whether we could observe similar behaviour in USP18-deficient cells.

3.5 Monitoring ISG expression upon hIFNa2 treatment in cells lacking components of ISG15 machinery

To study whether ISG expression upon drug treatment is altered when ISG15 machinery is depleted, we utilised HAP1 and HCT116 cells carrying USP18 depletion.

In HAP1 cells, absence of USP18 did not alter the sensitivity of cells against olaparib (Fig. 3.6A). Since we did not observe the change of sensitivity upon ISG15 loss in RPE1 cells, it was not surprising to witness that lack of ISG15 machinery proteins does not affect cells' sensitivity to PARPi.

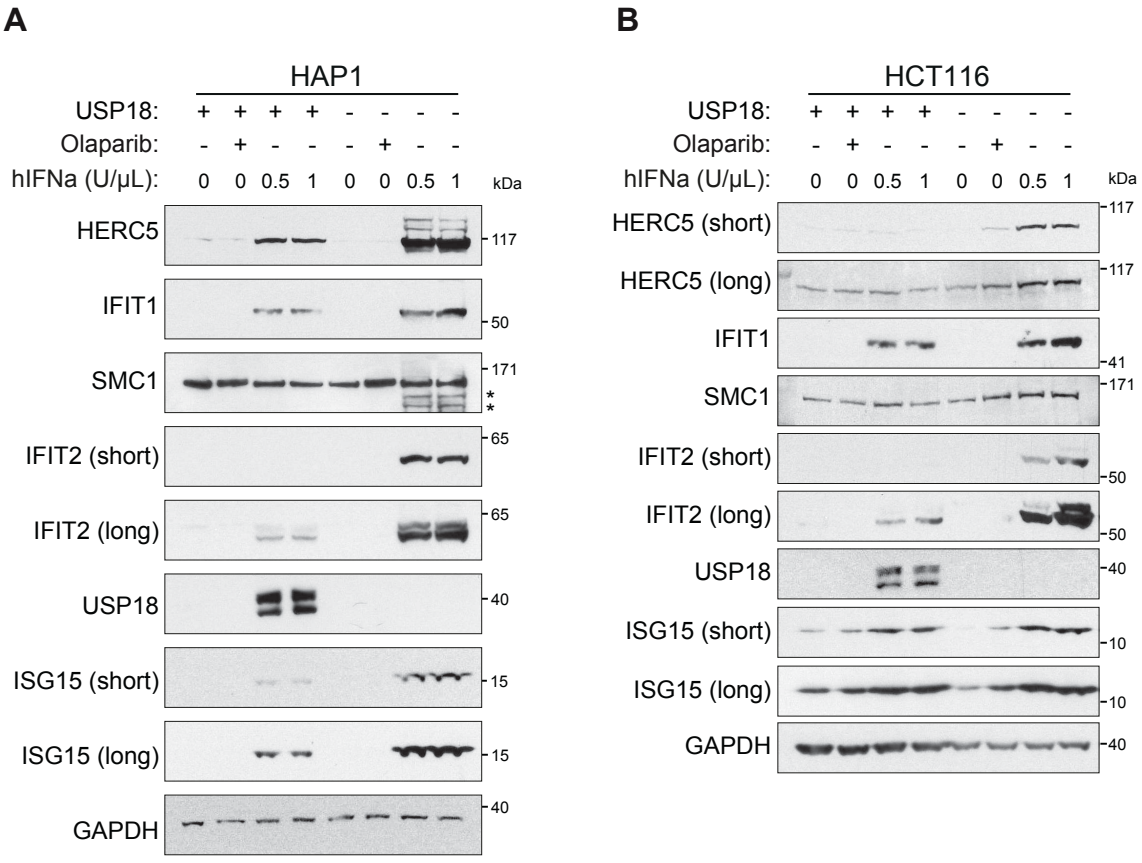


Figure 3.6 Sensitivity of USP18-deficient cells to hIFNa2 and olaparib treatment

(A) ISG expression of chronic myeloid leukaemia (CML)-derived HAP1 WT and *USP18*$^{-/-}$ cells. (B) ISG expression of colorectal carcinoma-

derived HCT116 WT and *USP18*$^{-/-}$ cells. (A, B) Cells were treated with olaparib (10μM) for 5 days or hIFNa2 (500U/mL, 1,000U/mL) for 24 hours. Whole-cell extracts are prepared and immunoblotted as shown. SMC1 and GAPDH were used as loading control. The data represents 2 independent biological experiments.

As previously reported [232], loss of USP18 resulted in increased ISGylation upon hIFNa2 treatment, as can be seen in ISG15-conjugated HERC5. Increased ISG15 induction is also observed as well. Moreover, *USP18*$^{-/-}$ cells seem to show better stabilisation of ISGs upon hIFNa2 treatment; IFIT1, IFIT2 both showed increased induction level at the same dose on USP18-depleted cells.

Similar pattern is also detected in HCT116 cells. In the absence of USP18, ISG were stabilised. ISG15-conjugated HERC5 was barely detectable, but it may be due to the very low expression of HERC5 in HCT116 cells. Interestingly, ISG15 expression show little to no difference between HCT116 WT and *USP18*$^{-/-}$ cells. We speculated that the very low ISG15 machinery protein expression in HCT116 cell line is responsible for the phenotype. From this experiment, we have concluded that depletion of ISG15 machinery protein results in stabilisation of ISGs upon hIFNa2 treatment, and it was consistent among different cell types despite the different level of ISG15 machinery protein expression.

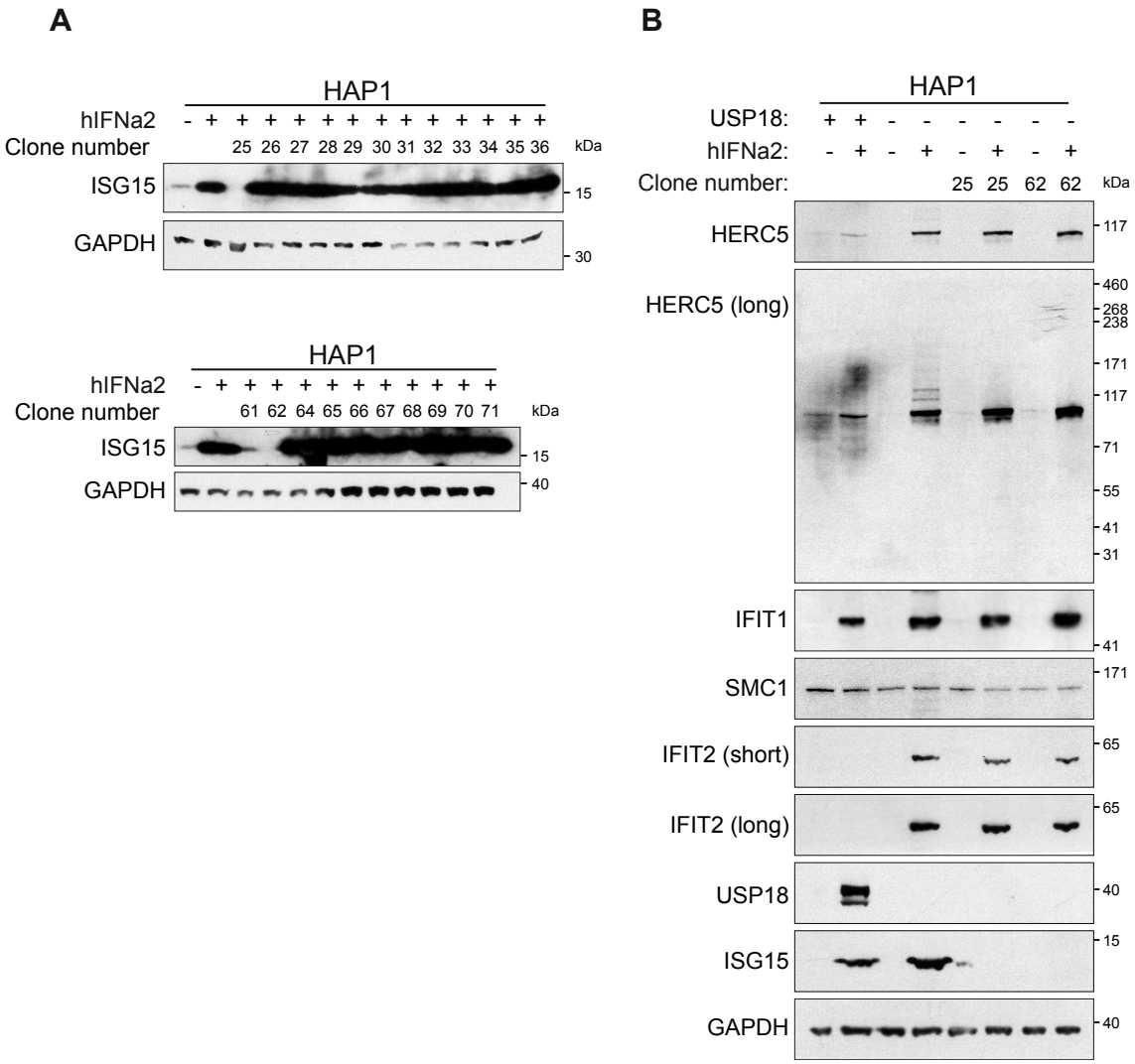


Figure 3.7 Generation of ISG15 and USP18 dKO in HAP1 cell line and studying the effect of double knockout upon hIFNa2 treatment

(A) Test result of the shortlisted single cell clones. HAP1 *USP18*$^{-/-}$ cells were transfected with single guide RNA (sgRNA) targeting *ISG15*. Each sample is treated with 500U/mL hIFNa2 for 24 hours to induce ISG expression. Whole-cell extracts were prepared and immunoblotted as shown. GAPDH was used as a loading control. (B) Cells were treated with hIFNa2 (500U/mL) for 24 hours. Whole-cell extracts are prepared and immunoblotted as shown. SMC1 and GAPDH were used as loading control. The data represents 3 independent biological experiments.

Intrigued by this, we wanted to investigate the possibility that ISG15 and USP18 play epistatic role in hIFNa2 response. Therefore, we took human HAP1 *USP18*$^{-/-}$ cells to generate a double knockout of *USP18* and *ISG15*. Briefly, cells are

transfected with sgRNA against ISG15 and underwent single-cell cloning as previously described (Fig. 3.3A). In HAP1 *USP18*$^{-/-}$ cells, 71 candidate clones are obtained. Among these clones, 22 candidate clones are selected. These candidates are treated with 500U/mL of hIFNa2 for 24 hours to induce ISG expression, which is then followed by whole cell extraction and immunoblotting (Fig. 3.7A). After successfully establishing HAP1 *ISG15*$^{-/-}$ *USP18*$^{-/-}$ cell line, we then utilised HAP1 *ISG15*$^{+/+}$ *USP18*$^{+/+}$, HAP1 *USP18*$^{-/-}$, and HAP1 *ISG15*$^{-/-}$ *USP18*$^{-/-}$ to study effect of hIFNa2 treatment on ISG expression (Fig. 3.7B). Loss of USP18 increased expression of hIFNa2-induced HERC5, IFIT1, IFIT2 levels. Similarly to previous results, increased expression of ISG15 and ISG15-conjugated HERC5 is observed as well. However, additional loss of ISG15 did not change the expression of IFIT1 and IFIT2. Interestingly, there was a marginal increase of HERC5 expression in HAP1 *ISG15*$^{-/-}$ *USP18*$^{-/-}$ cells compared to HAP1 *USP18*$^{-/-}$ cells.

3.6 ISG15 loss results in alteration of cell cycle

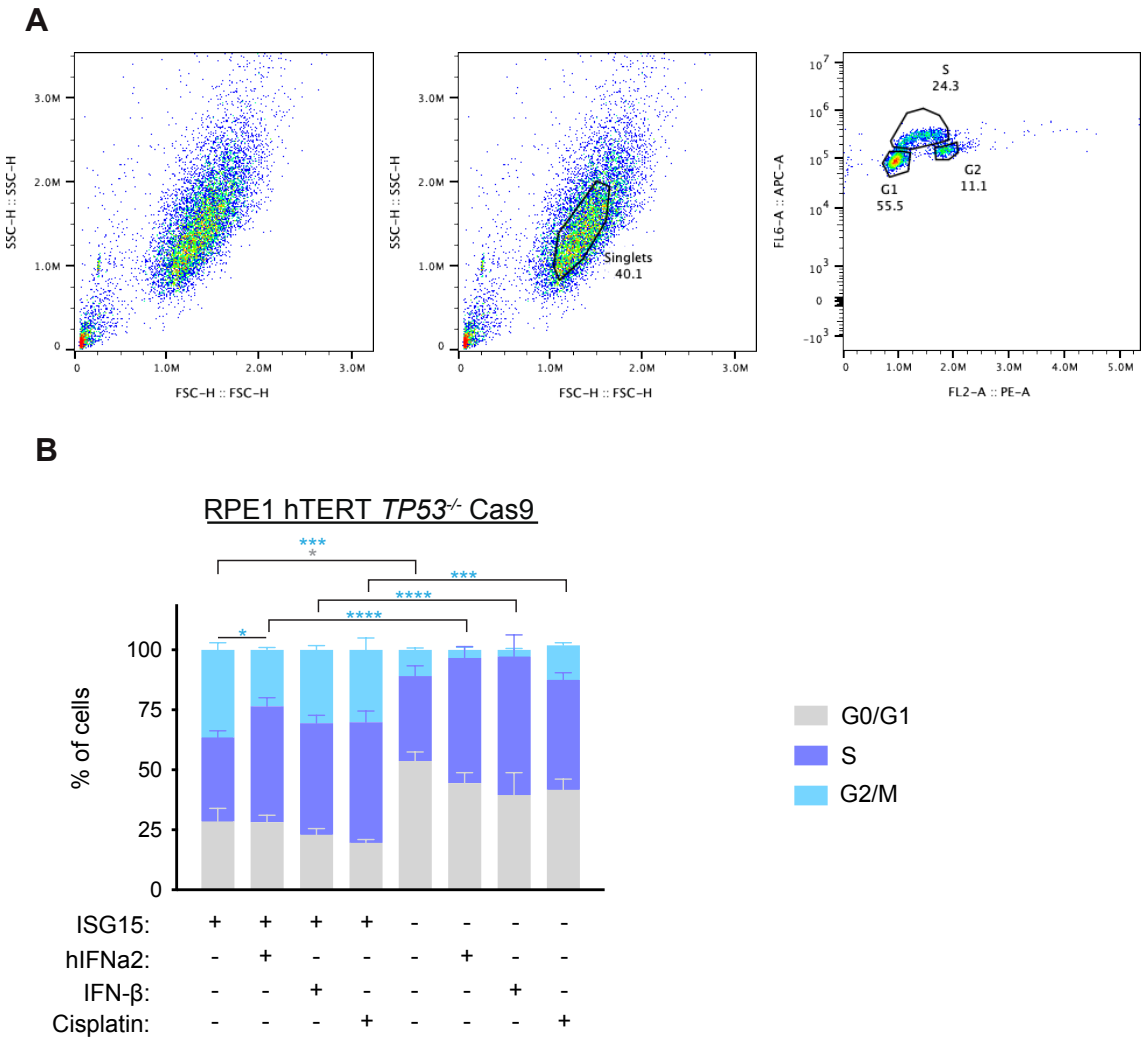


Figure 3.8 Effect of ISG15 loss in cell cycle progression

(A) Gating strategy to isolate single cell population and determine cell cycle phases. (B) RPE1 hTERT *TP53*$^{-/-}$ cells were subjected to indicated treatment; hIFNa2 (500U/mL) and IFN-β (50U/mL), and cisplatin (5μM) are treated for 24 hours. Following the treatment, cells were pulse-labelled with EdU for 30 min and subsequently stained with propidium iodide. Percentage of cells in G1, S, and G2/M phase was determined via flow cytometry analysis by using FlowJo. Error bars represent S.E.M of n=3 independent experiments. NS, p > 0.05; *, p<0.1; **, p<0.01; ***, p <0.001; ****, p <0.0001 (Cell cycle-specific one-way ANOVA followed by post-hoc Tukey's HSD testing.)

Since we have observed increased ISG expression upon hIFNa2 treatment in ISG15-deficient cells, we then questioned whether loss of ISG15 can affect

physiological aspect of the cells. To address this question, we carried out cell cycle analysis on RPE1 hTERT *TP53*$^{-/-}$ Cas9 *ISG15*$^{+/+}$ and *ISG15*$^{-/-}$ cells.

In addition to monitor the difference between ISG15-proficient and deficient cells, we also questioned whether the cells' response towards the drug treatment is altered upon ISG15 loss. In this experiment, two different types of type I IFN (hIFNa2, IFN-β) and cisplatin are selected for drug treatment.

Losing ISG15 resulted in prolonged G1 and shortened G2 phase, suggesting that ISG15 may play a role in regulating cell cycle. The observed change in cell cycle profile might be explained by disruption in equilibrium of SKP2 pools, minor ISG15-conjugated SKP2 and more abundant free SKP2 [240]. Briefly, SKP2 is involved in degradation of p27, plays a role in checkpoint progression during S phase. SKP2 can interact with both USP18 and ISG15, ISG15-conjugated SKP2 serves as a reservoir from self-ubiquitination, whereas most of free SKP2 interacts with USP18. The equilibrium regulates SKP2 pool, therefore contributing to the cell cycle progression. However, if the free ISG15 or USP18 level changes, the equilibrium is tilted, resulting in perturbation of cell cycle progression.

In WT cells, only hIFNa2 treatment resulted in change of cell cycle; hIFNa2-treated cells experienced shortened G2 phase. Cisplatin treatment did not alter the cell cycle profile but given that the cells used in the experiment are capable of carrying out faithful DNA repair, the result was not surprising.

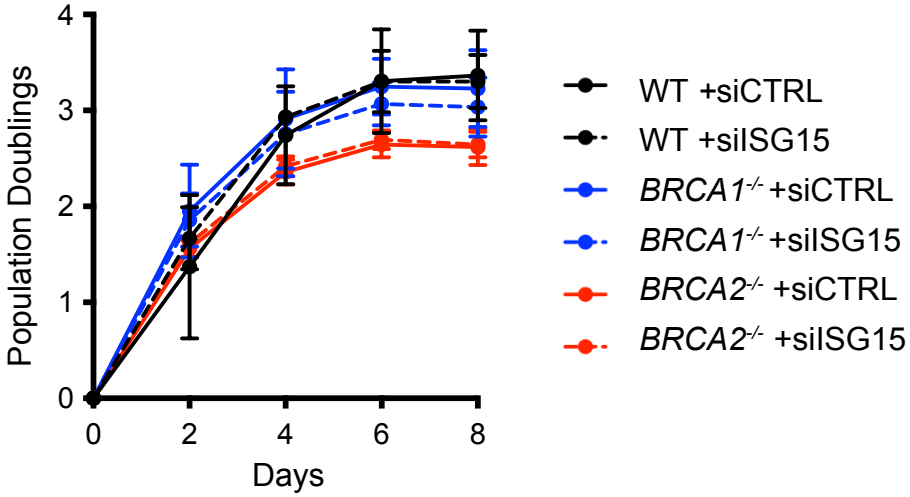
In ISG15 KO cells, however, none of the drug treatment resulted in change of cell cycle. Since the cells showed increased sensitivity toward hIFNa2 (Fig. 3.4A), the result was surprising.

Interestingly, ISG15 KO cells showed shortened G2 phase compared to their WT counterparts, regardless of the treatment. The shortened G2 phase may suggest that cells are progressing more rapidly from DNA synthesis to mitosis, which may compromise fidelity of cell division and genomic integrity [241, 242].

3.7 ISG15 loss does not affect proliferation of BRCA1/2-proficient or deficient cells

Since the experiment confirmed that loss of ISG15 results in the change of cell cycle, particularly elongation of G1 and shortening of G2, we then questioned whether losing ISG15 would affect the survival and proliferation of cells.

A



B

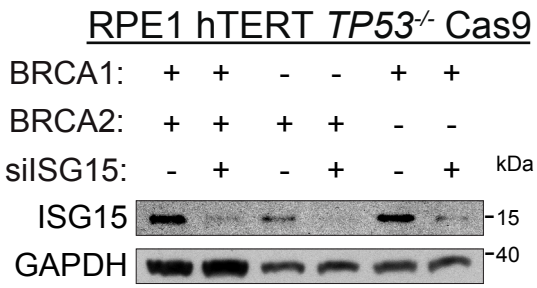


Figure 3.9 Effect of silencing ISG15 in BRCA1/2-proficient and deficient cells

(A) RPE1 hTERT *TP53*$^{-/-}$ Cas9 *BRCA1*$^{+/+}$ *BRCA2*$^{+/+}$, *BRCA1*$^{-/-}$ and *BRCA2*$^{-/-}$ cells were transfected with siRNA against ISG15 or non-targeting control siRNA. Following the 48-hour transfection, cells were seeded on 96 well plates. Resazurin-based viability assay to measure population doublings was conducted at indicated days and reported relative to day 0. Error bars represent the S.E.M of biologically

independent experiments, each performed in triplicate. Statistical significance was determined by an unpaired two-tailed t test. (B) Following the siRNA transfection described in (A), samples were harvested and whole cell extracts were immunoblotted as indicated. SMC1 was used as a loading control.

To answer this question, we utilised RPE1 hTERT *TP53*$^{-/-}$ *BRCA1*$^{+/+}$ *BRCA2*$^{+/+}$, *BRCA1*$^{-/-}$ and *BRCA2*$^{-/-}$ cells. The cells were transfected with siRNA against ISG15 or non-targeting control siRNA for 48 hours, and the knockdown of the protein was monitored by immunoblotting. Depleting ISG15 did not affect cell growth in either BRCA-proficient or deficient cells. Regarding the previous cell cycle analysis, these results suggest that ISG15 may play a crucial role in cell cycle regulation and its loss results in disrupted cell cycle. However, the effect does not directly translate to lethality. Therefore, we concluded that ISG15 does not itself affect the proliferation of both BRCA-proficient and deficient cells.

From the experiments featured in Chapter 3, we have found that BRCA1/2-deficient cells show differential ISG upregulation upon PARPi or hIFNa2 treatment (Fig. 3.1), implying that ISG regulation varies in different physiological contexts, especially in HR-deficient environments. In BRCA1/2-proficient cells, ISG15 deficiency alters sensitivity to hIFNa2 treatment but not to PARPi treatment (Fig. 3.4), suggesting a limited role for ISG15 in HR-related PARPi response. In addition, ISG15 loss results in prolonged G1 and shortened G2 phases in BRCA1/2-proficient cells (Fig. 3.8), highlighting its role in cell cycle regulation.

Chapter 4

Experiment results II – Upregulated ISG15 expression in PARPi talazoparib-resistant cells and its role in replication fork progression

4.1 PARP inhibitors potentiate innate immune responses

From the previous study published in the lab [170], it has been observed that treatment with the PARP inhibitor olaparib induces upregulation of interferon-stimulated genes (ISGs) at mRNA level. It is widely known that PARP inhibitors can selectively target BRCA-deficient cells by stabilising PARP-DNA complexes at SSB sites, converting them into lethal DSB lesions [146, 150].

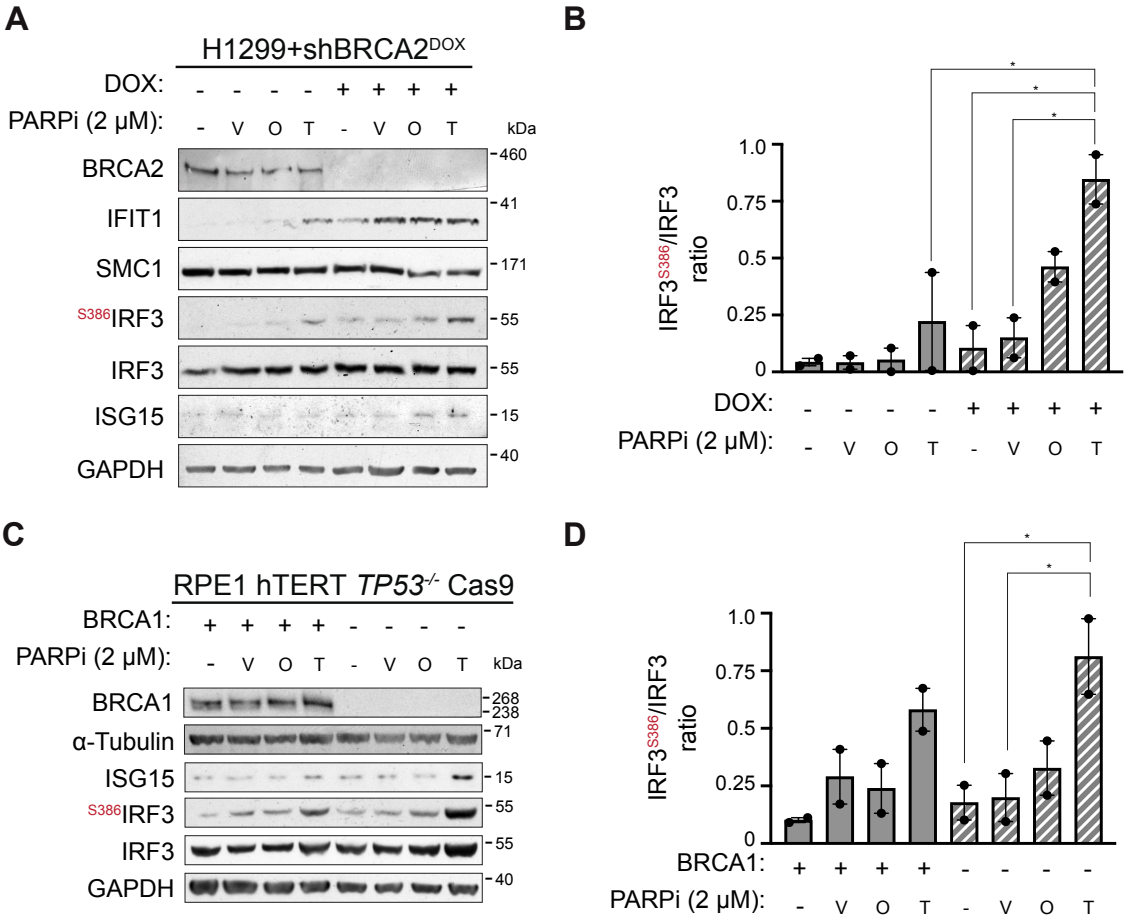


Figure 4.1 Upregulated ISG expression PARPi treatment in H1299+shBRCA2^{DOX} and RPE1 hTERT *TP53*$^{-/-}$ Cas9 (*BRCA1*$^{-/-}$, *BRCA2*$^{-/-}$)

(A) H1299+shBRCA2^{DOX} cells were grown with or without Doxycycline for 48 hours before PARPi treatment. The cells are then subjected to 48-hour treatment of indicated PARPi. (B) Relative quantified expression of pIRF3/IRF3 in (A). (C)RPE1 hTERT *TP53*$^{-/-}$ Cas9 cells were subjected to 48-hour treatment of indicated PARPi. Phosphorylation sites are indicated

in red. GAPDH was used as loading control. (D) Relative quantified expression of pIRF3/IRF3 in (C). The WB data are representative of 2 independent experiments. Error bars represent S.E.M of n=2 independent experiments. NS, $p > 0.05$; *, $p<0.1$ (One-way ANOVA followed by post-hoc Tukey's HSD testing)

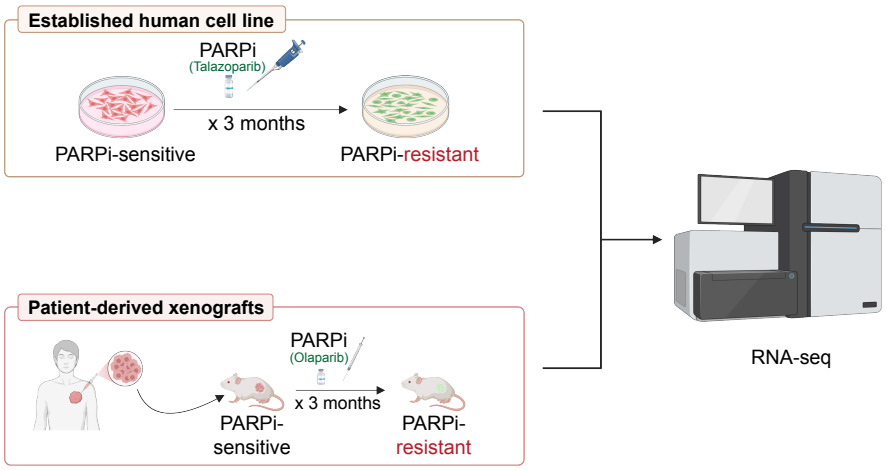
Clinical PARP inhibitors vary in their PARP trapping potency [243]. Talazoparib is known as one of the most potent PARP-trapping drugs, while veliparib is one of the least efficient in PARP trapping. Olaparib, the most widely used PARP inhibitor in clinics, shows higher PARP trapping ability than veliparib, but lesser trapping potency than talazoparib. We hypothesised that the type I IFN response is correlated with trapping potency of PARP inhibitors.

To test this, we monitored markers of cGAS-STING pathway by assessing phosphorylation of serine residue 386 of IRF3 and expression of IFIT1 or ISG15, the ISGs induced upon type I IFN response, via WB (Fig. 4.1). We observed induction of IRF3 phosphorylation upon addition of olaparib and talazoparib in both BRCA2-proficient and deficient cells (Fig. 4.1A, B). The induction level was higher in BRCA2-deficient cells, especially when compared between talazoparib-treated samples (Fig. 4.1B). In BRCA2-deficient cells, activation of cGAS-STING pathway seems to be dependent on PARP trapping potency (Fig. 4.1A, B). In BRCA2-deficient cells, the IRF3 phosphorylation rate was notably higher in talazoparib-treated sample compared to that of veliparib-treated sample (Fig. 4.1B). Interestingly, in BRCA2-proficient cells, endogenous IFIT1 expression was too low to be detected and only induced upon talazoparib treatment. However, in BRCA2-deficient cells, the endogenous IFIT1 expression was elevated to detectable level, and it is further potentiated upon PARPi treatment (Fig. 4.1A). Similarly, ISG15 was upregulated upon olaparib and talazoparib treatment in

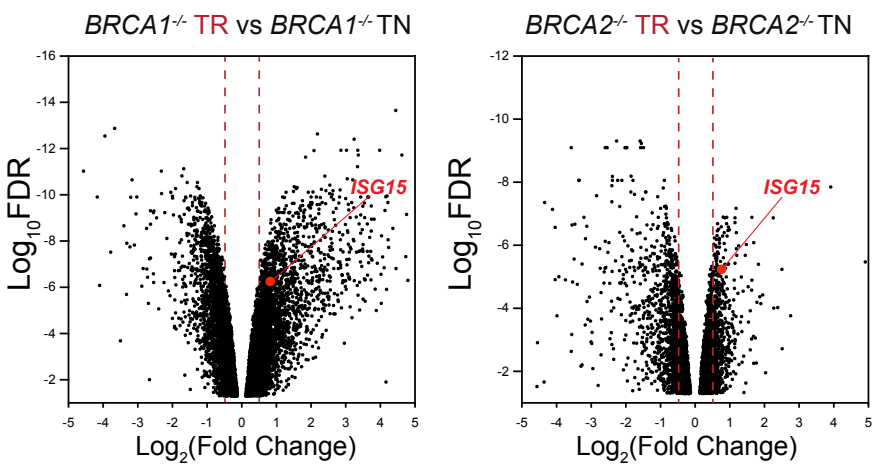
BRCA2-deficient cells. We then tested the BRCA1-deficient cells as well. As we have seen in BRCA2-deficient cells, we could observe increased phosphorylation of IRF3 corresponding with the PARP inhibitors' PARP trapping potency (Fig. 4.1D). Interestingly, talazoparib treatment in RPE1 cells seem to strongly induce phosphorylation of IRF3 in both BRCA1-proficient and deficient cells (Fig. 4.1D) We also detected the increase of ISG15 expression upon talazoparib addition in BRCA1-deficient cells (Fig. 4.1C). These results confirm that there is a correlation between PARP inhibitor's PARP-trapping potency and induction of cGAS-STING pathway. PARP inhibitor-induced innate immune response may have derived from accumulation of DNA lesions developed from stabilisation of PARP1-DNA complex at SSB sites. Given these results, we wanted to assess whether use of PARP inhibitor has an immunomodulatory effect, and if so, whether developing resistance against PARP inhibitor could alter the transcriptome profiles as well.

4.2 Development of PARPi resistance alters transcriptome profile of BRCA-deficient cells

A



B



C

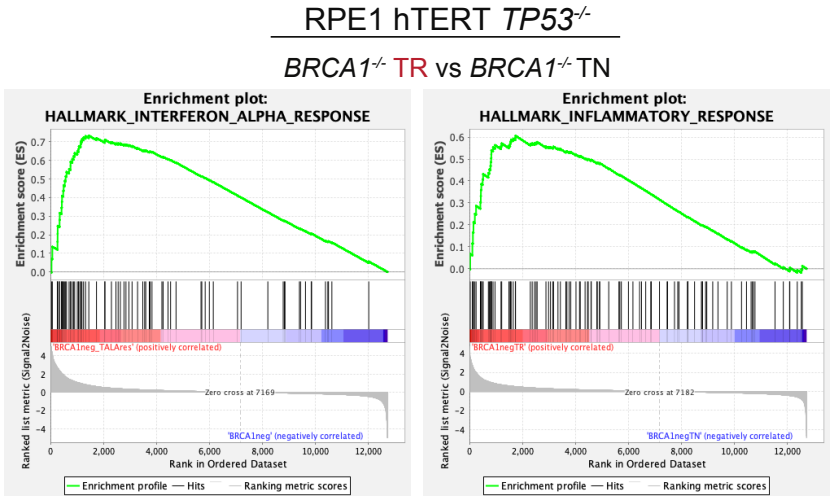


Figure 4.2 Upregulation of innate immune response genes in BRCA-deficient cells that have developed PARPi resistance

(A) Schematic of generating PARPi-resistant human cell lines and patient-derived xenografts (PDXs), and its further processing with RNA-seq. (B) Volcano plot showing differentially expressed genes in *BRCA1*$^{-/-}$ TR and TN cells and *BRCA2*$^{-/-}$ TR and TN cells. Dashed red lines represents cut-off at $|Log_2(\text{Fold change})| > 0.5$ (C) Pathway analysis using GSEA in RPE1 *BRCA1*$^{-/-}$ TR and TN cells. The x-axis represents the genes that belong to gene sets (Interferon α-response genes and inflammatory response genes, respectively) and y-axis shows the enrichment score. The data are representative of n=3 biologically independent experiments. All RNA-seq data processing was done by Birbal Prasad.

To study the change of transcriptome upon acquiring PARPi resistance in vitro and in vivo, we first established PARPi-resistant cell model and patient-derived xenograft (PDX) model. For the cell model, we utilised human retinal pigment epithelial RPE1 cells carrying deletion of BRCA1 or BRCA2. We cultured these cells in increasing doses of talazoparib over 3 months. The developed resistance was confirmed by conducting viability assays with talazoparib (Fig. S1.B). For PDXs, we used samples from BRCA1-mutated tumours of breast or ovarian cancer patients. These tumour tissues were injected into mice and half of the mice were treated with olaparib over 3 months to develop resistance against the drug. The development of resistance was initially measured by the growth of tumour; the tumours in the mice initially decreased, but then over the course of the treatment window, they began to grow again at high rates, indicating resistance to the drug. The development of PDX model is done by Dr Violeta Serra at Vall d'Hebron Institute of Oncology, Barcelona (VHIO). Both the naïve

and resistant models from cell lines and PDXs were then subjected into RNA-seq analysis (Fig. 4.2A).

To address differences in gene expression in robust manner, we determined cut-off of differential expression of genes with a |Log2(Fold change)| > 0.5 and FDR < 0.05 for the analysis. Interestingly, our analysis revealed that ISG15 is commonly upregulated in both BRCA1- and BRCA2-deficient talazoparib-resistant cells, when compared to their naïve counterparts (Fig. 4.2B). We then proceed with GSEA analysis to study the enriched pathways upon acquiring resistance. In BRCA2-deficient talazoparib resistant (TR) cells, there was no pathways with FDR < 0.05. However, in BRCA1-deficient TR cells, we found out that interferon alpha response and inflammatory response pathways are upregulated as compared to BRCA1-deficient TN cells. Therefore, we concluded that developing resistance against PARPis elicits innate immune response.

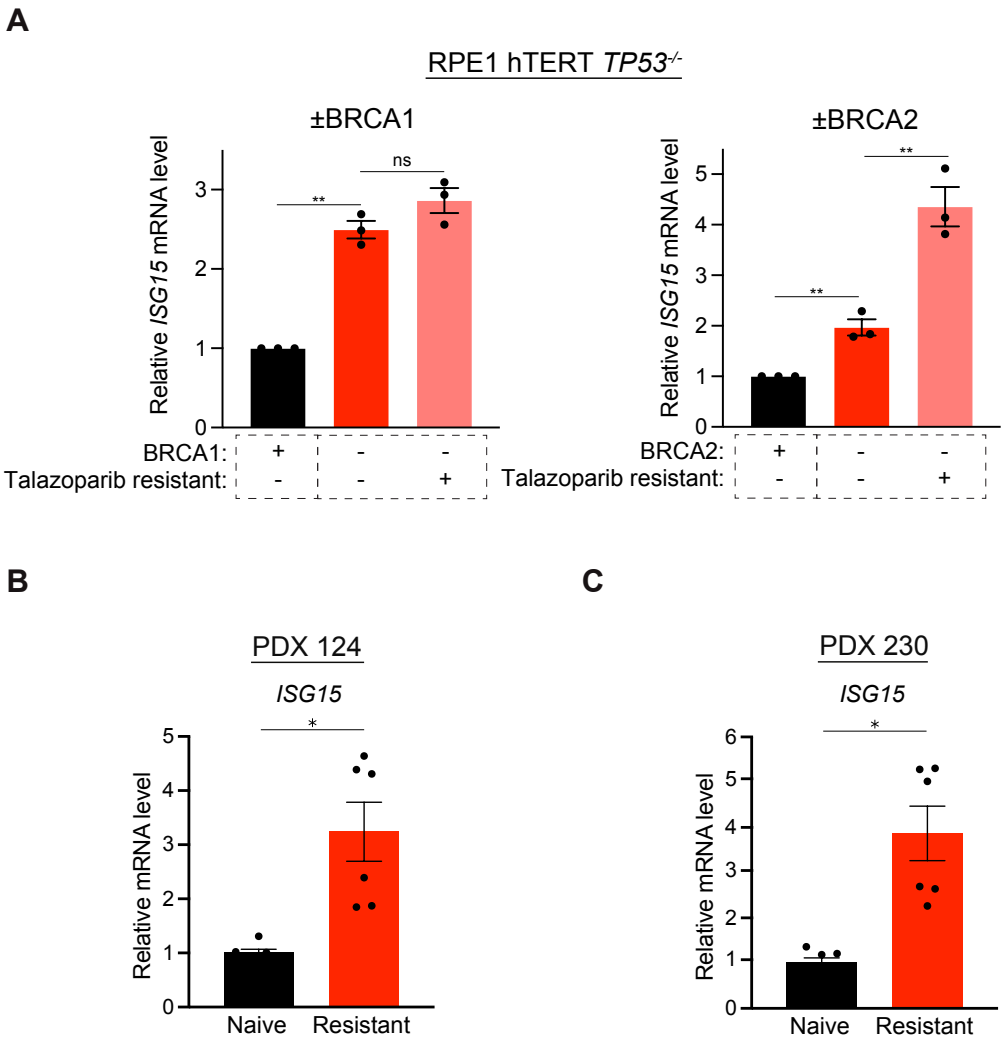


Figure 4.3 Interferon-stimulated gene 15 (ISG15) expression in BRCA1-deficient PARPi-naïve and resistant cells

(A) Total RNA was extracted from RPE1 cells and processed into RT-qPCR analysis using primers targeting indicated genes. mRNA levels were expressed relative to mRNA levels of GAPDH and to wild type samples. (B) Total RNA was extracted from BRCA1-mutated patient-derived PDX124 and processed into RT-qPCR analysis as described above. (C) Total RNA was extracted from BRCA1-mutated patient-derived PDX230 and processed as previous samples. Values were expressed as $2^{-\Delta\Delta Ct}$. Error bars represent S.E.M value of n=3 biologically independent experiments, in which performed technical triplicates. *NS*, $p > 0.05$; **, $p < 0.01$ (unpaired two-tailed t-test). Each dot represents mean

of technical triplicates. All RT-qPCR data was generated with help of Teressa Paulsen and Rebecca Dagg.

To confirm the data from RNA-seq, we performed RT-qPCR to measure mRNA expression of ISG15 in RPE1 cells. There was a two-fold increase of ISG15 expression upon loss of BRCA1 (Fig. 4.3A). The data illustrates a slight upregulation in ISG15 expression upon the development of resistance to talazoparib. However, this increase did not reach statistical significance. We could observe similar trend in BRCA2-deficient cells. In BRCA2-deficient cells, the increase of gene expression was more noticeable. We observed two-fold increase of ISG15 gene expression upon loss of BRCA2. Upon acquiring resistance, ISG15 gene expression was again increased in two-fold; the expression was almost five-fold higher than that of wild type (Fig. 4.3A). We then used BRCA1-mutated PDXs to measure ISG15 gene expression. We used two different PDX models for more reliable results; PDX124 is breast cancer-originated, and PDX230 is ovarian cancer-originated. In both PDXs, we could observe at least two-fold increase in ISG15 gene expression upon acquiring resistance (Fig. 4.3B).

We then proceed with immunoblotting of ISG15 to confirm that the observed increase of gene expression is correlated with an increase of protein expression as well (Fig. 4.4). This was done in order to ensure the robustness of our RNA-seq analysis, and to validate previous findings within the literature [244] whereby ISGylation was found to be related with tumour progression in patients: increased ISG15 expression is observed in pancreatic, endometrial and bladder cancers, implying that it is positively associated with tumour development [245-247].

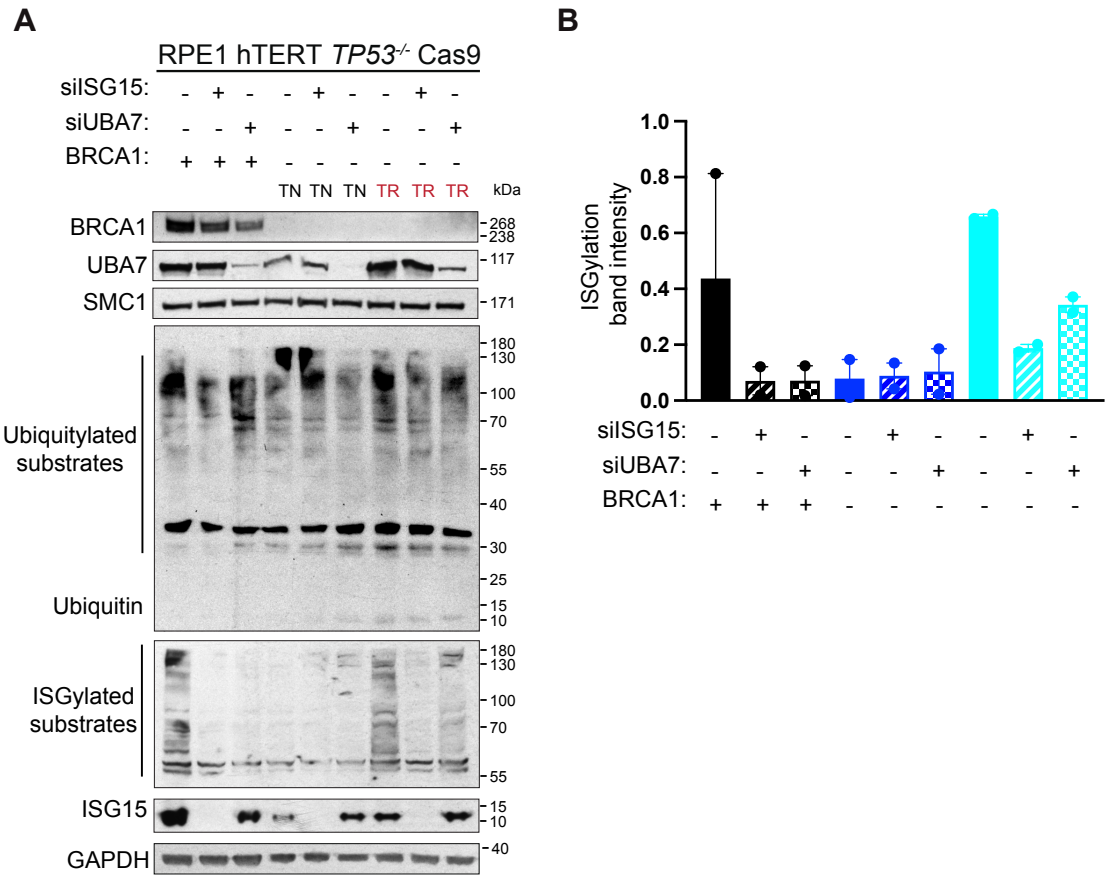


Figure 4.4 Monitoring ISGylation level in BRCA1-deficient talazoparib-naïve and resistant cells

(A) RPE1 hTERT *TP53*$^{-/-}$ Cas9 cells were transfected with siRNA against indicated target genes for 48 hours. Following the treatment, samples were harvested and whole cell extracts were immunoblotted as indicated. GAPDH and SMC1 were used as loading controls. (B) Quantification of band intensity of ISGylated substrates. Values are measured through ImageJ software and normalised against loading control GAPDH. Error bars represent S.E.M of n=2 independent experiments. (One-way ANOVA followed by post-hoc Tukey's HSD testing)

Since ISG15 can exist as free molecule and conjugated form, we monitored the level of both free ISG15 and ISGylated ISG15 in RPE1 cells. Moreover, we studied the ubiquitination as well, given that ISG15 can form mixed chain with ubiquitin [248]. To ensure that we are observing bona fide ISGylation, we have included samples treated with siISG15, or siUBA7, a siRNA targeting E1 enzyme

of ISGylation. Ubiquitination levels were not altered in the three cell utilised cell lines WT, TN or TR, regardless of BRCA1 status or acquired resistance. Given that ISG15 can form mixed chains with ubiquitin [248], we expected that alterations in the ISG15 machinery would affect ubiquitination. However, it seems like silencing ISG15 or UBA7 does not change free ubiquitin or ubiquitination level. We have observed that free ISG15 and ISGylation level is highest in WT cells, and lowest in BRCA1-deficient TN cells. We could not explain the discrepancy between mRNA levels with corresponding protein levels. It is possible that transcriptional changes have been modified by translational process, or the protein degradation rate is changed to sync the protein level with changing transcription level. However, we did observe similar tendency of increase in ISG15 expression between TN and TR cells (Fig. 4.4A). We also measured the band intensity of ISGylated substrates. There was no statistical significance among the samples, but we could clearly observe the trend in which BRCA1-deficient TR cells experiencing higher rate of ISGylation compared to BRCA1-deficient TN cells (Fig. 4.4B).

Hence, we concluded that protein expression of ISG15 and ISGylation in BRCA1-deficient cells is increased upon developing talazoparib resistance.

4.3 ISG15 plays a role in cell cycle progression and replication fork progression

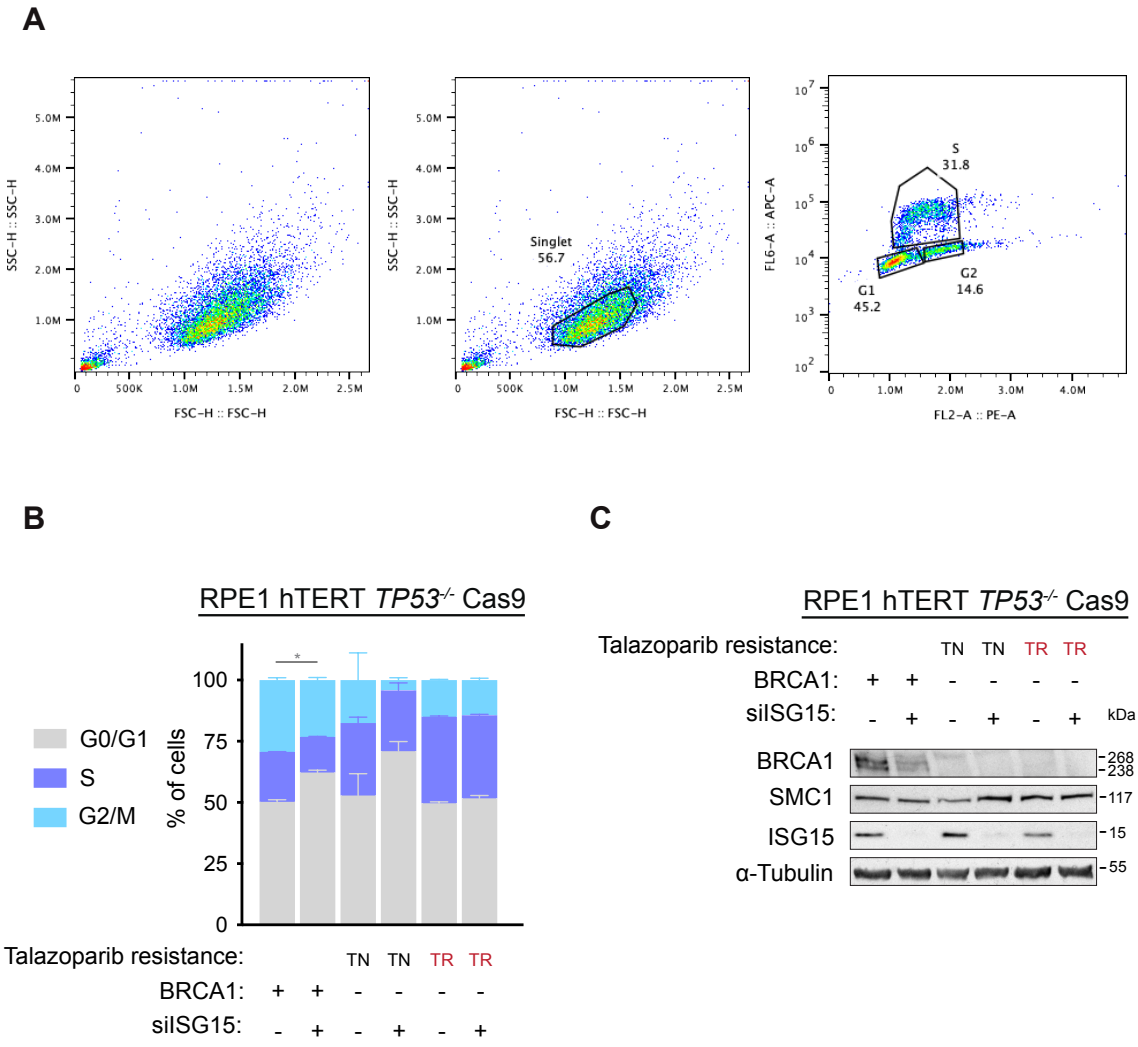


Figure 4.5 Effect of silencing ISG15 in cell cycle progression

(A) Gating strategy to isolate single cell population and determine cell cycle phases. RPE1 hTERT *TP53*$^{-/-}$ Cas9 cells were transfected with siRNA against ISG15 for 48 hours. (B) Following the treatment, samples were pulse-labelled with EdU for 30 min and subsequently stained with propidium iodide. Percentage of cells in G1, S, and G2/M phase was determined via flow cytometry analysis by using FlowJo. Error bars represent S.E.M of n=3 independent experiments. *NS*, $p > 0.05$; **, $p < 0.01$ (unpaired two-tailed t-test). (C) The same samples were harvested and whole cell extracts were immunoblotted as indicated. SMC1 and α-Tubulin were used as loading controls.

Next, we determined to elucidate the physiological relevance of increased ISG15 expression in BRCA1-deficient TR cells. To address this question, we first carried out cell cycle analysis using siRNA against ISG15. The knockdown of ISG15 is confirmed by immunoblotting (Fig. 4.5C). In wild type cells, we have observed that silencing ISG15 led to G1 accumulation, as we have observed from previous experiment (Fig. 3.8B). However, we could not see the same effect on BRCA1-deficient TN and TR cells (Fig. 4.5B). Given that losing BRCA1 leads to cell cycle dysregulation [114], it is possible that the effect by ISG15 has been masked.

Knowing that ISG15 can interact with replication machinery proteins [230, 231, 249, 250], we then determined to investigate the possible roles of ISG15 in replication fork progression. Considering that ISG15 plays a role in cell cycle progression, studying its role in replication fork progression would provide complementary information about understanding its physiological role in resistance cells. To address this, we utilised replication fork progression assay (Fig. 4.6A). We pulsed cells with CldU and IdU for 30 min, following the 48-hour siRNA transfection. We observed a decrease of fork speed upon loss of BRCA1, in line with previous studies[152, 251]. Interestingly, BRCA1-deficient TR cells showed highest fork progression rates. Silencing ISG15 resulted in decrease of fork speed in all three cell lines. The RT-qPCR data (Fig. 4.6B) confirms the knockdown of ISG15 was successful. We were particularly interested in replication fork progression of BRCA1-deficient TR cells, since the cells show pathologically high fork speed. We hypothesised that the in BRCA1-deficient environment, fork progression might be corelated to upregulation of ISGylation level. BRCA1-deficient TN cells had shown lowest ISGylation level and lowest

replication fork speed, whereas BRCA1-deficient TR cells had shown second-highest ISGylation level, and highest replication fork speed.

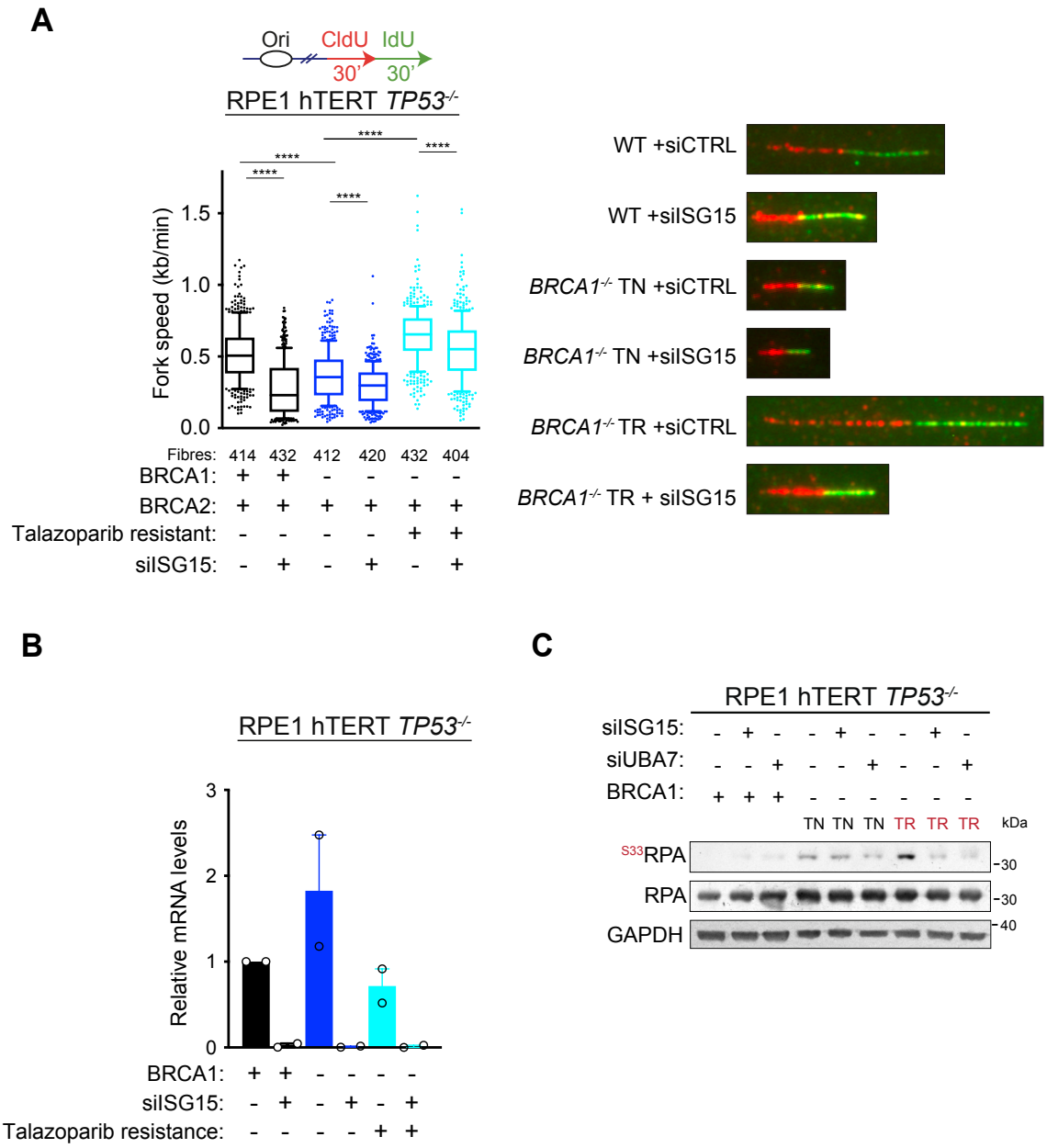


Figure 4.6 Effects of ISG15 in replication fork progression

(A) Left top: diagram for DNA labelling strategy: CldU (red), IdU (green). Right top: representative image of DNA fibre. Left bottom: Analysis of replication tracts on RPE1 hTERT *TP53*$^{-/-}$ Cas9 cells. Following 48 hour of siRNA transfection against target gene, cells were pulsed with CldU and IdU for 30 min each. At least 200 fibres were analysed for each condition of each replicate. Error bars represent S.E.M of n=2

independent experiments. *NS*, $p > 0.05$; ***, $p < 0.001$; ****, $p < 0.0001$ (One-way ANOVA followed by post-hoc Tukey's HSD testing) (B) Total RNA was extracted and processed into RT-qPCR analysis using primers targeting indicated genes to confirm knockdown of the protein. mRNA levels were expressed relative to mRNA levels of GAPDH and to wild type samples. (C) RPE1 hTERT *TP53*$^{-/-}$ Cas9 cells were transfected with siRNA against indicated target genes for 48 hours. Following the treatment, samples were harvested and whole cell extracts were immunoblotted as indicated. Phosphorylated sites are indicated in red. GAPDH and SMC1 were used as loading controls. The data are representative of n=2 biologically independent experiments.

A previous study [231] suggests that high levels of ISG15 expression leads to acceleration of fork speed, supporting our hypothesis. Hence, we investigated the level of replication stress in the wild type, BRCA1-deficient TN and TR cells since dysregulation of replication fork progression often leads to perturbed replication [152]. To study the replication stress level, we monitored phosphorylation of serine residue 33 of RPA via WB (Fig. 4.6C). As previously reported, BRCA1-deficient cells show higher replication stress compared to BRCA1-proficient cells [252, 253]. Strikingly, BRCA1-deficient TR cells showed highest phosphorylation of RPA. This phenotype is rescued upon silencing ISG15 or UBA7, the E1 enzyme of ISGylation, suggesting that ISGylation contributes to increased replication stress in BRCA1-deficient TR cells, by accelerating replication fork progression.

This confirms that ISGylation in BRCA1-deficient TR cells results in increased replication fork speed and higher replication stress, we further explored how ISG15 regulates replication fork progression.

4.4 ISG15 interacts with replication machinery proteins

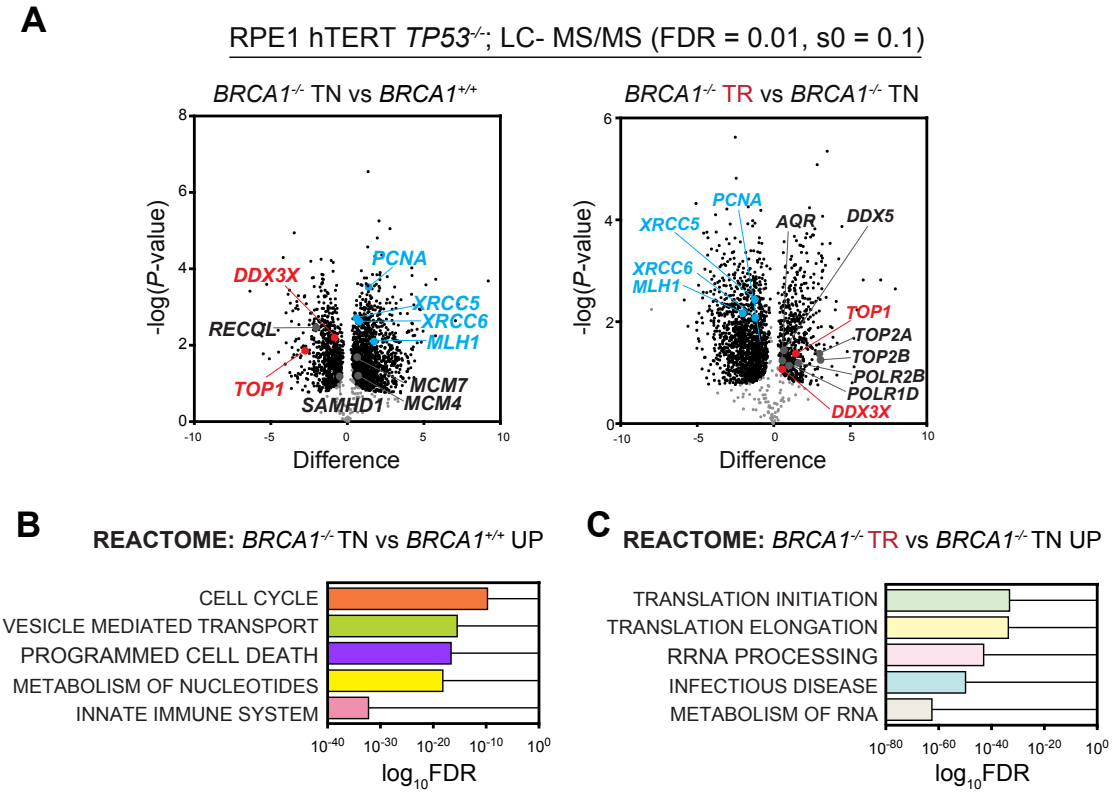


Figure 4.7 ISG15 interacts with replication machinery proteins and its interaction with RNA metabolism proteins are upregulated in PARPi-resistant cells

(A) Comparative volcano plot of ISG15-interactome in RPE1 hTERT *TP53*$^{-/-}$ Cas9 BRCA1-proficient and deficient cells (left) and RPE1 BRCA1-talazoparib naïve and resistant cells (right). In red are shown the proteins upregulated with ISG15 interaction in *BRCA1*$^{-/-}$ TR cells, and in blue are shown the proteins downregulated with ISG15 interaction in *BRCA1*$^{-/-}$ TN cells. (B) GSEA pathway enrichment analysis of ISG15-interacting proteins in RPE1 hTERT *TP53*$^{-/-}$ Cas9 *BRCA1*$^{-/-}$ talazoparib naïve cells and wild type cells. (C) GSEA pathway enrichment analysis of ISG15-interacting proteins in RPE1 hTERT *TP53*$^{-/-}$ Cas9 *BRCA1*$^{-/-}$ talazoparib naïve cells and talazoparib resistant cells. The data are representative of n=3 biologically independent experiments. All MS/MS experiments were carried out by Adan Pinto Fernandez.

To study the proteins interacting with ISG15, we decided to implement MS/MS analysis. In order to evaluate ISG15 interactome, we first silenced USP18 expression by using siRNA. This process was necessary since USP18 functions as a de-ISGylating enzyme, removing ISG15 from its conjugated substrates [239]. We then immunoprecipitated the samples with ISG15 antibody and subjected it to the LC-MS/MS analysis in order to enrich and identify the accumulation of potential ISGylated substrates in the different samples.

After mass spectrometry analysis (Fig. 4.7A), we observed that ISG15 is interacting with replication machinery proteins, including PCNA and RECQL, as previously reported [230, 231, 250]. Interestingly, we found out that BRCA1-deficient TN and TR cells presented opposite trend in ISG15 interaction. As in the volcano plot (Fig. 4.7A), we could observe PCNA, XRCC5, XRCC6 and MLH1 exhibits increased interaction with ISG15 in BRCA1-deficient TN cells. However, these proteins showed decreased interaction with ISG15 in BRCA1-deficient TR cells. Similarly, DDX3X and TOP1 showed decreased interaction with ISG15 in BRCA1-deficient TN cells but, interestingly, increased interaction with ISG15 in BRCA1-deficient TR cells. Moreover, we have observed that ISG15 is also interacting with DEAD-box helicases, DDX5 and DDX3X, and RNA helicase AQR. It is also notable that ISG15 is interacting with RNAPII subunit B (*POLR2B*), which constitutes RNAPII, a DNA-dependent RNA polymerase known to have a role in R-loop regulation [254].

Intrigued by the results, we then proceeded to pathway analysis (Fig. 4.7B, C) using the reactome dataset from Gene Set Enrichment Analysis (GSEA). In BRCA1-deficient TN cells, the pathway analysis showed upregulated ISG15 interaction of pathways involved in innate immune response. It showed ISG15

interaction is also increased in proteins involved in nucleotide metabolism pathway as well (Fig. 4.7B). In BRCA1-deficient TR cells, however, showed upregulation of ISG15 interaction in pathways such as RNA metabolism and RNA processing (Fig. 4.7C). It is notable that pathways involved in translation initiation and elongation are also enriched in interaction with ISG15.

Following the MS/MS analysis, we then proceed to validate the interaction between ISG15 and selected proteins via WB. For validation, we have selected TOP1, DDX5 and Ku70. We have selected TOP1 among other topoisomerases because firstly, TOP1 is the primary topoisomerase that acts in front of replication forks to relieve negative supercoiling. Secondly, Top1 in yeast has been suggested to promote fork progression [255]. We chose DDX5 among other DEAD-box helicases since previous study [256] suggested that DDX5 is involved in regulating DNA replication, and also has the ability to interact with BRCA2.

We also selected Ku70 for validation because the protein has shown opposite trend of ISG15 interaction in BRCA1-deficient TN and TR cells. Prior to validation, we transfected the cells with siRNA against USP18, to ensure the enrichment of ISG15 interaction with its substrates. We then immunoprecipitated the proteins using antibody against ISG15 under native conditions. From this validation, we confirmed an interaction between TOP1 and ISG15 (Fig. 3.8A) and this interaction was higher in BRCA1-deficient TR cells than BRCA1-deficient TN cells, as we have observed from LC-MS/MS analysis. Next, we also confirmed that DDX5 is interacting with ISG15 (Fig. 3.8B) and confirmed the interaction was higher in BRCA1-deficient TR than BRCA1-deficient TN cells, as we have observed in previous experiment. Lastly, we have shown that Ku70 interaction

with ISG15 (Fig.4.8C) is higher in BRCA1-deficient TN cells than BRCA1-deficient TR cells.

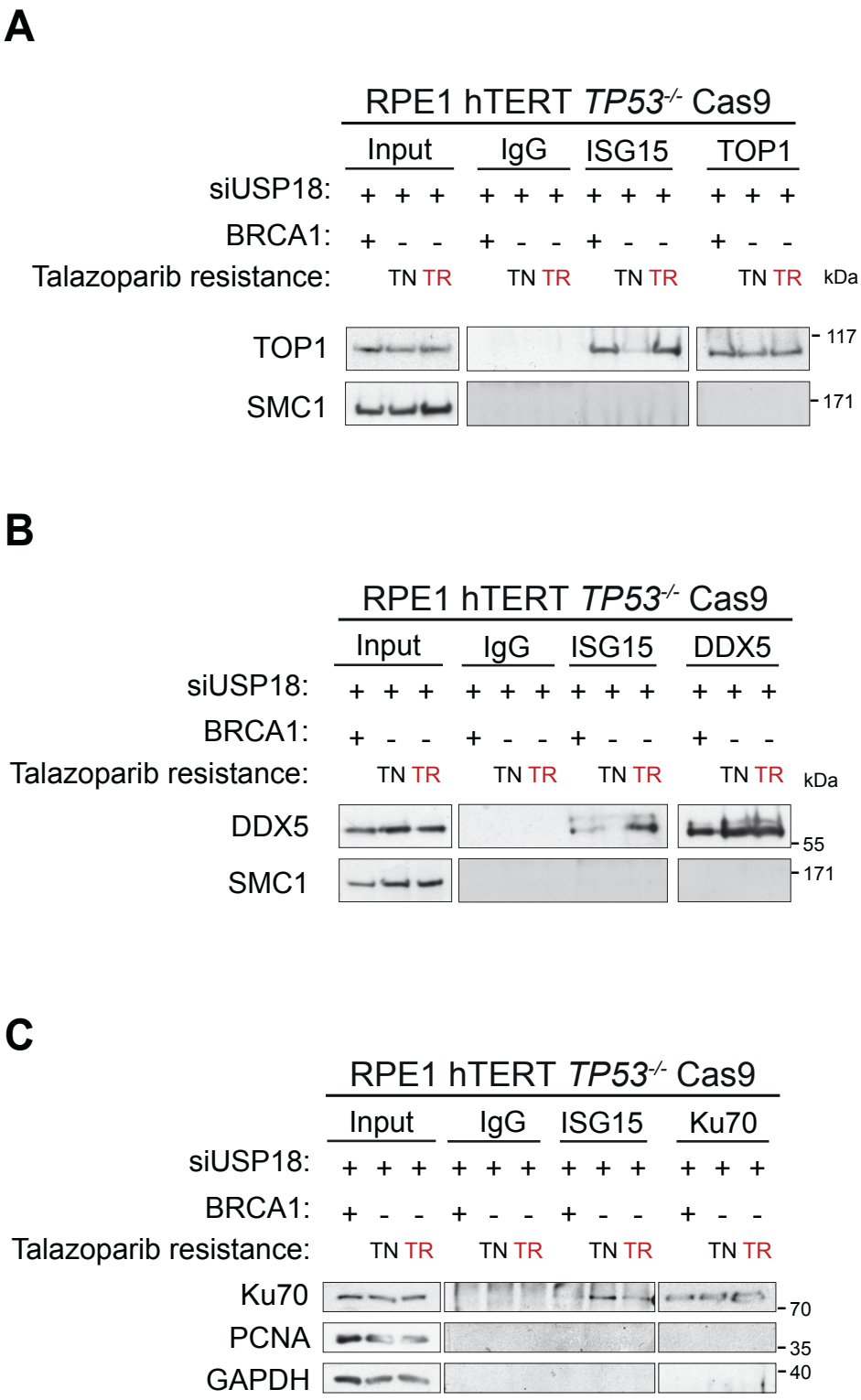


Figure 4.8 ISG15 interacts with TOP1, DDX5 and Ku70

(A), (B), (C) RPE1 hTERT *TP53*$^{-/-}$ Cas9 cells are transfected with siUSP18 for 48 hours to ensure enrichment of ISGylation on its substrates. ISG15

was immunoprecipitated under native conditions using magnetic beads. (A) TOP1 was immunoprecipitated under native conditions. (B) DDX5 was immunoprecipitated under native conditions. (C) Ku70 and PCNA was immunoprecipitated under native conditions, respectively. The data are representative of n=3 biologically independent experiments.

Among the proteins validated from WB, we were particularly interested in TOP1 because it is involved in both replication and transcription to alleviate torsional stress, which is known to have an effect on replication-transcription conflicts [257] that cause subsequent impact on replication fork progression [258].

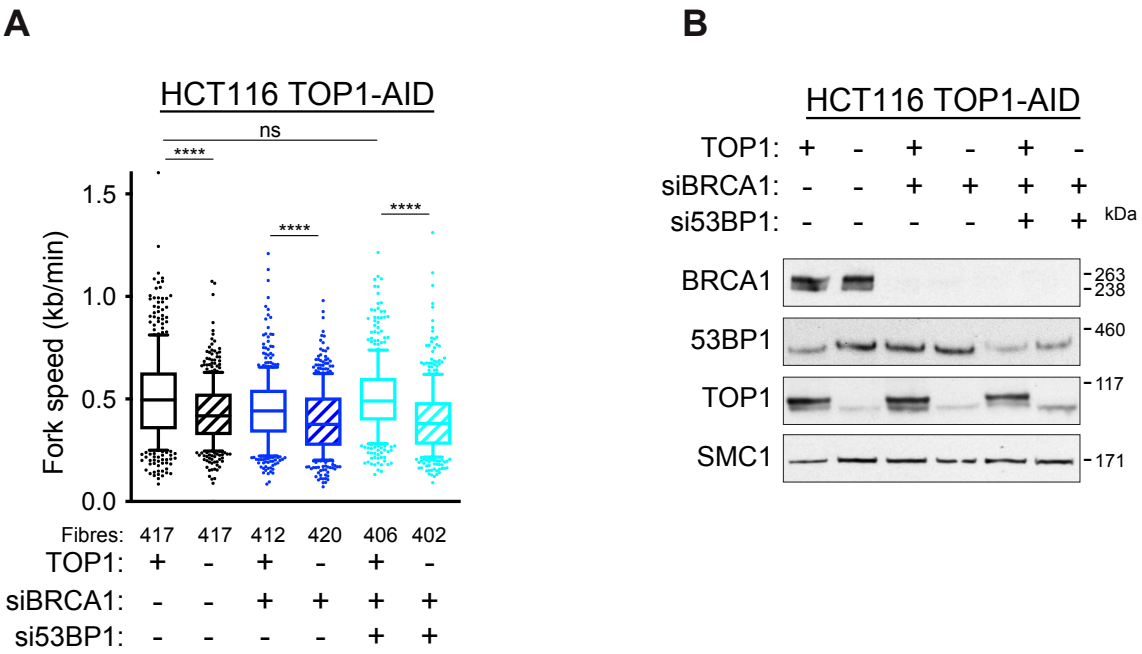


Figure 4.9 TOP1 depletion in HCT116 cells results in decrease of fork speed

(A) Analysis of replication tracts on HCT116 TOP1-AID cells. Cells underwent 48 hours of siRNA transfection to knock down the target genes and 24 hours of auxin addition to deplete TOP1. Following the procedure, cells were pulsed with CldU and IdU for 20 min each. At least 200 fibres were analysed for each condition of each replicate. Error bars represent S.E.M of n=2 independent experiments. *NS*, $p > 0.05$; ***, $p < 0.001$; ****, $p < 0.0001$ (One-way ANOVA followed by post-hoc Tukey's HSD testing)

(B) The same cells were harvested and whole cell extracts were immunoblotted as indicated. SMC1 was used as loading control.

Knowing that TOP1 plays a role in replication and interacts with ISG15, we then questioned whether the protein participates in replication fork progression as ISG15 does. To answer this question, we carried out a replication fork progression assay to study the role of TOP1 (Fig. 4.9A). For this experiment, we utilised HCT116 cells carrying an Auxin-inducible degron (AID) tagged against TOP1. To mimic the PARPi-naïve and resistant phenotype of RPE1 cells, we have transfected the cells with siRNA against BRCA1 or siRNA against BRCA1 and 53BP1[259]. Silencing of BRCA1 and 53BP1 expression was confirmed via WB (Fig. 4.9B). Similar to RPE1 cells, BRCA1-depleted samples showed decrease of fork speed compared to the siCTRL-transfected samples. Similar to the phenotype between RPE1 BRCA1-deficient TR and BRCA1-deficient TN cells, the siBRCA1 and si53BP1 co-transfected HCT116 cells showed rescue of fork speed when compared to siBRCA1-transfected HCT116 cells. Interestingly, we observed that TOP1 depletion leads to a decrease of fork speed regardless of genotype, as ISG15 depletion in RPE1 cells did.

Since we know that TOP1 can play a role in replication fork progression, we then asked whether ISG15 and TOP1 are regulating replication fork speed through the same pathway. To address this, we utilised RPE1 cells for replication fork progression assay. Due to slow turnover of TOP1 protein, we had to double-transfect the siTOP1 to ensure the successful knockdown of TOP1. The knockdown of proteins was validated by WB.

In this experiment, we have observed that BRCA1-deficient TN cells showed decreased replication fork progression when compared to their wild type

counterparts (Fig. 4.10A), and the phenotype is rescued in BRCA1-deficient TR cells, as we have previously shown. In RPE1 wild type cells, depleting TOP1 did not change the replication fork speed, unlike we have seen in HCT116 cells. Silencing TOP1 with ISG15, however, resulted in decreased replication fork progression rate, consistent with the previous results.

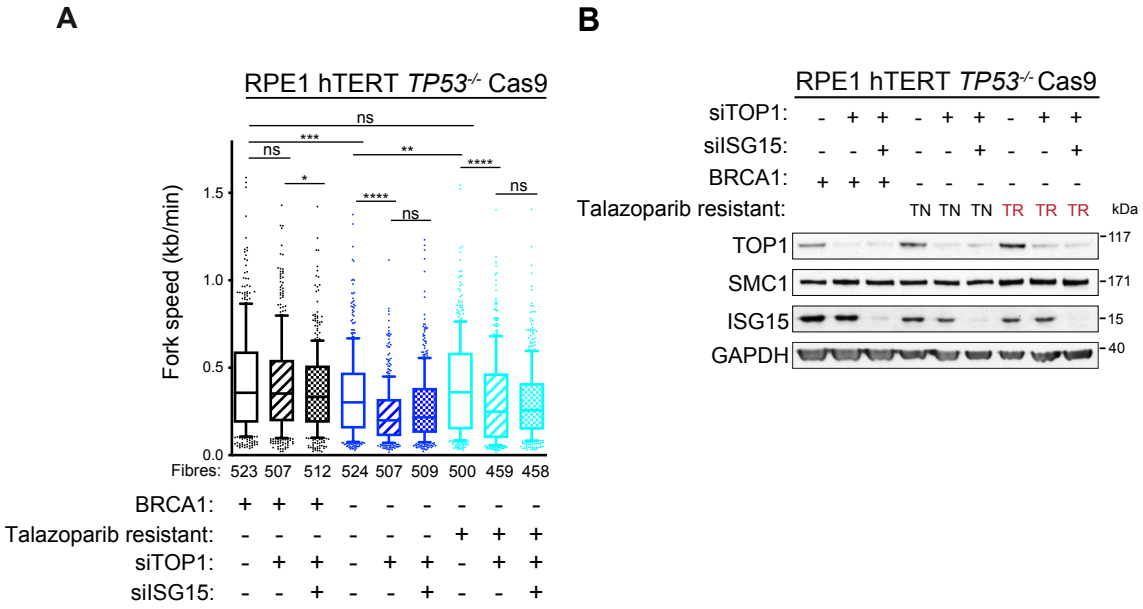


Figure 4.10 ISG15 and TOP1 regulates replication fork progression in the same pathway in BRCA1-deficient talazoparib resistant cells

(A) Analysis of replication tracts on RPE1 hTERT *TP53*$^{-/-}$ Cas9 cells. Cells were initially transfected against target gene for 48 hours and underwent second transfection for additional 24 hours. Following the double transfection, cells were pulsed with CldU and IdU for 30 min each. At least 200 fibres were analysed for each condition of each replicate. Error bars represent S.E.M of n=2 independent experiments. *NS*, $p > 0.05$; *, $p < 0.05$; **, $p < 0.01$; ***, $p < 0.001$; ****, $p < 0.0001$ (One-way ANOVA followed by post-hoc Tukey's HSD testing) (B) RPE1 hTERT *TP53*$^{-/-}$ Cas9 cells were double-transfected with siRNA against target genes. Following the treatment, samples were harvested and whole cell extracts were immunoblotted as indicated. SMC1 and GAPDH were used as loading controls.

In BRCA1-deficient cells, depleting TOP1 resulted in decreased fork speed, regardless of their sensitivity towards PARPi. It was consistent with the previous observation in HCT116 cells. Interestingly, co-depleting ISG15 with TOP1 in BRCA1-deficient TN and TR cells did not have any effect on replication fork speed. Therefore, we conclude that TOP1-mediated regulation of replication fork progression is not a cell-line specific phenotype, and TOP1 and ISG15 work in the same pathway in BRCA1-deficient cells to regulate the replication fork speed.

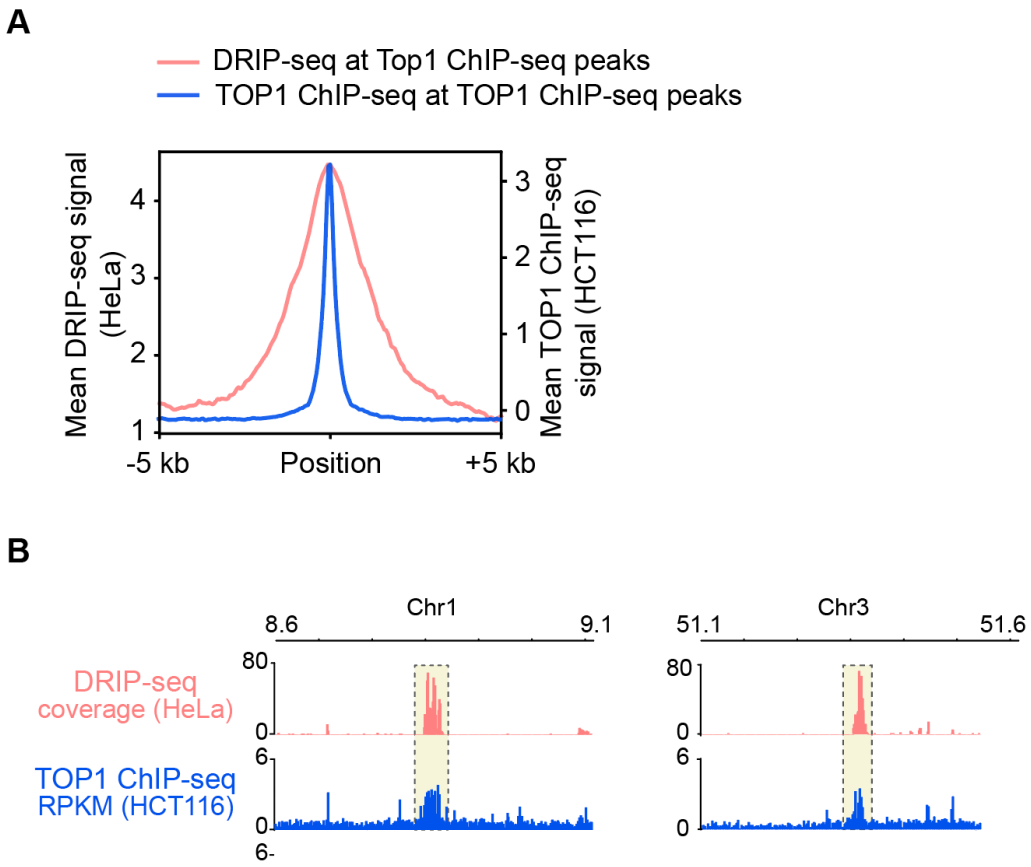


Figure 4.11 TOP1 can bind to the R-loop forming sites

(A) Profile plots of average DRIP-seq signal (HeLa) and TOP1 ChIP-seq signal (HCT116), centred across TOP1 ChIP-seq peaks. Span of genomic region, 10 kb. (B) Top row: DRIP-seq coverage profile at representative genomic regions in HeLa cells. Bottom row: TOP1 ChIP-seq profile (RPKM) at the same genomic sites. Bin resolution, 50 bp. Span of genomic region, 500 kb. All of analysis is done by Birbal Prasad.

One possible explanation for replication fork slowdown upon depletion of TOP1 is that TOP1 can resolve the structure that can pose a barrier to replication fork progression [260, 261]. Previous studies have also shown that TOP1 can prevent R-loop formation by alleviating torsional stress [262, 263]. R-loop, the three-stranded RNA:DNA hybrid, can cause arrest or slowdown of replication forks [88]. Given that BRCA1-deficient TR cells showed enhanced interaction between TOP1 and ISG15, and showed an epistatic relationship in regulating replication fork progression, we hypothesise that ISGylation might be involved in TOP1-mediated R-loop regulation; the replication fork slowdown upon silencing TOP1 might be due to the increased numbers of R-loops.

We used publicly available TOP1 ChIP-seq and DRIP-seq data to test the hypothesis and to see whether TOP1 can bind at R-loop prone sites. We compared the mean value of the DRIP-seq signal profile and the mean value of the TOP1 ChIP-seq profile at TOP1 ChIP-seq peak sites (Fig. 4.11A). The analysis showed that TOP1 can localise to the R-loop forming sites. When we compared the average DRIP-seq profile with average TOP1 ChIP-seq profile, the DRIP signal peaked at the TOP1-binding sites as well (Fig. 4.11B), showing a correlation between TOP1-binding sites and R-loop prone sites.

From the experiments featured in Chapter 4, we have observed that PARPi induces upregulation of ISGs, which correlates with the drugs' PARP-trapping abilities (Fig. 4.1). Most importantly, we have found that mRNA expression of ISG15 (Fig. 4.3) and ISGylation levels increase in BRCA-deficient PARPi-resistant cells compared to BRCA-deficient PARPi-naïve cells (Fig. 4.4), which seems to correlate with elevated replication fork speed and stress (Fig. 4.6). Moreover, we have observed that ISG15 can interact with proteins TOP1, DDX5,

and Ku70 (Fig. 4.7, Fig. 4.8), the proteins involved in replication fork machinery and stress response. Furthermore, we observed that ISG15 and TOP1 regulate replication fork progression through the same pathway in BRCA1-deficient talazoparib-resistant cells (Fig. 4.10). Due to the enhanced interaction between TOP1 and ISG15 in BRCA1-deficient talazoparib-resistant cells (Fig. 4.8A) and TOP1's ability to localise to R-loop prone sites, we have speculated that ISG15 may contribute to R-loop regulation through interaction with TOP1, via maintaining replication fork speed in BRCA1-deficient talazoparib resistant cells.

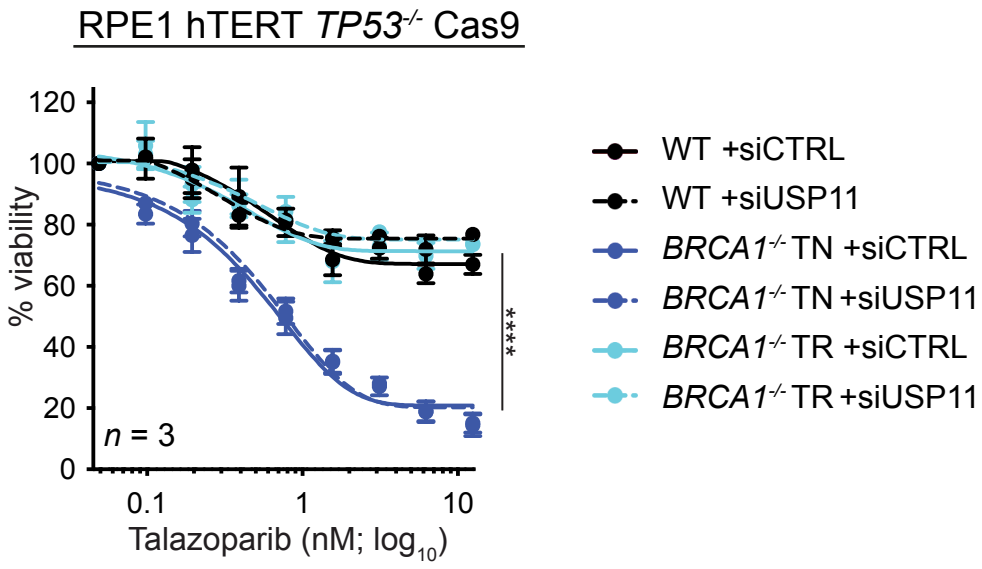
Chapter 5

Experiment results III – R-loop regulating proteins does not directly affect survival of BRCA1-deficient talazoparib-resistant cells

5.1 Studying the role of proteins regulating R-loop homeostasis in the context of PARPi resistance

Since we have discovered the putative link between the PARPi resistance in BRCA1-deficient cells and R-loop homeostasis, we then determined to study whether the R-loop regulating factors play a role in survival of BRCA1-deficient talazoparib resistant cells.

A



B

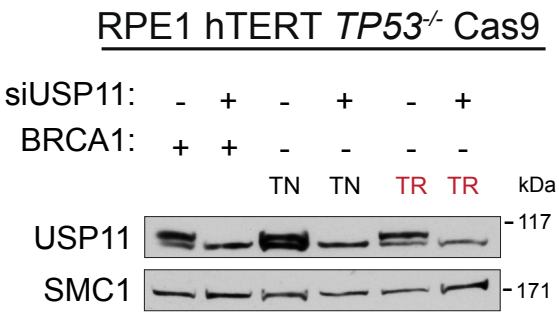


Figure 5.1 Silencing USP11 does not affect cell viability of RPE1 hTERT *TP53*$^{-/-}$ Cas9 cells upon talazoparib treatment

(A) RPE1 hTERT *TP53*$^{-/-}$ Cas9 *BRCA1*$^{+/+}$ and *BRCA1*$^{-/-}$ cells, with or without talazoparib resistance were transfected with siRNA against USP11 or non-targeting control siRNA. Following the 48-hour transfection, cells were treated with talazoparib at the indicated doses.

Six days after, cell viability was measured using resazurin-based assay. Error bars represent standard error of the mean (SEM) of n = 3 biologically independent experiments, each performed in triplicate. *NS*, $p > 0.05$; *, $p < 0.05$; **, $p < 0.01$; ***, $p < 0.001$; ****, $p < 0.000$ (unpaired two-tailed t test) (B) Following the siRNA transfection described in (A), samples were harvested and whole cell extracts were immunoblotted as indicated. SMC1 was used as a loading control.

To answer this question, we first carried out survival assay using siRNA against ubiquitin specific peptidase 11 (USP11). We selected USP11 among other R-loop regulating proteins because the protein de-ubiquitinates Senataxin (SETX), an established BRCA1-binding partner and the R-loop specific helicase, thereby regulating its proteostasis [264, 265]. Moreover, previous study has observed that loss of USP11 leads to decreased SETX level, increased R-loop accumulation and subsequent genomic instability [266].

In this experiment, we monitored whether depletion of USP11 affects survival of BRCA1-deficient talazoparib resistant cells upon talazoparib treatment. As we have observed before (Fig. S1.B), BRCA1-deficient talazoparib-naïve cells exhibited sensitivity to talazoparib while BRCA1-deficient talazoparib-resistant cells illustrated decreased sensitivity to talazoparib; the survival rate was similar to that of BRCA1-proficient cells.

In all three cell lines, depleting USP11 seems to have no effect on viability. We suspected that the residual expression of USP11 (Fig. 5.1B) might be sufficient for maintaining proteostasis of SETX. Moreover, regarding that R-loop regulation is a multifaceted process managed by a network of proteins, and various helicases are involved in R-loop resolution [82], it may also be possible that depleting USP11 alone may not be enough to have effect on R-loop formation.

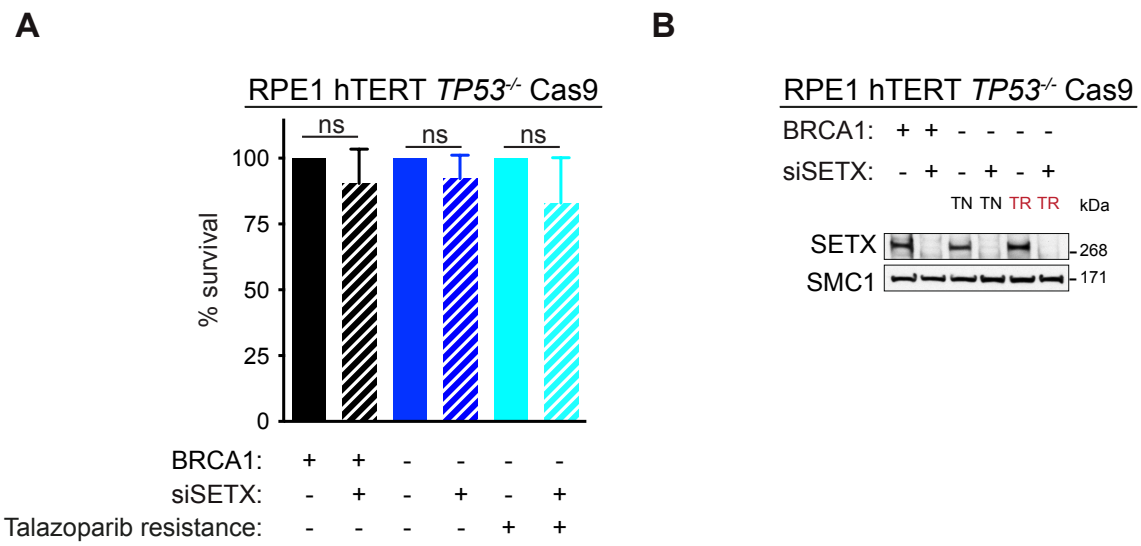


Figure 5.2 SETX depletion does not affect cell survival of RPE1 hTERT *TP53*$^{-/-}$ Cas9 cells

(A) RPE1 hTERT *TP53*$^{-/-}$ Cas9 *BRCA1*$^{+/+}$ and *BRCA1*$^{-/-}$ cells, with or without talazoparib resistance were transfected with siRNA against SETX or non-targeting control siRNA. Following the 48-hour transfection, cells were plated on 6-well plates. Surviving fraction of cells was quantified after 7-15 day of incubation. Error bars represent standard error of the mean (SEM) of n = 3 biologically independent experiments, each performed in triplicate. *NS*, $p > 0.05$ (unpaired two-tailed t test) (B) Following the siRNA transfection described in (A), samples were harvested and whole cell extracts were immunoblotted as indicated. SMC1 was used as a loading control.

Since the siRNA-mediated USP11 depletion was insufficient to fully silence the gene expression, and the residual protein expression may have been sufficient to manage the proteostasis of SETX, we then decided to target the SETX for silencing. To interrogate the role of SETX in viability of BRCA1-deficient talazoparib resistant cells, we implemented a survival assay using crystal violet. Briefly, cells were transfected with siRNA targeting SETX or non-targeting control siRNA and seeded on 6-well plates, which were stained and quantified after 7-15 days of incubation.

From this experiment, we could confirm that there was little to no residual expression of SETX (Fig. 5.2B). However, it seems like SETX depletion does not affect cell viability in three cell lines. We suspected that the effect of depleting SETX may have been masked, since SETX is not the only helicase that can resolve R-loop; cells may have complemented the role of SETX with other available R-loop helicases.

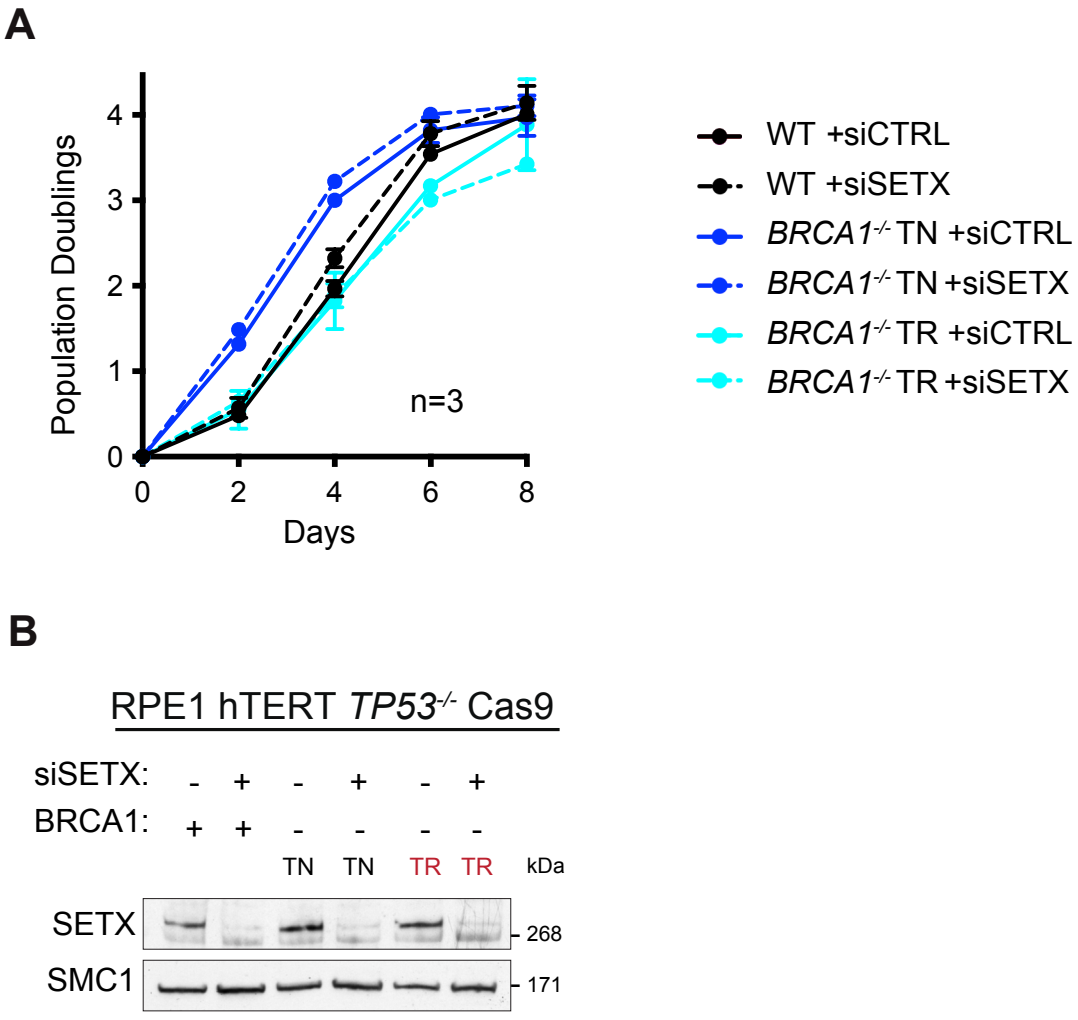


Figure 5.3 SETX depletion does not affect cell proliferation of RPE1 hTERT *TP53*$^{-/-}$ Cas9 cells

(A) RPE1 hTERT *TP53*$^{-/-}$ Cas9 *BRCA1*$^{+/+}$ and *BRCA1*$^{-/-}$ cells, with or without talazoparib resistance were transfected with siRNA against SETX or non-targeting control siRNA. Following the 48-hour transfection, cells were seeded on 96 well plates. Resazurin-based viability assay to measure population doublings was conducted at indicated days and

reported relative to day 0. Error bars represent the S.E.M of biologically independent experiments, each performed in triplicate. (B) Following the siRNA transfection described in (A), samples were harvested and whole cell extracts were immunoblotted as indicated. SMC1 was used as a loading control.

We have speculated that SETX may not have direct effect on cell survival, but it may have a role in cell health or behaviour. Therefore, we determined to study the effect of SETX depletion on cell proliferation. Briefly, cells were transfected with siRNA targeting SETX or non-targeting control siRNA for 48 hours and then seeded on 96-well plate. Population doubling was quantified in 2-day intervals by using resazurin-based assay. We observed little to no difference in cell growth between SETX-proficient and deficient cells.

From these experiments, we have observed that depleting R-loop regulating factor SETX and USP11 does not affect the cells' response towards talazoparib treatment and proliferative ability. We concluded that impact of SETX and USP11 depletion may be more pronounced under specific stress conditions or in different cellular contexts.

To interrogate the putative relationship between PARPi-resistance and R-loop accumulation in more precise manner, we then moved on to establishing the cell model (Fig. 5.4).

Briefly, FLAG-tagged RNaseH1 plasmid (RNH1-FLAG [267]; gift from Dr García-Rubio) was amplified and transduced into HeLa-TetON cells. Following the transduction, cells underwent Puromycin (5µg/mL) selection. The surviving fraction of cells then proceeded with single-cell cloning (Fig. 5.4A).

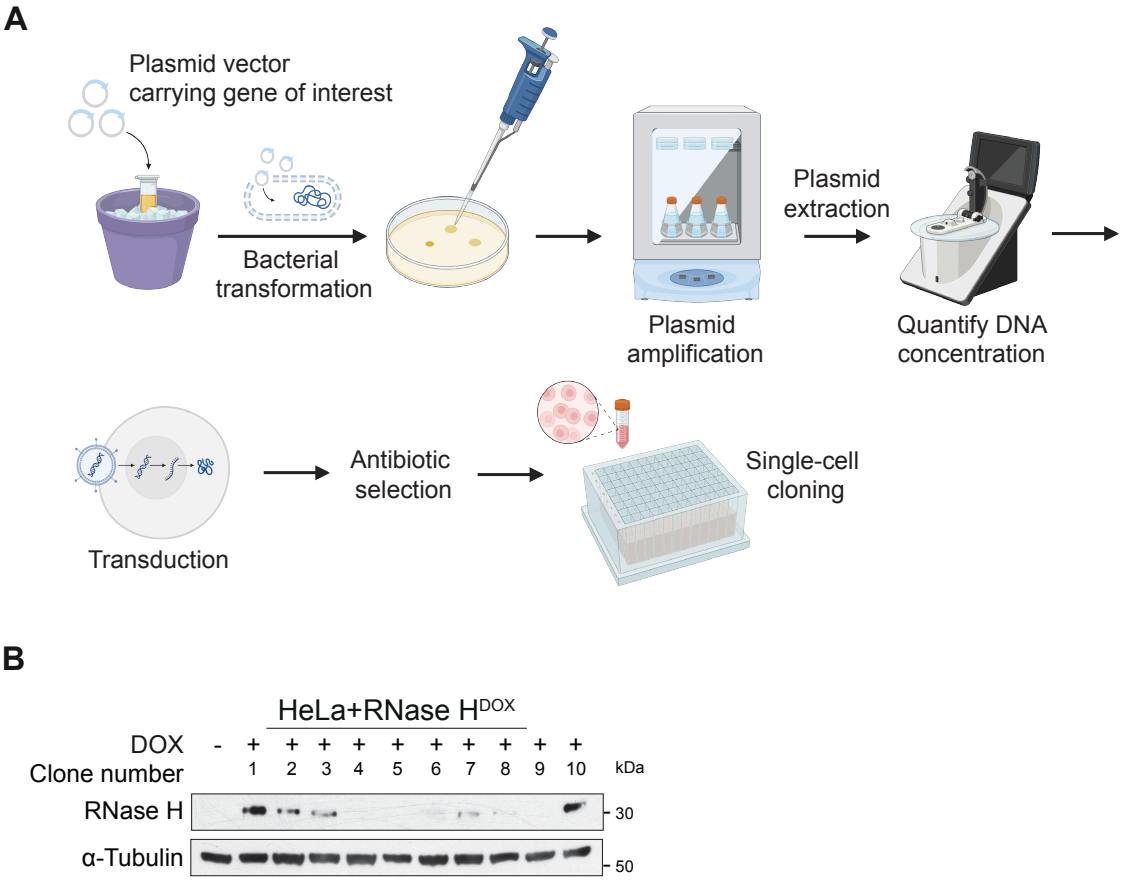


Figure 5.4 Establishing HeLa cell line carrying DOX-inducible FLAG-tagged RNaseH cassette

(A) Schematic of developing HeLa cell line carrying DOX-inducible FLAG-tagged RNaseH cassette. (B) Candidate clones were treated with 2μg/mL DOX for 48 hours. Following the treatment, cells were harvested and immunoblotted against Rnase H. α-Tubulin was used as loading control.

After obtaining significant number of single-cell clones, we then selected 10 samples for screening. To induce the RNaseH expression, the candidate cells were treated with 2μg/mL DOX for 48 hours. We selected clones #1 and #4 from the screening for further use (Fig. 5.4B). In addition to generating HeLa cells carrying DOX-inducible RNaseH cassette, we also tested the efficiency of transiently transfecting GFP-tagged RNaseH^{D210N} mutant plasmid to visualise R-loop in further experiments (Data not shown).

These experiments concluded that USP11 and SETX depletion did not influence cell survival or proliferation (Fig. 5.1, Fig 5.2, Fig. 5.3), suggesting their roles may be more pronounced under specific stress conditions. To further explore the connection between PARPi resistance and R-loop accumulation, a HeLa cell line with a DOX-inducible FLAG-tagged RNAseH1 plasmid was established. The obtained clones #1 and #4 from screening (Fig. 5.4) would be suitable for further research.

Chapter 6

Discussion and conclusion

6.1 Increased type I IFN protein expression in BRCA1/2-deficient cells and impact of ISG15 loss on cell cycle regulation

From this study, we observed that BRCA1- and BRCA2-deficient cells exhibit increased type I IFN protein expression upon PARPi treatment, which aligns with previous reports [168, 170] that suggest a heightened innate immune response in cells with compromised DNA repair capabilities.

Interestingly, our experiments demonstrated that ISG15 loss results in significant cell cycle dysregulation. This observation suggests that ISG15 plays a crucial role in maintaining proper cell cycle progression, potentially through the regulation of key cell cycle proteins. The dysregulation observed might lead to an accumulation of cells in specific cell cycle phases, thereby affecting cellular proliferation and survival, especially under stress conditions such as those induced by PARPi treatment.

To study the effect of ISG15 in the context of impaired DNA repair and PARPi treatment, utilising siRNA against BRCA1/2 on RPE1 hTERT *TP53*$^{-/-}$ Cas9 *ISG15*$^{-/-}$ cells could be an option to mimic the BRCA-deficient cell models. Monitoring the cell cycle upon the PARPi treatment in these models would help to clarify the physiological relevance of ISG15 in BRCA1/2-deficient cells' survival and their resistance development against PARPi.

In addition to monitoring cell cycle regulation, it may be helpful to use Incucyte for monitoring the subtle changes in proliferation rates between ISG15-proficient and deficient cells.

Moreover, carrying out RNA-seq analysis between ISG15-proficient and deficient cells would be helpful in visualising the transcriptomic changes upon the loss of

ISG15. This would contribute to finding the key regulation pathways and proteins affected by ISG15 loss, elucidating the role of ISG15 in cellular physiology.

6.2 ISG15 deficiency and sensitivity to hIFNa2 treatment

Our experiments demonstrated decreased survival of ISG15-deficient cells upon hIFNa2 treatment. It indicates that ISG15 is essential for cell survival in the presence of hIFNa2; the absence of ISG15 may impair the cellular response to hIFNa2. This suggests that ISG15 could be a protective factor, helping cells mitigate the cytotoxic effects of heightened IFN signalling. To study the role of ISG15 in regulating IFN signalling, it would be useful to start by silencing ISG15 machinery proteins. For instance, silencing UBA7, the E1 enzyme of ISG15, and treating with hIFNa2 would determine whether the conjugative role of ISG15 is important in the regulation.

In addition to this, monitoring the phenotypical difference between double knockouts and single knockouts would be helpful in understanding the role of ISG15 machinery in regulating type I IFN response, as previous literature suggests that USP18 deficiency results in decreased cell survival upon type I IFN treatment [232].

6.3 Enhanced ISG15 expression and ISGylation in BRCA1-deficient TR cells

Previous studies show that ISG15 expression levels are altered in various cancers, including breast, ovarian, and colorectal [268]. However, due to the protein's multifaceted nature and context-dependent effect, the role of ISG15 in tumours remains elusive. A large number of studies have suggested that ISG15

has both tumour-promoting and tumour-suppressive effects, depending on the type of tumour [269].

From this study and previously published data by our research group, we have observed that mRNA expression of ISG15 is upregulated in BRCA-deficient cells compared to BRCA-proficient cells. An increase in ISG15 mRNA expression was observed between BRCA-deficient TN and TR cells; BRCA-deficient TR cells showed higher ISG15 expression than TN cells. A similar trend was also observed in BRCA1-mutated breast and ovarian cancer patient-derived xenografts.

We have also observed that protein expression of ISG15 is upregulated in BRCA1-deficient TR cells, compared to BRCA1-deficient TN cells. However, we could not see an increase in protein expression of ISG15 between BRCA1-deficient TN cells and BRCA1-WT cells. The disparity between mRNA levels and protein levels can be attributed to various factors and post-transcriptional regulations, such as protein degradation, protein stability, protein translation, cellular signalling and post-translational modifications [270]. However, pinpointing the factors contributing to the varied expression pattern between transcription and translation was beyond the scope of this thesis.

Interestingly, we have observed that ISGylation is almost abolished in BRCA1-deficient TN cells but restored in BRCA1-deficient TR cells, which is practically similar to WT cells. Since we know that ISG15 can play a role in post-translational modification by ISGylation [214, 271], we have suspected that an increase of ISGylation at the cellular level favours the survival of BRCA1-deficient cells under the PARPi treatment. Previous study has suggested that increased expression of innate immune genes is correlated with resistance to chemotherapy and/or

radiation [272]. Therefore, examining the effect of inhibition of ISG15 in response to PARPi treatment in PARPi-naïve and resistant cells, in addition to studying the impact of overexpression of ISG15 in PARPi-naïve cells using inducible ISG15 vector, would help to understand the role of ISG15 in acquiring PARPi resistance. In addition, utilising hIFNa2 to induce ISG15 overexpression would also be an alternative. Moreover, it would be informative to compare the effect of vector-induced ISG15 overexpression and hIFNa2-induced upregulation of ISG15 to understand better how type I IFN response modulates the PARPi resistance in BRCA1-deficient cells. However, further work to address the question was not possible due to the significant interruption caused by the COVID-19 pandemic and the time restraint of the DPhil programme.

6.4 Role of ISG15 in replication fork machinery

It is well known that ISG15 has a multifaceted role in the cellular context, ranging from antiviral defence and immune regulation to involvement in DNA damage response and cell cycle regulation [268]. Moreover, two independent studies suggested its involvement in DNA replication [231, 250].

One study utilised mouse embryonic fibroblasts (MEFs) with a 4-OHT inducible system targeting Nbs1, which plays a crucial role in maintaining genome integrity as a DNA damage sensor and effector [273], to study the role of ISG15 in the context of replication stress. It revealed that ISG15 conjugates to the proteins present on nascent replication forks, such as TOP2A, FEN1 and VCP, under normal conditions and its enrichment was upregulated upon replication stress [250].

The other study showed that the increased expression of ISG15 results in replication fork acceleration, which is mediated by the non-covalent interaction

between ISG15 and DNA helicase RecQ1. Most importantly, the study showed that the increased replication fork speed caused by upregulated ISG15 expression leads to replication stress and, ultimately, genomic instability [231].

This study has shown a correlation between high replication fork speed and PARPi resistance. Most importantly, we have confirmed that the accelerated fork speed in BRCA1-deficient TR cells depends on ISG15. Moreover, we have elucidated that ISG15 can interact with proteins involved in replication and DDR, such as TOP1 and Ku70. Further studies are required to study the thorough mechanism of how ISG15 regulates replication fork machinery.

Given that ISG15 can interact with its target proteins through both conjugation and non-covalent protein-protein interaction, it may be possible that ISG15 is mediating protein interactions via different mechanisms depending on the cellular context. Since previous studies using the *Listeria*-infected mural liver cells show that most ISGylation sites of the target proteins overlap with catalytic sites [274], it is also possible that ISG15 can conjugate with the protein to regulate the protein activity.

To study how ISG15 contributes to the regulation of replication machinery and to differentiate potential ISGylated proteins from ISG15 interactors, it would be insightful to carry out an MS/MS analysis using RPE1 ISG15 KO cell lines expressing ISG15 mutant lacking the C-terminal di-Glycine motif, which is crucial for its conjugation to target proteins. The MS/MS analysis would reveal whether ISG15 interacts with the proteins of interest through non-covalent interaction or conjugation.

In parallel to this, it may be useful to apply BioID to screening protein-protein interactions since the technique is known to be more effective in capturing weak

and/or transient interactions between proteins [275]. Moreover, the BirA tag used in BioID can be fused to the E3 ligases of ISG15, enabling the study of which E3 ligase of ISG15 is responsible for the interaction.

Moreover, to achieve more in-depth understanding of its role in replication fork progression, it would be effective to implement in-situ analysis of protein interactions at DNA replication fork (SIRF) assay to measure the quantitative interaction between ISG15 and its target protein in BRCA1-deficient TN and TR cells. This would give a more comprehensive understanding of how ISG15 accelerates replication fork progression in BRCA1-deficient TR cells.

6.5 Possible role of ISG15 in regulating R-loop levels

Previous studies showed that TOP1 is implicated in preventing excessive R-loop accumulation by resolving positive supercoiling and preventing transcription-induced torsional stress [258, 276]. Moreover, a recent study shows a link between TOP1 and R-loop homeostasis [258].

Our study confirmed that ISG15 interacts with TOP1 in TR cells, and several DEAD-box helicases and proteins are involved in RNA metabolism. Since previous studies suggest that ISGylation can stabilise the protein and inhibit proteasomal degradation via competition with ubiquitination [206, 277], we have speculated that interaction between ISG15 and TOP1 may enhance the activity of the protein by stabilising the TOP1, therefore decreasing R-loop levels.

To study the hypothesis, we would like to carry out TOP1 relaxation assay on RPE1 models to study whether increased interaction between ISG15 and TOP1 influence the enzymatic activity. In parallel to this, utilising ISGylation site mutant TOP1 (K540A) to study its ability to be recruited to chromatins compared to its

WT proteins would give more comprehensive understanding about the relationship between ISG15 and TOP1.

In addition to this, it would be helpful to utilise Quantitative-image based cytometry (QIBC) to visualise R-loop levels with RPE1 cells transfected with GFP-tagged catalytically inactive RNaseH (D210N). It would show the R-loop levels of RPE1 BRCA1-deficient TN and TR cells compared to BRCA1-proficient cells. This would provide an insight into the potential relationship between TOP1-mediated R-loop regulation and replication fork progression.

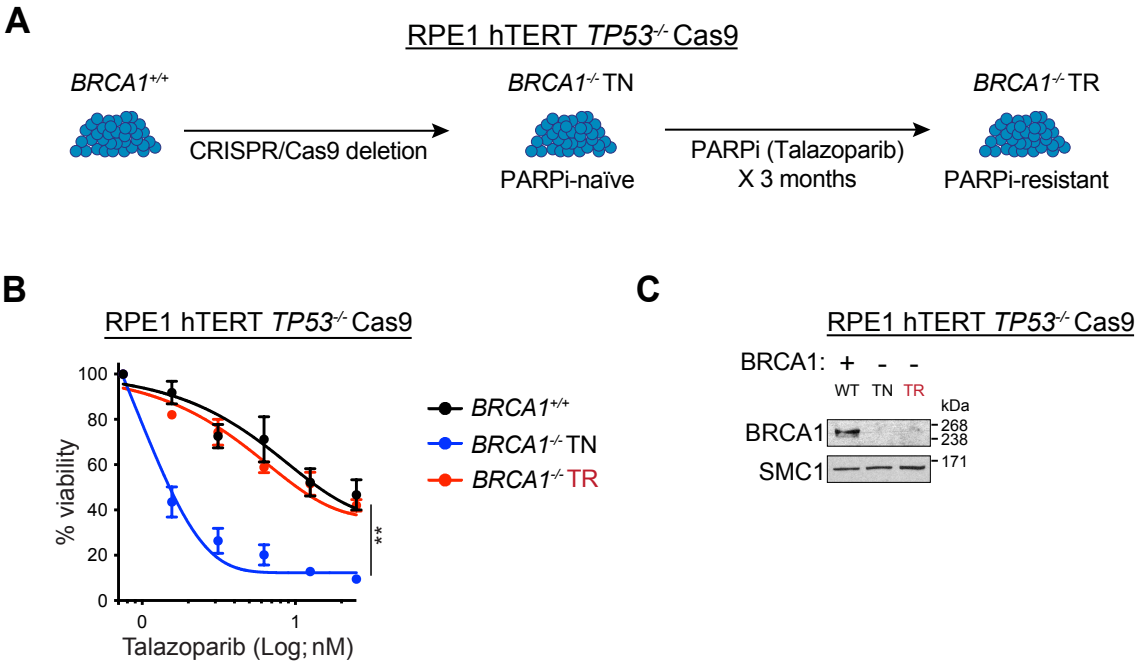
Taken together, this thesis demonstrates the putative link between ISG15-TOP1 interaction and R-loops and R-loop binding proteins. This is particularly important because it may provide a broader perspective in understanding how genomic instability triggered innate immune response regulates DNA replication and DDR and, ultimately, how it contributes to acquiring resistance. Therefore, fully elucidating the link between R-loop homeostasis and ISG15 expression might elucidate a novel biomarker for future cancer treatments.

6.6 Studying the putative relationships between R-loop accumulation and PARPi resistance

While the depletion of SETX and USP11 did not impact cell proliferation or survival in our models, the role of R-loops in PARPi resistance remains a critical area of investigation. Future studies focusing on the detailed characterization of R-loop dynamics and their interactions with DNA damage response pathways will be essential. To achieve this goal, it would be useful to perform DRIP-seq to quantify and map R-loops in BRCA1-deficient talazoparib-naïve and resistant cells. It would help determine if R-loop levels and locations differ upon acquiring PARPi resistance. Furthermore, exploring the effects of combining PARPi

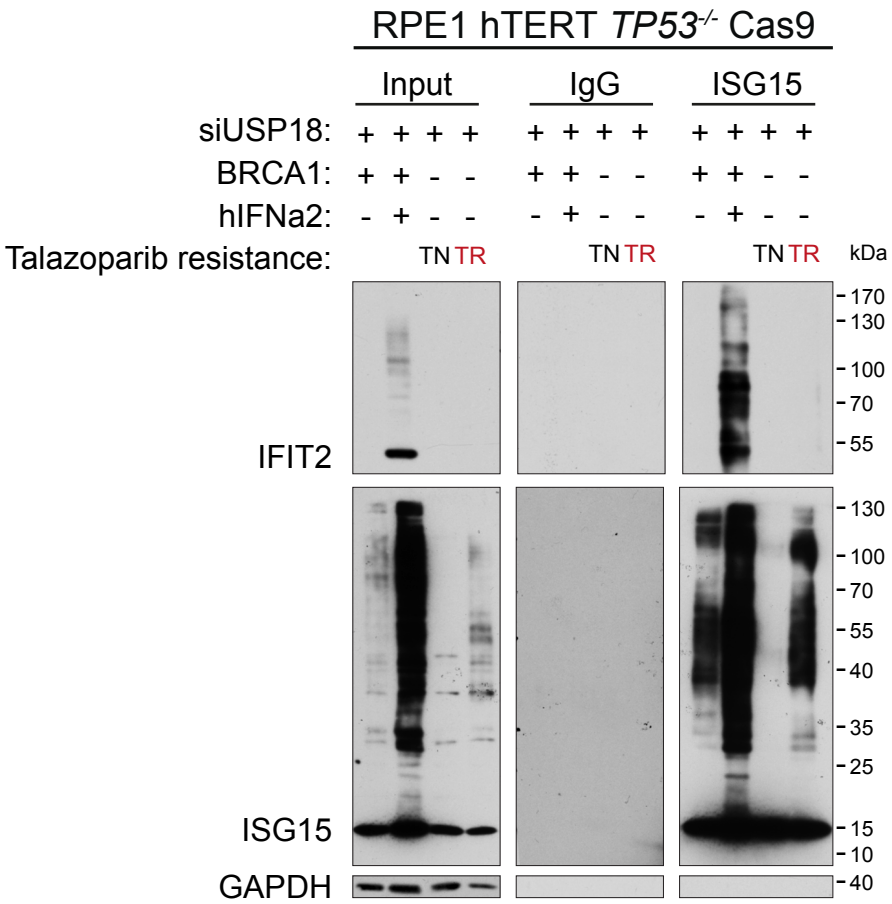
treatment with agents that target R-loop formation or resolution would help the understanding between physiological role of R-loops in DNA damage response. For instance, evaluating whether co-treatment with RNaseH1 or helicase inhibitors increases the sensitivity of BRCA1-deficient cells to PARPi would be informative. These efforts will enhance our understanding of PARPi resistance mechanisms and may identify novel therapeutic strategies to improve the treatment of BRCA1-deficient cancers.

Appendix



Supplemental Figure 1. Model of RPE1 hTERT *TP53*$^{-/-}$ Cas9 cell line developed resistance against PARPi talazoparib

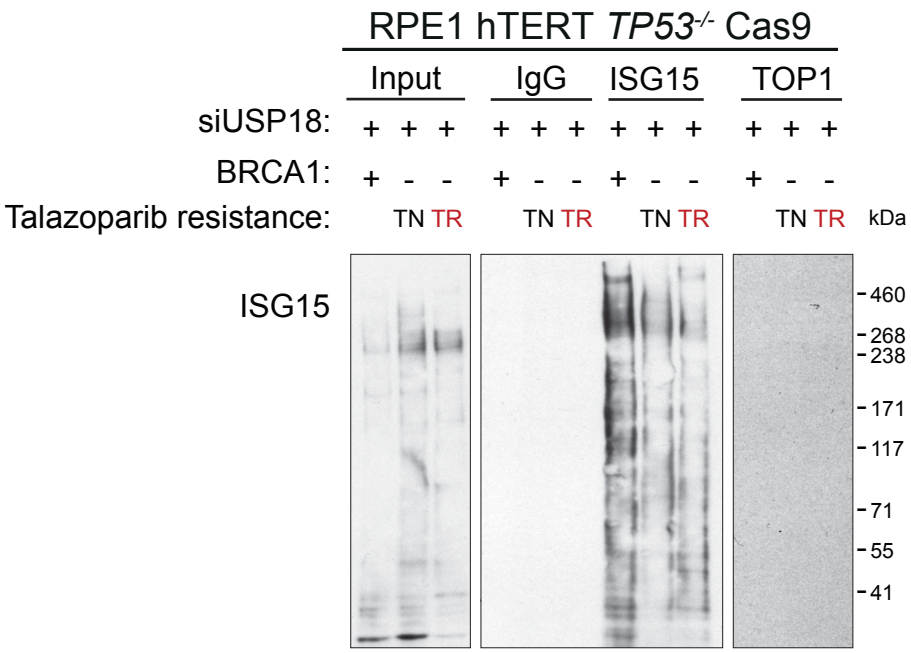
(A) Schematic of developing talazoparib-resistant RPE1 hTERT *TP53*$^{-/-}$ Cas9 *BRCA1*$^{-/-}$ cell line. (B) RPE1 hTERT *TP53*$^{-/-}$ Cas9 *BRCA1*$^{+/+}$ and *BRCA1*$^{-/-}$ cells, with or without talazoparib resistance, were treated with talazoparib at the indicated doses. Six days later, cell viability was measured using a resazurin-based assay. Error bars represent the standard error of the mean (SEM) of n = 3 biologically independent experiments, each performed in triplicate. Statistical significance was determined by an unpaired two-tailed t-test. (C) The samples used in (B) were harvested, and whole cell extracts were immunoblotted as indicated. SMC1 was used as a loading control. The cell line was established by Guiliana De Gregoriis. All work shown in Supplemental Figure 1 was performed by Giuliana de Gregoriis.



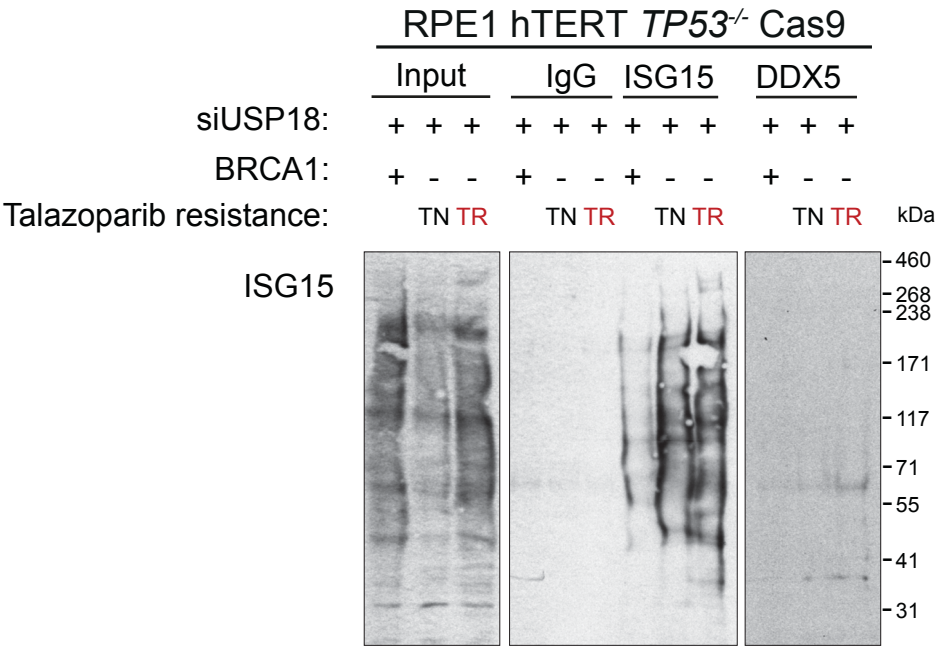
Supplemental Figure 2. Detection of IFIT2 in immunoprecipitated samples upon hIFNa2 treatment

RPE1 hTERT *TP53*$^{-/-}$ Cas9 cells are transfected with siUSP18 to ensure enrichment of ISGylation on its substrates. After 24 hours of transfection, cells were treated with 500U/mL of hIFNa2 for 24 hours. The treatment is to maximise ISG15 expression and ISG15 conjugation on its substrates. After 48 hours of transfection, ISG15 was immunoprecipitated under native conditions using magnetic beads.

A



B

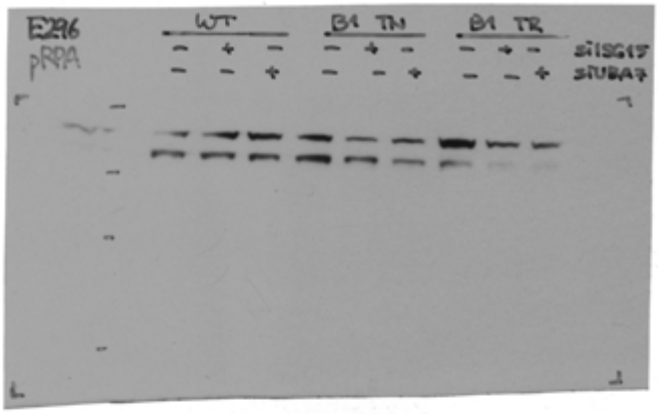


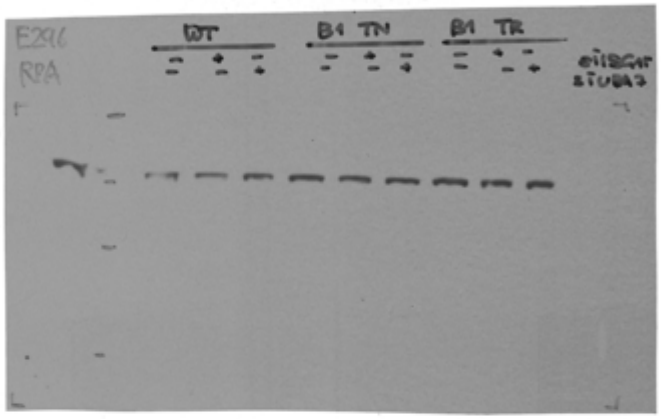
Supplemental Figure 3. Detection of ISG15-conjugated substrates from immunoprecipitated samples

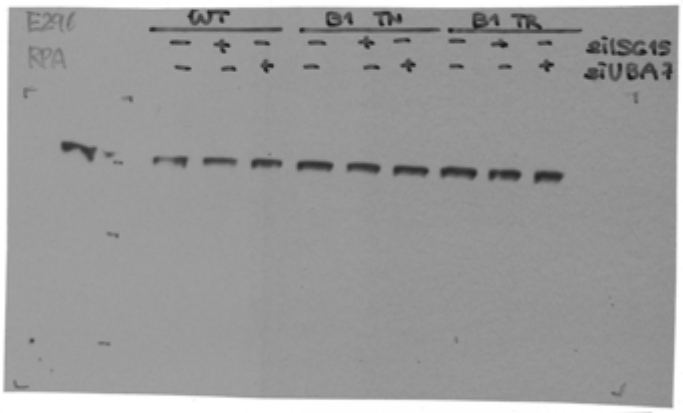
(A), (B) hTERT *TP53*$^{-/-}$ Cas9 cells are transfected with siUSP18 for 48 hours to ensure enrichment of ISGylation on its substrates. ISG15 was immunoprecipitated under native conditions using magnetic beads.

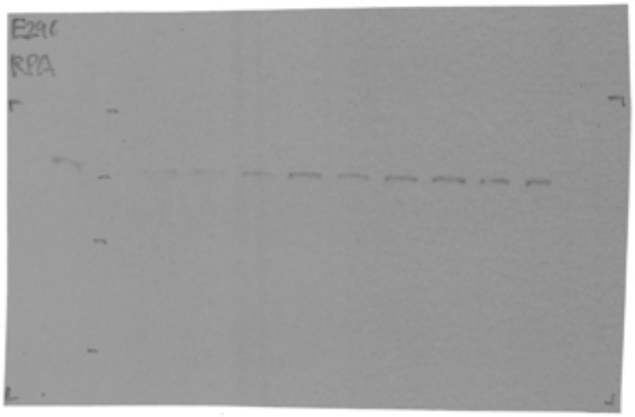
Supplemental Figure 3A is from the same experiment with Fig. 3.8A. Supplemental Figure 3B is from the same experiment with Fig. 3.8B. (Fig.3.8C was not probed with ISG15.) The data are representative of n=3 biologically independent experiments.

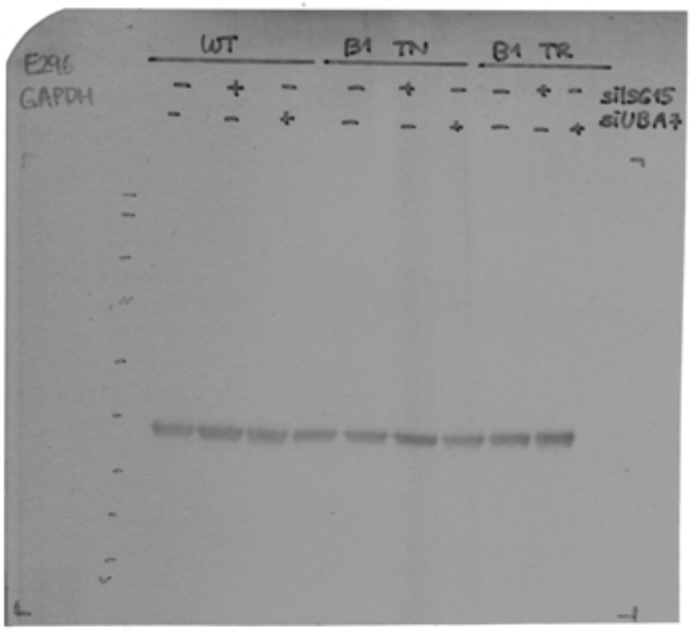
Raw Western Blot Image scans (Fig 4.4)

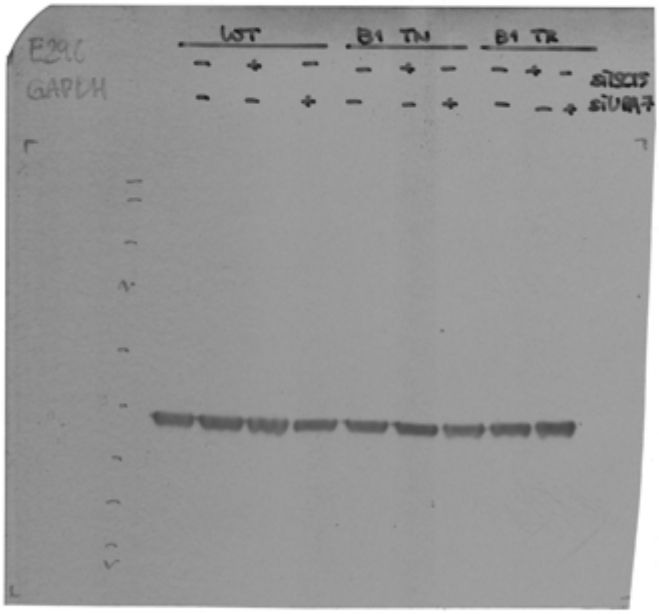

E2F6
pRPA
WT
B1 TN
B1 TR
siISG15
siUBA7

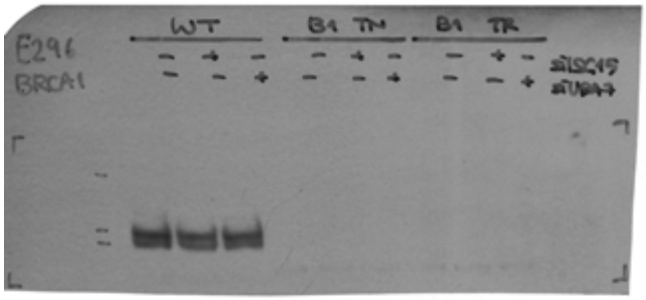

E2F6
RPA
WT
B1 TN
B1 TR

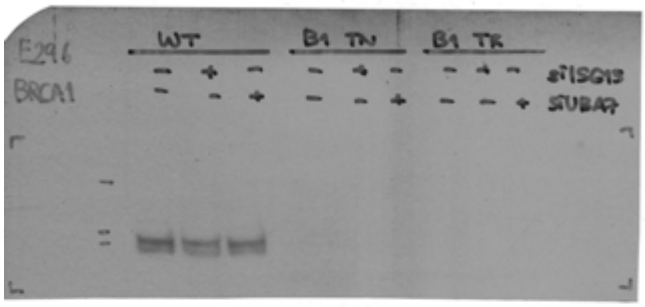

E2F6
RPA
WT
B1 TN
B1 TR
siISG15
siUBA7

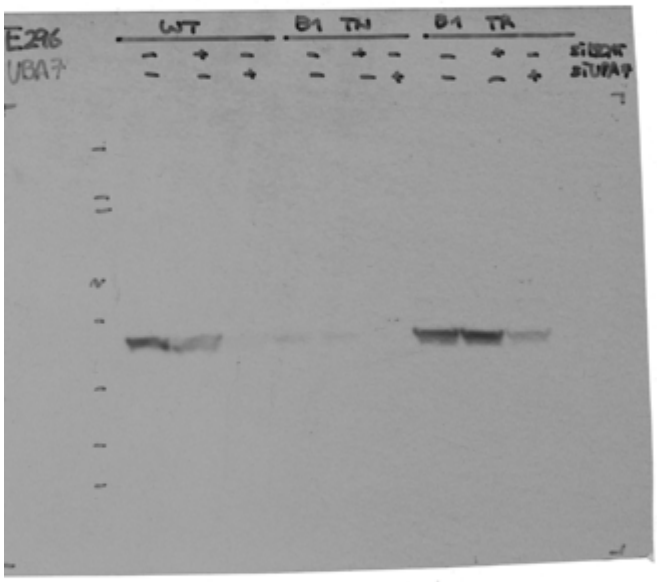

E2F6
RPA

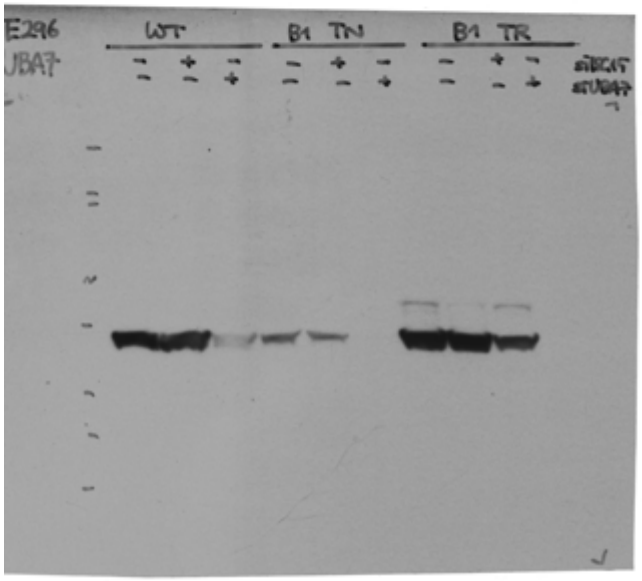

E2C
GAPDH
WT
B1 TN
B1 TR
siISG15
siUBA7

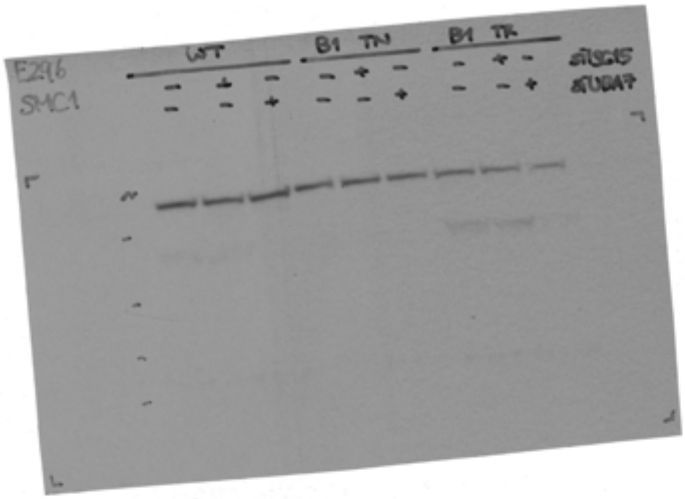

E2C
GAPDH
WT
B1 TN
B1 TR

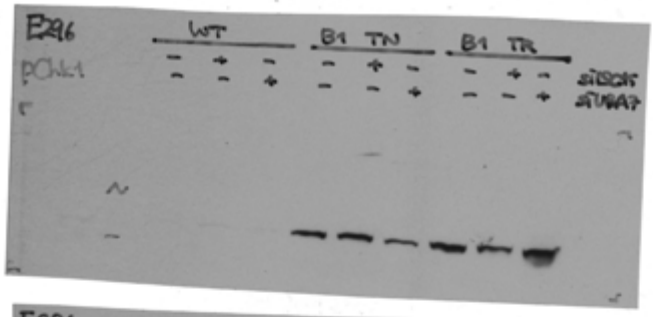

E296
BRCA1
WT
B1 TN
B1 TR

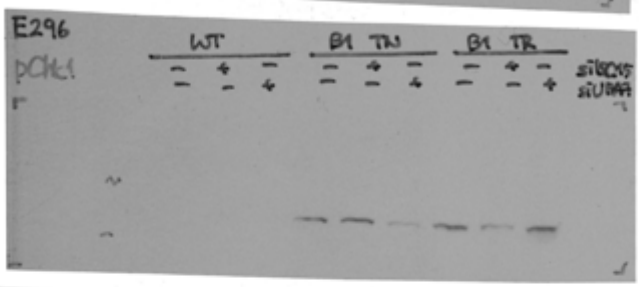

E296
BRCA1
WT
B1 TN
B1 TR

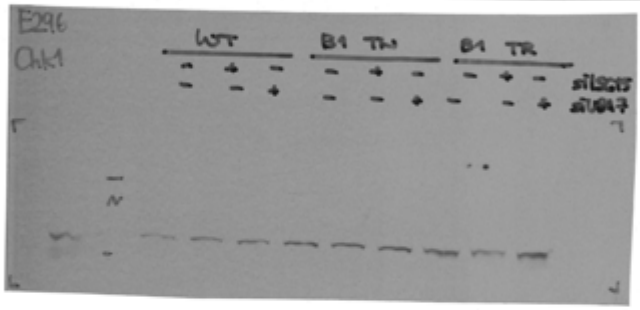

E296
UBA7
WT
B1 TN
B1 TR

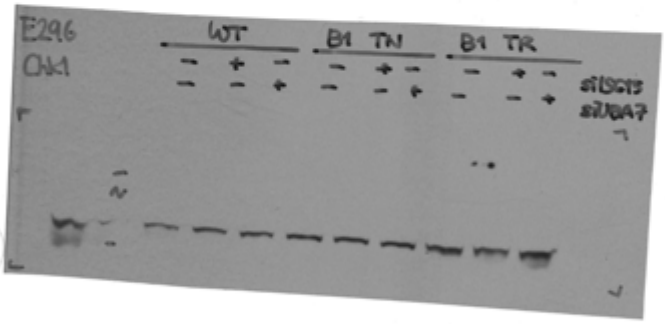

E296
UBA7
WT
B1 TN
B1 TR

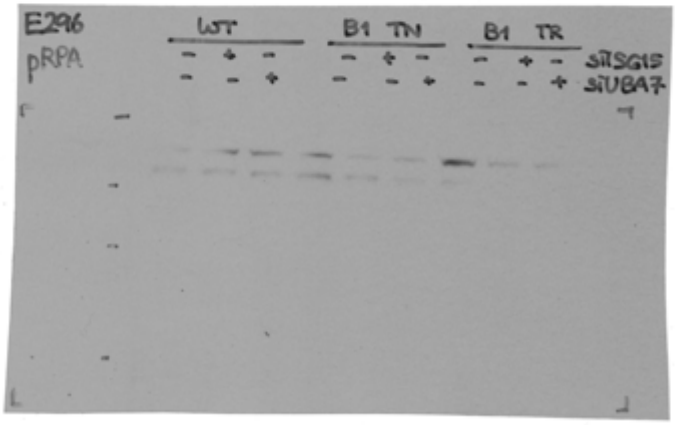

E2f6
SMC1
WT
B1 TN
B1 TK

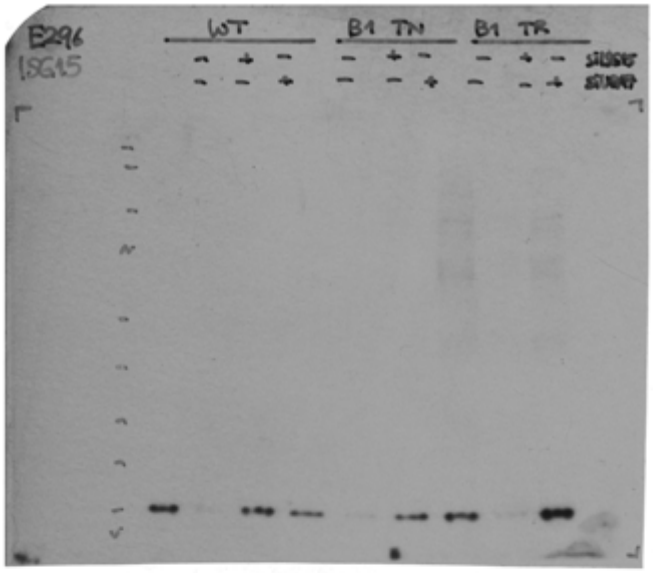

E296
WT
B1 TN
B1 TR
pCHK1
siTSG15
siUBA7

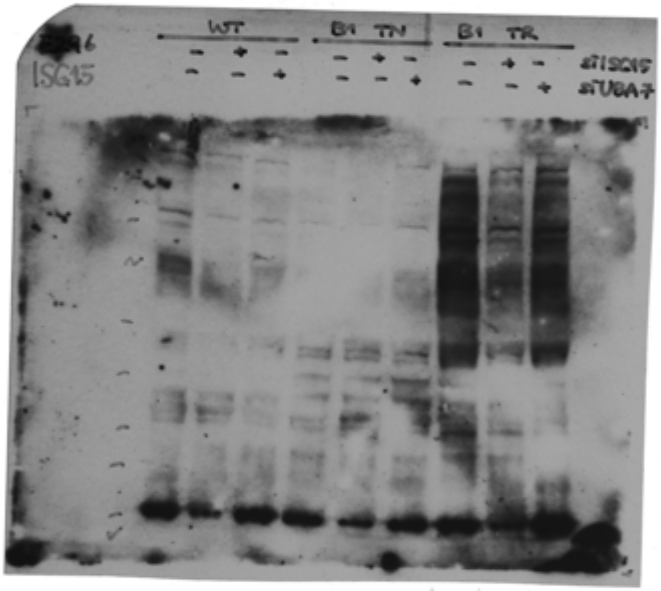

E296
WT
B1 TN
B1 TR
pCHK1

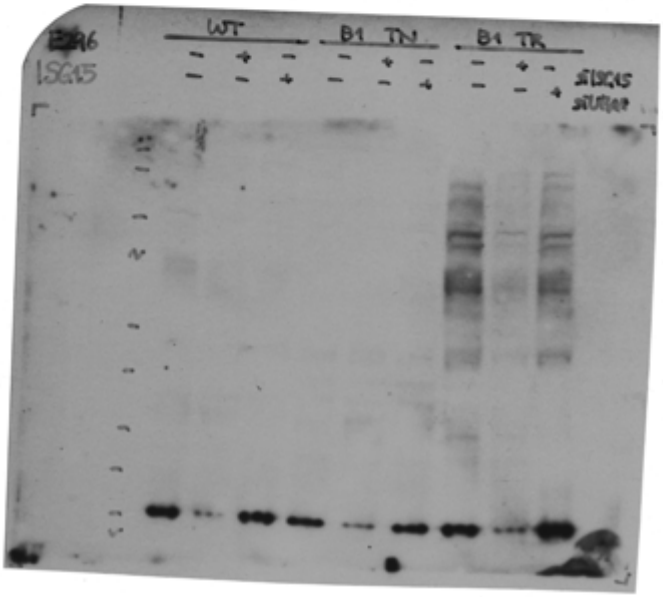

E296
WT
B1 TN
B1 TR
CHK1

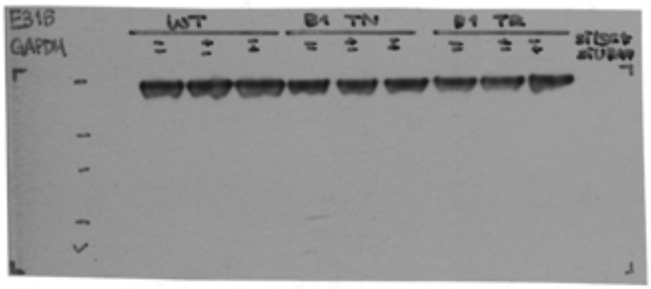

E296
WT
B1 TN
B1 TR
CHK1

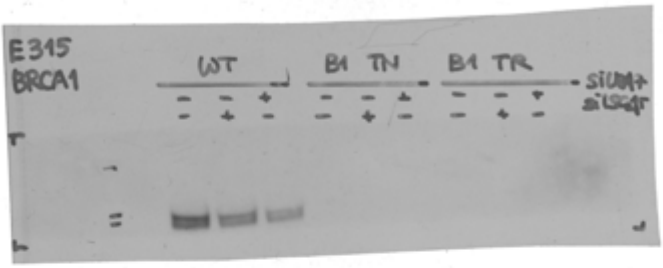

E296
WT
B1 TN
B1 TR
pRPA

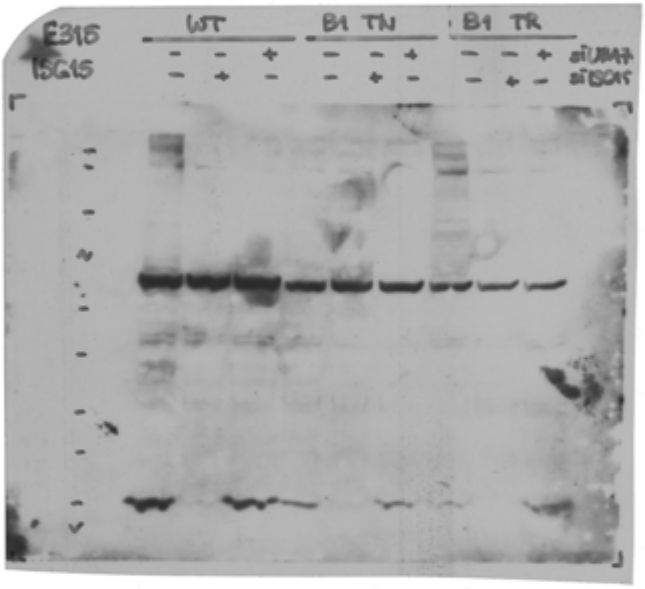

E2f6
ISG15
WT
B1 TN
B1 TR

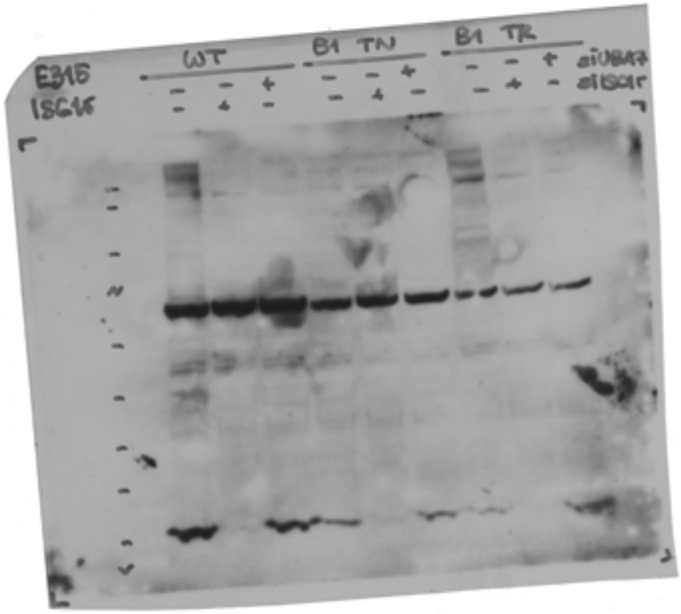

E2f6
ISG15
WT
B1 TN
B1 TR

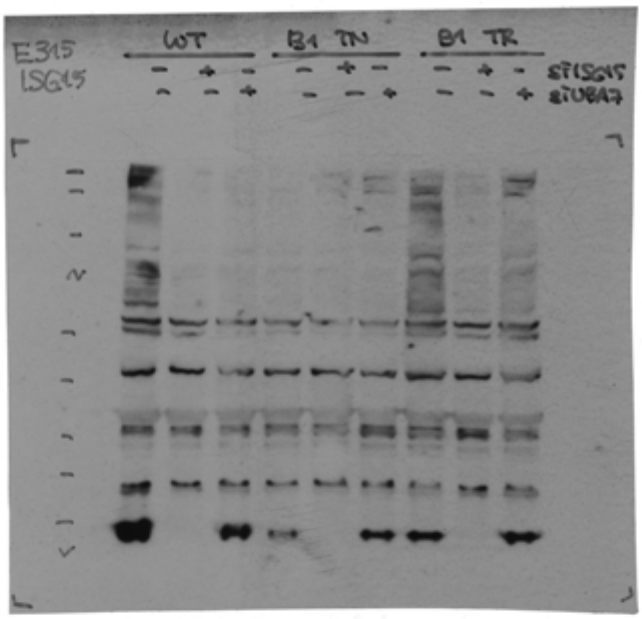

E2f6
ISG15
WT
B1 TN
B1 TR

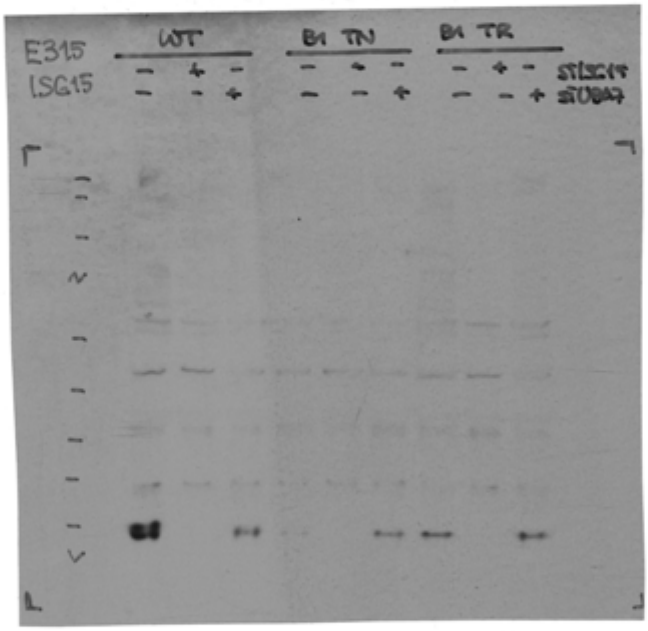

E315
GAPDH
WT
B1 TN
B1 TR

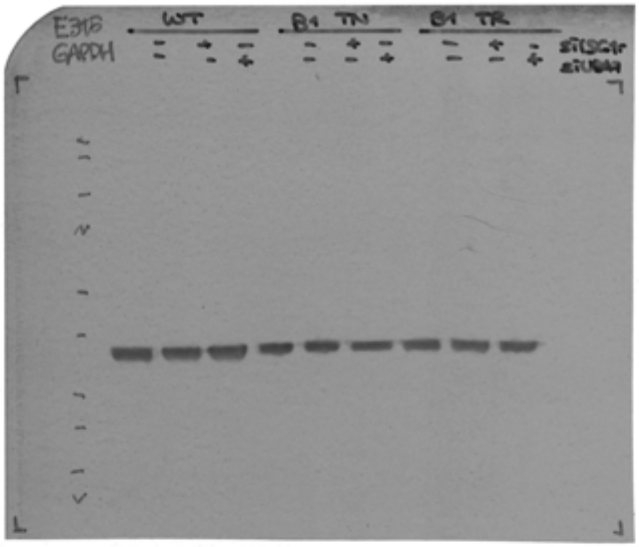

E315
BRCA1
WT
B1 TN
B1 TR

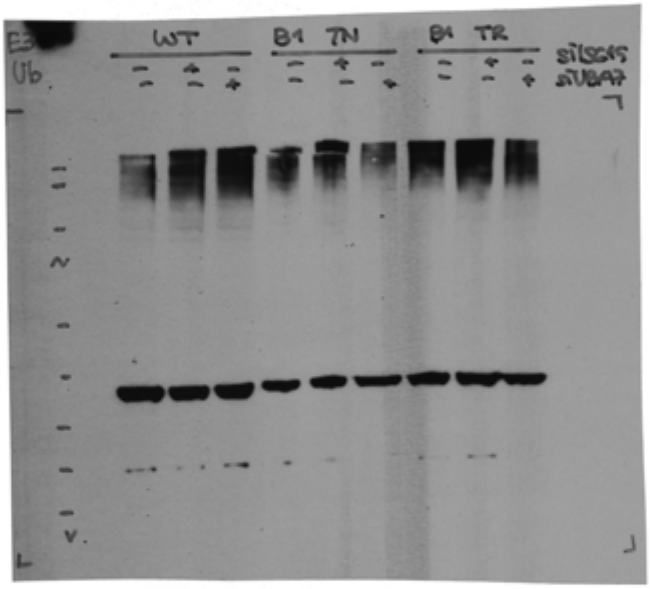

E315
ISG15
WT
B1 TN
B1 TR

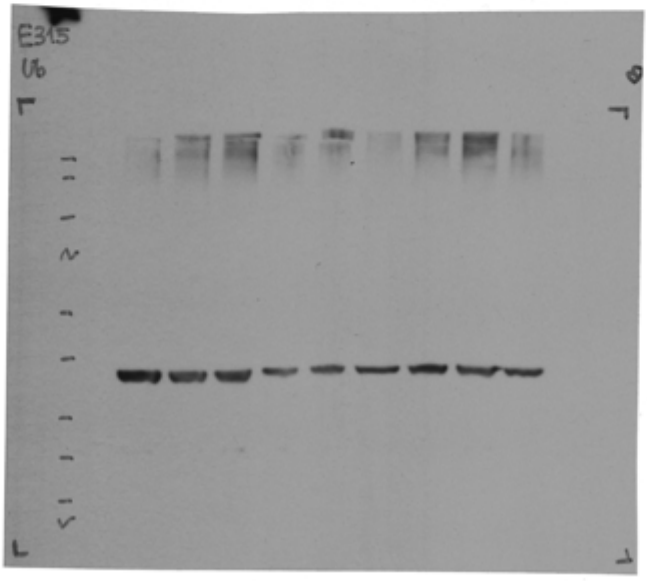

E315
ISG15
WT
B1 TN
B1 TR

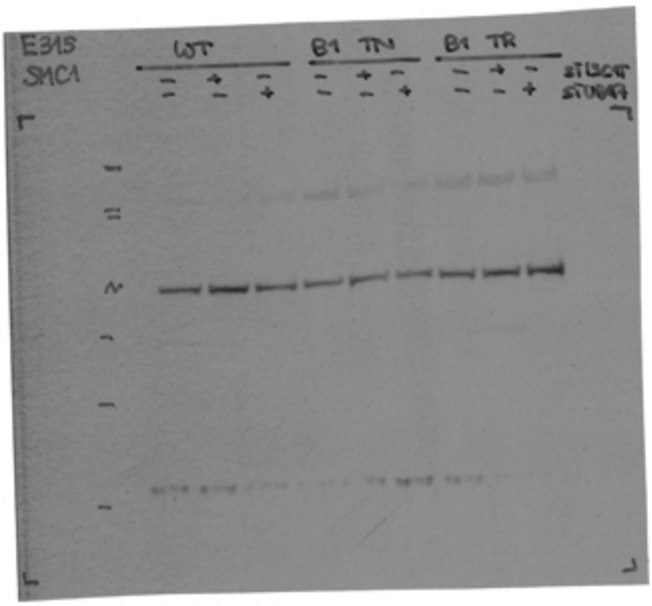

E315
LSG15
WT
B1 TN
B1 TR

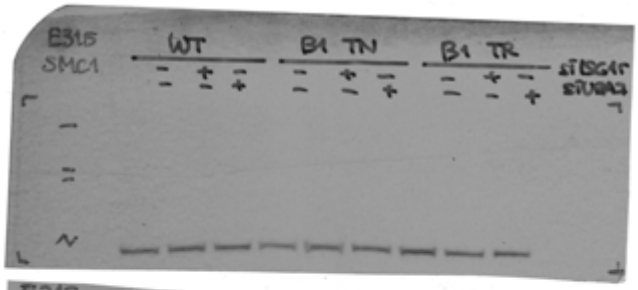

E315
LSG15
WT
B1 TN
B1 TR

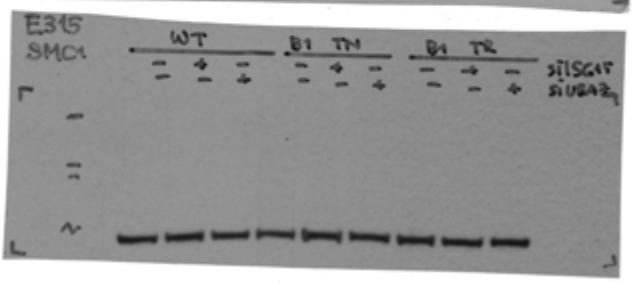

E3l6
GAPDH
WT
B1 TN
B1 TR

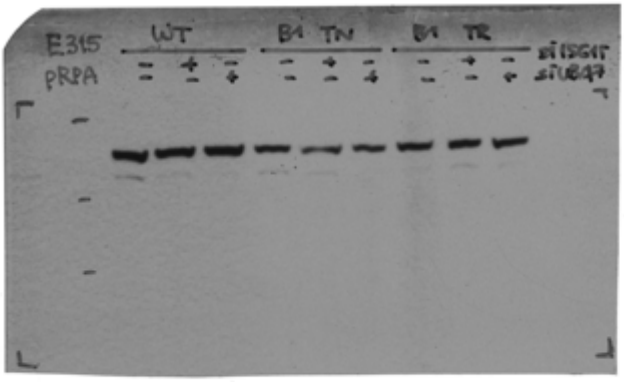

Ub
WT
B1 TN
B1 TR

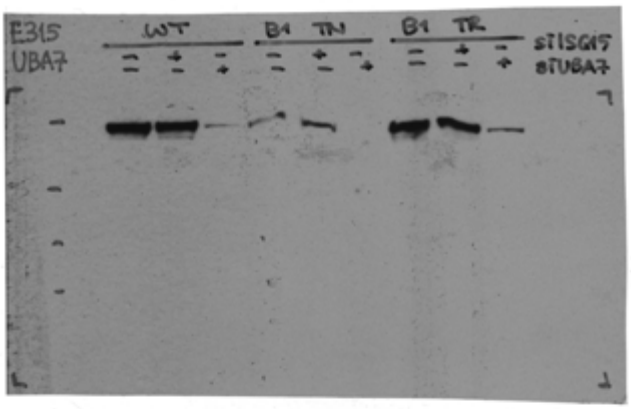

E3l5
Ub

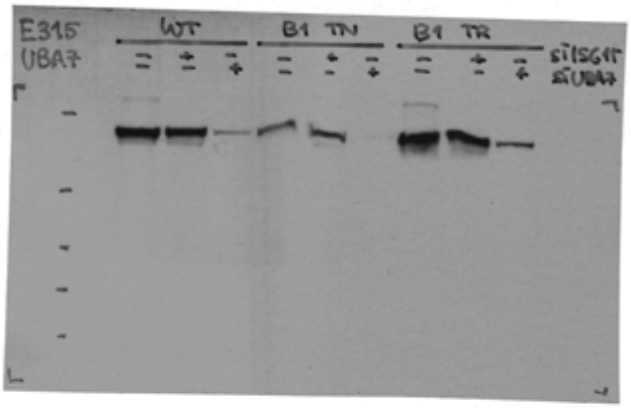

E315
SMC1
WT
B1 TN
B1 TR

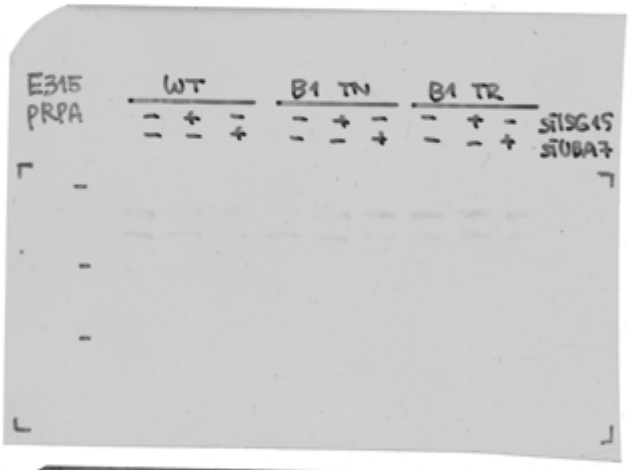

E315
SMC1
WT
B1 TN
B1 TR

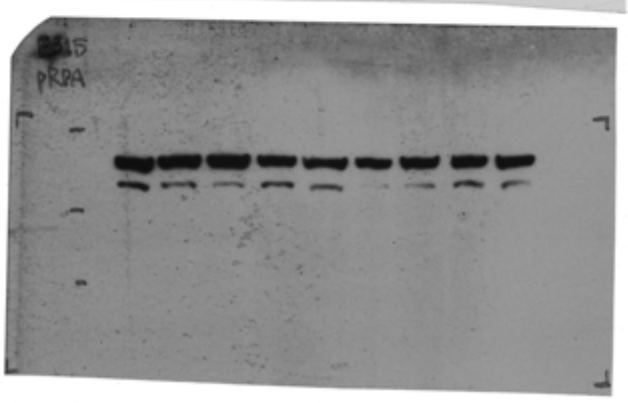

E315
SMC1
WT
B1 TN
B1 TR

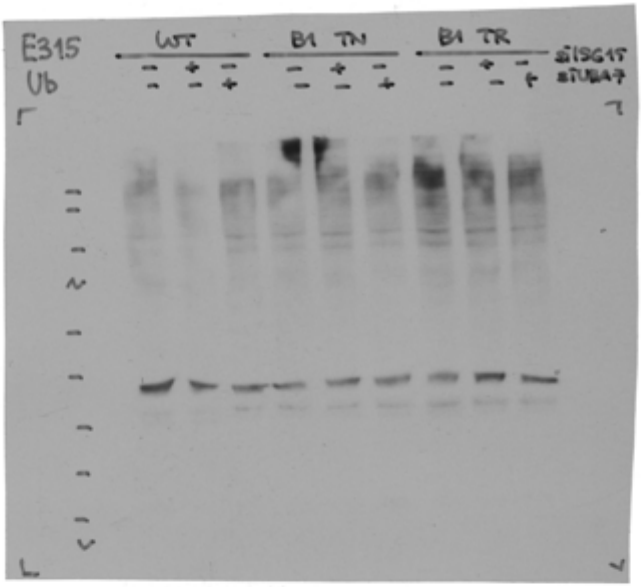

E315
pRPA
WT
B1 TN
B1 TR

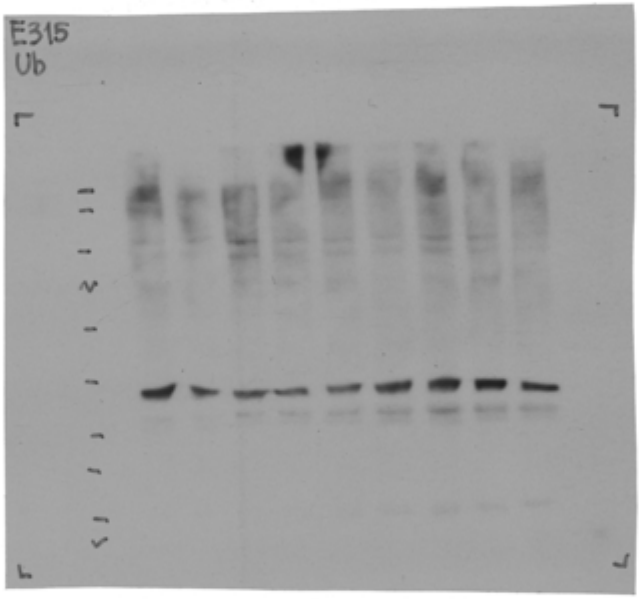

E315
UBA7
WT
B1 TN
B1 TR
siISG15
siUBA7

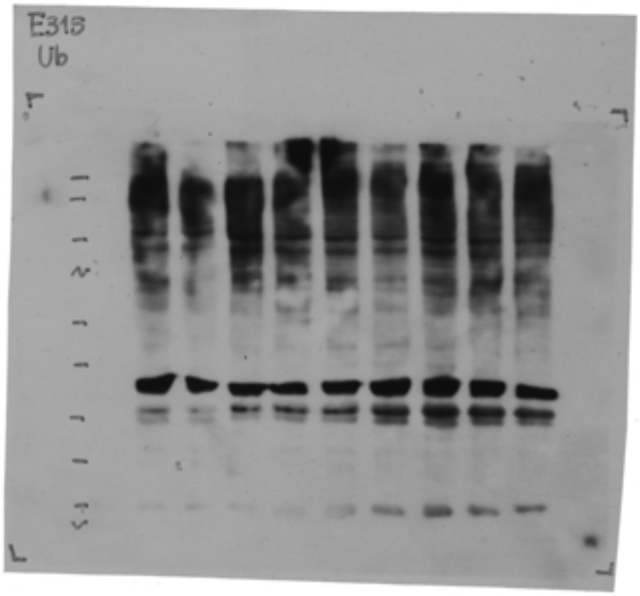

E315
UBA7
WT
B1 TN
B1 TR
siISG15
siUBA7

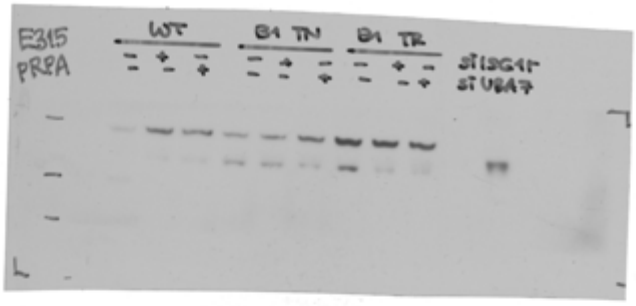

E315
PRPA
WT
B1 TN
B1 TR
siISG15
siUBA7

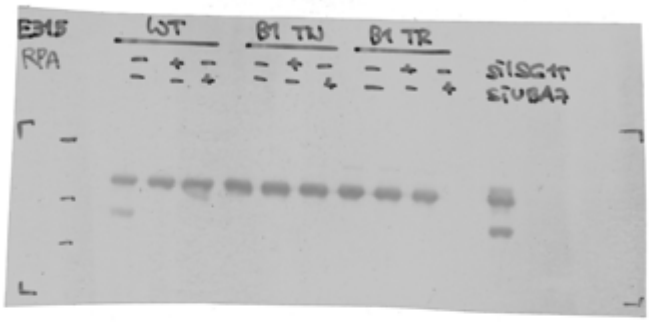

E315
PRPA

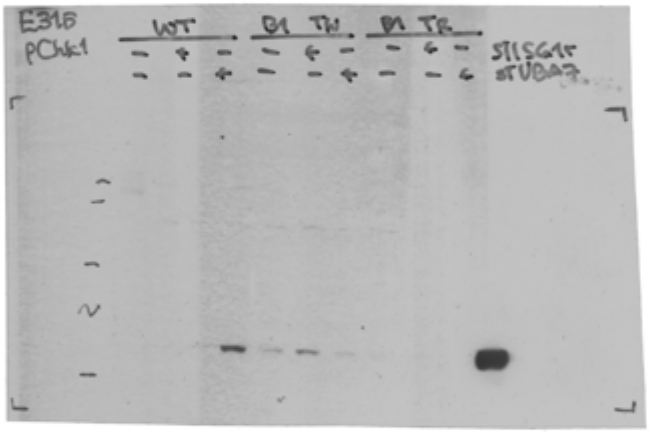

E315
Ub
WT
B1 TN
B1 TR
siISG15
siUBA7

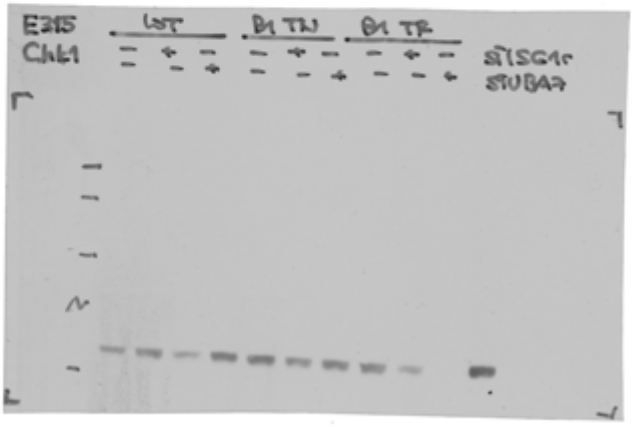

E315
Ub


E315
Ub


E315
PRPA
WT
B1 TN
B1 TR
ATR
ATM


E315
RPA
WT
B1 TN
B1 TR
ATR
ATM


E315
pChk1
WT
B1 TN
B1 TR
ATR
ATM


E315
Chk1
WT
B1 TN
B1 TR
ATR
ATM

References

1. Sender, R., S. Fuchs, and R. Milo, *Revised Estimates for the Number of Human and Bacteria Cells in the Body.* PLoS Biol, 2016. **14**(8): p. e1002533.

2. Bianconi, E., et al., *An estimation of the number of cells in the human body.* Ann Hum Biol, 2013. **40**(6): p. 463-71.

3. Roth, S.C., *What is genomic medicine?* J Med Libr Assoc, 2019. **107**(3): p. 442-448.

4. Gartler, S.M., *The chromosome number in humans: a brief history.* Nat Rev Genet, 2006. **7**(8): p. 655-60.

5. Taanman, J.W., *The mitochondrial genome: structure, transcription, translation and replication.* Biochim Biophys Acta, 1999. **1410**(2): p. 103-23.

6. Maki, H., *Origins of spontaneous mutations: specificity and directionality of base-substitution, frameshift, and sequence-substitution mutageneses.* Annu Rev Genet, 2002. **36**: p. 279-303.

7. Halliday, J.A. and B.W. Glickman, *Mechanisms of spontaneous mutation in DNA repair-proficient Escherichia coli.* Mutat Res, 1991. **250**(1-2): p. 55-71.

8. Aparicio, T., R. Baer, and J. Gautier, *DNA double-strand break repair pathway choice and cancer.* DNA Repair (Amst), 2014. **19**: p. 169-75.

9. Sirbu, B.M. and D. Cortez, *DNA damage response: three levels of DNA repair regulation.* Cold Spring Harb Perspect Biol, 2013. **5**(8): p. a012724.

10. Bhargava, R., D.O. Onyango, and J.M. Stark, *Regulation of Single-Strand Annealing and its Role in Genome Maintenance.* Trends Genet, 2016. **32**(9): p. 566-575.

11. Alexander, J.L. and T.L. Orr-Weaver, *Replication fork instability and the consequences of fork collisions from rereplication.* Genes Dev, 2016. **30**(20): p. 2241-2252.

12. Branzei, D. and M. Foiani, *Regulation of DNA repair throughout the cell cycle.* Nat Rev Mol Cell Biol, 2008. **9**(4): p. 297-308.

13. Jackson, S.P. and J. Bartek, *The DNA-damage response in human biology and disease.* Nature, 2009. **461**(7267): p. 1071-8.

14. Ciccia, A. and S.J. Elledge, *The DNA damage response: making it safe to play with knives.* Mol Cell, 2010. **40**(2): p. 179-204.

15. Pilie, P.G., et al., *State-of-the-art strategies for targeting the DNA damage response in cancer.* Nat Rev Clin Oncol, 2019. **16**(2): p. 81-104.

16. Norbury, C.J. and I.D. Hickson, *Cellular responses to DNA damage.* Annu Rev Pharmacol Toxicol, 2001. **41**: p. 367-401.

17. Caldecott, K.W., *DNA single-strand break repair and human genetic disease.* Trends Cell Biol, 2022. **32**(9): p. 733-745.

18. Beck, C., et al., *Poly(ADP-ribose) polymerases in double-strand break repair: focus on PARP1, PARP2 and PARP3.* Exp Cell Res, 2014. **329**(1): p. 18-25.

19. Gibson, B.A. and W.L. Kraus, *New insights into the molecular and cellular functions of poly(ADP-ribose) and PARPs.* Nat Rev Mol Cell Biol, 2012. **13**(7): p. 411-24.

20. Ryu, K.W., D.S. Kim, and W.L. Kraus, *New facets in the regulation of gene expression by ADP-ribosylation and poly(ADP-ribose) polymerases.* Chem Rev, 2015. **115**(6): p. 2453-81.

21. Rack, J.G.M., L. Palazzo, and I. Ahel, *(ADP-ribosyl)hydrolases: structure, function, and biology.* Genes Dev, 2020. **34**(5-6): p. 263-284.

22. London, R.E., *XRCC1 - Strategies for coordinating and assembling a versatile DNA damage response.* DNA Repair (Amst), 2020. **93**: p. 102917.

23. Fairlamb, M.S., et al., *Visualizing the coordination of apurinic/apyrimidinic endonuclease (APE1) and DNA polymerase beta during base excision repair.* J Biol Chem, 2023. **299**(5): p. 104636.

24. Liu, Y., et al., *Coordination between polymerase beta and FEN1 can modulate CAG repeat expansion.* J Biol Chem, 2009. **284**(41): p. 28352-28366.

25. Ceccaldi, R., B. Rondinelli, and A.D. D'Andrea, *Repair Pathway Choices and Consequences at the Double-Strand Break.* Trends Cell Biol, 2016. **26**(1): p. 52-64.

26. Chang, H.H.Y., et al., *Non-homologous DNA end joining and alternative pathways to double-strand break repair.* Nat Rev Mol Cell Biol, 2017. **18**(8): p. 495-506.

27. Prakash, R., et al., *Homologous recombination and human health: the roles of BRCA1, BRCA2, and associated proteins.* Cold Spring Harb Perspect Biol, 2015. **7**(4): p. a016600.

28. Stok, C., et al., *Shaping the BRCAness mutational landscape by alternative double-strand break repair, replication stress and mitotic aberrancies.* Nucleic Acids Res, 2021. **49**(8): p. 4239-4257.

29. Kawale, A.S. and P. Sung, *Mechanism and significance of chromosome damage repair by homologous recombination.* Essays Biochem, 2020. **64**(5): p. 779-790.

30. Wyatt, H.D., et al., *Coordinated actions of SLX1-SLX4 and MUS81-EME1 for Holliday junction resolution in human cells.* Mol Cell, 2013. **52**(2): p. 234-47.

31. Swuec, P. and A. Costa, *Molecular mechanism of double Holliday junction dissolution.* Cell Biosci, 2014. **4**: p. 36.

32. Matos, J. and S.C. West, *Holliday junction resolution: regulation in space and time.* DNA Repair (Amst), 2014. **19**(100): p. 176-81.

33. Tacconi, E.M. and M. Tarsounas, *How homologous recombination maintains telomere integrity.* Chromosoma, 2015. **124**(2): p. 119-30.

34. Shah Punatar, R., et al., *Resolution of single and double Holliday junction recombination intermediates by GEN1.* Proc Natl Acad Sci U S A, 2017. **114**(3): p. 443-450.

35. Fugger, K. and S.C. West, *Keeping homologous recombination in check.* Cell Res, 2016. **26**(4): p. 397-8.

36. Burgess, R.C., et al., *Activation of DNA damage response signaling by condensed chromatin.* Cell Rep, 2014. **9**(5): p. 1703-1717.

37. Scully, R., et al., *DNA double-strand break repair-pathway choice in somatic mammalian cells.* Nat Rev Mol Cell Biol, 2019. **20**(11): p. 698-714.

38. Zeman, M.K. and K.A. Cimprich, *Causes and consequences of replication stress.* Nat Cell Biol, 2014. **16**(1): p. 2-9.

39. Meng, X. and X. Zhao, *Replication fork regression and its regulation.* FEMS Yeast Res, 2017. **17**(1).

40. Routh, E.D., et al., *A G-quadruplex DNA-affinity Approach for Purification of Enzymatically Active G4 Resolvase1.* J Vis Exp, 2017(121).

41. Zyner, K.G., et al., *G-quadruplex DNA structures in human stem cells and differentiation.* Nat Commun, 2022. **13**(1): p. 142.

42. Valton, A.L. and M.N. Prioleau, *G-Quadruplexes in DNA Replication: A Problem or a Necessity?* Trends Genet, 2016. **32**(11): p. 697-706.

43. Lin, Y.L. and P. Pasero, *Replication stress: from chromatin to immunity and beyond.* Curr Opin Genet Dev, 2021. **71**: p. 136-142.

44. Perry, M. and G. Ghosal, *Mechanisms and Regulation of DNA-Protein Crosslink Repair During DNA Replication by SPRTN Protease.* Front Mol Biosci, 2022. **9**: p. 916697.

45. Zhang, H., Y. Xiong, and J. Chen, *DNA-protein cross-link repair: what do we know now?* Cell Biosci, 2020. **10**: p. 3.

46. Hegazy, Y.A., C.M. Fernando, and E.J. Tran, *The balancing act of R-loop biology: The good, the bad, and the ugly.* J Biol Chem, 2020. **295**(4): p. 905-913.

47. Crossley, M.P., M. Bocek, and K.A. Cimprich, *R-Loops as Cellular Regulators and Genomic Threats.* Mol Cell, 2019. **73**(3): p. 398-411.

48. Garcia-Muse, T. and A. Aguilera, *Transcription-replication conflicts: how they occur and how they are resolved.* Nat Rev Mol Cell Biol, 2016. **17**(9): p. 553-63.

49. Hamperl, S. and K.A. Cimprich, *Conflict Resolution in the Genome: How Transcription and Replication Make It Work.* Cell, 2016. **167**(6): p. 1455-1467.

50. Mirkin, E.V. and S.M. Mirkin, *Replication fork stalling at natural impediments.* Microbiol Mol Biol Rev, 2007. **71**(1): p. 13-35.

51. Rinaldi, C., et al., *Sensing R-Loop-Associated DNA Damage to Safeguard Genome Stability.* Front Cell Dev Biol, 2020. **8**: p. 618157.

52. Hamperl, S., et al., *Transcription-Replication Conflict Orientation Modulates R-Loop Levels and Activates Distinct DNA Damage Responses.* Cell, 2017. **170**(4): p. 774-786 e19.

53. Saxena, S. and L. Zou, *Hallmarks of DNA replication stress.* Mol Cell, 2022. **82**(12): p. 2298-2314.

54. Branzei, D. and B. Szakal, *DNA damage tolerance by recombination: Molecular pathways and DNA structures.* DNA Repair (Amst), 2016. **44**: p. 68-75.

55. Byun, T.S., et al., *Functional uncoupling of MCM helicase and DNA polymerase activities activates the ATR-dependent checkpoint.* Genes Dev, 2005. **19**(9): p. 1040-52.

56. Marechal, A. and L. Zou, *RPA-coated single-stranded DNA as a platform for post-translational modifications in the DNA damage response.* Cell Res, 2015. **25**(1): p. 9-23.

57. Yates, L.A., et al., *A structural and dynamic model for the assembly of Replication Protein A on single-stranded DNA.* Nat Commun, 2018. **9**(1): p. 5447.

58. Quinet, A., D. Lemacon, and A. Vindigni, *Replication Fork Reversal: Players and Guardians.* Mol Cell, 2017. **68**(5): p. 830-833.

59. Kolinjivadi, A.M., et al., *Smarcal1-Mediated Fork Reversal Triggers Mre11-Dependent Degradation of Nascent DNA in the Absence of Brca2 and Stable Rad51 Nucleofilaments.* Mol Cell, 2017. **67**(5): p. 867-881 e7.

60. Betous, R., et al., *Substrate-selective repair and restart of replication forks by DNA translocases.* Cell Rep, 2013. **3**(6): p. 1958-69.

61. Couch, F.B., et al., *ATR phosphorylates SMARCAL1 to prevent replication fork collapse.* Genes Dev, 2013. **27**(14): p. 1610-23.

62. Hishiki, A., et al., *Structure of a Novel DNA-binding Domain of Helicase-like Transcription Factor (HLTF) and Its Functional Implication in DNA Damage Tolerance.* J Biol Chem, 2015. **290**(21): p. 13215-23.

63. Kile, A.C., et al., *HLTF's Ancient HIRAN Domain Binds 3' DNA Ends to Drive Replication Fork Reversal.* Mol Cell, 2015. **58**(6): p. 1090-100.

64. Garcia-Gomez, S., et al., *PrimPol, an archaic primase/polymerase operating in human cells.* Mol Cell, 2013. **52**(4): p. 541-53.

65. Rudd, S.G., J. Bianchi, and A.J. Doherty, *PrimPol-A new polymerase on the block.* Mol Cell Oncol, 2014. **1**(2): p. e960754.

66. Guilliam, T.A. and A.J. Doherty, *PrimPol-Prime Time to Reprime.* Genes (Basel), 2017. **8**(1).

67. Lange, S.S., K. Takata, and R.D. Wood, *DNA polymerases and cancer.* Nat Rev Cancer, 2011. **11**(2): p. 96-110.

68. Petermann, E., L. Lan, and L. Zou, *Sources, resolution and physiological relevance of R-loops and RNA-DNA hybrids.* Nat Rev Mol Cell Biol, 2022. **23**(8): p. 521-540.

69. Azzalin, C.M., et al., *Telomeric repeat containing RNA and RNA surveillance factors at mammalian chromosome ends.* Science, 2007. **318**(5851): p. 798-801.

70. Schoeftner, S. and M.A. Blasco, *Developmentally regulated transcription of mammalian telomeres by DNA-dependent RNA polymerase II.* Nat Cell Biol, 2008. **10**(2): p. 228-36.

71. Xu, Y., et al., *R-loop and diseases: the cell cycle matters.* Mol Cancer, 2024. **23**(1): p. 84.

72. Westover, K.R., P. Jin, and B. Yao, *Bridging the gap: R-loop mediated genomic instability and its implications in neurological diseases.* Epigenomics, 2024. **16**(8): p. 589-608.

73. Niehrs, C. and B. Luke, *Regulatory R-loops as facilitators of gene expression and genome stability.* Nat Rev Mol Cell Biol, 2020. **21**(3): p. 167-178.

74. Kotsantis, P., et al., *Increased global transcription activity as a mechanism of replication stress in cancer.* Nat Commun, 2016. **7**: p. 13087.

75. Kaneko, S., et al., *Human capping enzyme promotes formation of transcriptional R loops in vitro.* Proc Natl Acad Sci U S A, 2007. **104**(45): p. 17620-5.

76. Huertas, P. and A. Aguilera, *Cotranscriptionally formed DNA:RNA hybrids mediate transcription elongation impairment and transcription-associated recombination.* Mol Cell, 2003. **12**(3): p. 711-21.

77. Li, X. and J.L. Manley, *Inactivation of the SR protein splicing factor ASF/SF2 results in genomic instability.* Cell, 2005. **122**(3): p. 365-78.

78. Paulsen, R.D., et al., *A genome-wide siRNA screen reveals diverse cellular processes and pathways that mediate genome stability.* Mol Cell, 2009. **35**(2): p. 228-39.

79. Skourti-Stathaki, K. and N.J. Proudfoot, *A double-edged sword: R loops as threats to genome integrity and powerful regulators of gene expression.* Genes Dev, 2014. **28**(13): p. 1384-96.

80. Cerritelli, S.M. and R.J. Crouch, *Ribonuclease H: the enzymes in eukaryotes.* FEBS J, 2009. **276**(6): p. 1494-505.

81. Lockhart, A., et al., *RNase H1 and H2 Are Differentially Regulated to Process RNA-DNA Hybrids.* Cell Rep, 2019. **29**(9): p. 2890-2900 e5.

82. Yang, S., et al., *Helicases in R-loop Formation and Resolution.* J Biol Chem, 2023. **299**(11): p. 105307.

83. Dominguez-Sanchez, M.S., et al., *Genome instability and transcription elongation impairment in human cells depleted of THO/TREX.* PLoS Genet, 2011. **7**(12): p. e1002386.

84. Pefanis, E., et al., *RNA exosome-regulated long non-coding RNA transcription controls super-enhancer activity.* Cell, 2015. **161**(4): p. 774-89.

85. de Amorim, J.L., et al., *The putative RNA helicase DDX1 associates with the nuclear RNA exosome and modulates RNA/DNA hybrids (R-loops).* J Biol Chem, 2024. **300**(2): p. 105646.

86. Saha, S. and Y. Pommier, *R-loops, type I topoisomerases and cancer.* NAR Cancer, 2023. **5**(1): p. zcad013.

87. Herrera-Moyano, E., et al., *The yeast and human FACT chromatin-reorganizing complexes solve R-loop-mediated transcription-replication conflicts.* Genes Dev, 2014. **28**(7): p. 735-48.

88. Barroso, S., et al., *The DNA damage response acts as a safeguard against harmful DNA-RNA hybrids of different origins.* EMBO Rep, 2019. **20**(9): p. e47250.

89. Posse, V., et al., *RNase H1 directs origin-specific initiation of DNA replication in human mitochondria.* PLoS Genet, 2019. **15**(1): p. e1007781.

90. Yu, K., et al., *R-loops at immunoglobulin class switch regions in the chromosomes of stimulated B cells.* Nat Immunol, 2003. **4**(5): p. 442-51.

91. Ginno, P.A., et al., *R-loop formation is a distinctive characteristic of unmethylated human CpG island promoters.* Mol Cell, 2012. **45**(6): p. 814-25.

92. Sanz, L.A., et al., *Prevalent, Dynamic, and Conserved R-Loop Structures Associate with Specific Epigenomic Signatures in Mammals.* Mol Cell, 2016. **63**(1): p. 167-78.

93. Nadel, J., et al., *RNA:DNA hybrids in the human genome have distinctive nucleotide characteristics, chromatin composition, and transcriptional relationships.* Epigenetics Chromatin, 2015. **8**: p. 46.

94. Chen, L., et al., *R-ChIP Using Inactive RNase H Reveals Dynamic Coupling of R-loops with Transcriptional Pausing at Gene Promoters.* Mol Cell, 2017. **68**(4): p. 745-757 e5.

95. Dumelie, J.G. and S.R. Jaffrey, *Defining the location of promoter-associated R-loops at near-nucleotide resolution using bisDRIP-seq.* Elife, 2017. **6**.

96. Grunseich, C., et al., *Senataxin Mutation Reveals How R-Loops Promote Transcription by Blocking DNA Methylation at Gene Promoters.* Mol Cell, 2018. **69**(3): p. 426-437 e7.

97. Ohle, C., et al., *Transient RNA-DNA Hybrids Are Required for Efficient Double-Strand Break Repair.* Cell, 2016. **167**(4): p. 1001-1013 e7.

98. Lu, W.T., et al., *Drosha drives the formation of DNA:RNA hybrids around DNA break sites to facilitate DNA repair.* Nat Commun, 2018. **9**(1): p. 532.

99. Yasuhara, T., et al., *Human Rad52 Promotes XPG-Mediated R-loop Processing to Initiate Transcription-Associated Homologous Recombination Repair.* Cell, 2018. **175**(2): p. 558-570 e11.

100. Mackay, R.P., Q. Xu, and P.M. Weinberger, *R-Loop Physiology and Pathology: A Brief Review.* DNA Cell Biol, 2020. **39**(11): p. 1914-1925.

101. Aguilera, A. and T. Garcia-Muse, *R loops: from transcription byproducts to threats to genome stability.* Mol Cell, 2012. **46**(2): p. 115-24.

102. Vohhodina, J., et al., *BRCA1 binds TERRA RNA and suppresses R-Loop-based telomeric DNA damage.* Nat Commun, 2021. **12**(1): p. 3542.

103. Garcia-Rubio, M.L., et al., *The Fanconi Anemia Pathway Protects Genome Integrity from R-loops.* PLoS Genet, 2015. **11**(11): p. e1005674.

104. Schwab, R.A., et al., *The Fanconi Anemia Pathway Maintains Genome Stability by Coordinating Replication and Transcription.* Mol Cell, 2015. **60**(3): p. 351-61.

105. Groh, M., et al., *R-loops associated with triplet repeat expansions promote gene silencing in Friedreich ataxia and fragile X syndrome.* PLoS Genet, 2014. **10**(5): p. e1004318.

106. Lim, Y.W., et al., *Genome-wide DNA hypomethylation and RNA:DNA hybrid accumulation in Aicardi-Goutieres syndrome.* Elife, 2015. **4**.

107. Li, M.L. and R.A. Greenberg, *Links between genome integrity and BRCA1 tumor suppression.* Trends Biochem Sci, 2012. **37**(10): p. 418-24.

108. Chen, C.C., et al., *Homology-Directed Repair and the Role of BRCA1, BRCA2, and Related Proteins in Genome Integrity and Cancer.* Annu Rev Cancer Biol, 2018. **2**: p. 313-336.

109. Feng, W. and M. Jasin, *BRCA2 suppresses replication stress-induced mitotic and G1 abnormalities through homologous recombination.* Nat Commun, 2017. **8**(1): p. 525.

110. Gudas, J.M., et al., *Cell cycle regulation of BRCA1 messenger RNA in human breast epithelial cells.* Cell Growth Differ, 1996. **7**(6): p. 717-23.

111. Vaughn, J.P., et al., *BRCA1 expression is induced before DNA synthesis in both normal and tumor-derived breast cells.* Cell Growth Differ, 1996. **7**(6): p. 711-5.

112. Xu, X., et al., *Centrosome amplification and a defective G2-M cell cycle checkpoint induce genetic instability in BRCA1 exon 11 isoform-deficient cells.* Mol Cell, 1999. **3**(3): p. 389-95.

113. Scully, R., et al., *Genetic analysis of BRCA1 function in a defined tumor cell line.* Mol Cell, 1999. **4**(6): p. 1093-9.

114. Deng, C.X., *BRCA1: cell cycle checkpoint, genetic instability, DNA damage response and cancer evolution.* Nucleic Acids Res, 2006. **34**(5): p. 1416-26.

115. Cortez, D., et al., *Requirement of ATM-dependent phosphorylation of brca1 in the DNA damage response to double-strand breaks.* Science, 1999. **286**(5442): p. 1162-6.

116. Okada, S. and T. Ouchi, *Cell cycle differences in DNA damage-induced BRCA1 phosphorylation affect its subcellular localization.* J Biol Chem, 2003. **278**(3): p. 2015-20.

117. Xu, B., S. Kim, and M.B. Kastan, *Involvement of Brca1 in S-phase and G(2)-phase checkpoints after ionizing irradiation.* Mol Cell Biol, 2001. **21**(10): p. 3445-50.

118. Xu, B., et al., *Phosphorylation of serine 1387 in Brca1 is specifically required for the Atm-mediated S-phase checkpoint after ionizing irradiation.* Cancer Res, 2002. **62**(16): p. 4588-91.

119. Bertwistle, D., et al., *Nuclear location and cell cycle regulation of the BRCA2 protein.* Cancer Res, 1997. **57**(24): p. 5485-8.

120. Simhadri, S., et al., *PALB2 connects BRCA1 and BRCA2 in the G2/M checkpoint response.* Oncogene, 2019. **38**(10): p. 1585-1596.

121. Chin, K., et al., *In situ analyses of genome instability in breast cancer.* Nat Genet, 2004. **36**(9): p. 984-8.

122. Cohen, S.B., et al., *Protein composition of catalytically active human telomerase from immortal cells.* Science, 2007. **315**(5820): p. 1850-3.

123. Kocak, H., et al., *Hoyeraal-Hreidarsson syndrome caused by a germline mutation in the TEL patch of the telomere protein TPP1.* Genes Dev, 2014. **28**(19): p. 2090-102.

124. Vulliamy, T., et al., *Association between aplastic anaemia and mutations in telomerase RNA.* Lancet, 2002. **359**(9324): p. 2168-70.

125. Walne, A.J., et al., *TINF2 mutations result in very short telomeres: analysis of a large cohort of patients with dyskeratosis congenita and related bone marrow failure syndromes.* Blood, 2008. **112**(9): p. 3594-600.

126. Yamaguchi, H., et al., *Mutations in TERT, the gene for telomerase reverse transcriptase, in aplastic anemia.* N Engl J Med, 2005. **352**(14): p. 1413-24.

127. Xiong, J., et al., *BRCA1 inhibition of telomerase activity in cultured cells.* Mol Cell Biol, 2003. **23**(23): p. 8668-90.

128. Ballal, R.D., et al., *BRCA1 localization to the telomere and its loss from the telomere in response to DNA damage.* J Biol Chem, 2009. **284**(52): p. 36083-36098.

129. Badie, S., et al., *BRCA1 and CtIP promote alternative non-homologous end-joining at uncapped telomeres.* EMBO J, 2015. **34**(6): p. 828.

130. Daza-Martin, M., et al., *Isomerization of BRCA1-BARD1 promotes replication fork protection.* Nature, 2019. **571**(7766): p. 521-527.

131. Fradet-Turcotte, A., et al., *BRCA2 functions: from DNA repair to replication fork stabilization.* Endocr Relat Cancer, 2016. **23**(10): p. T1-T17.

132. Vallerga, M.B., et al., *Rad51 recombinase prevents Mre11 nuclease-dependent degradation and excessive PrimPol-mediated elongation of nascent DNA after UV irradiation.* Proc Natl Acad Sci U S A, 2015. **112**(48): p. E6624-33.

133. Tye, S., G.E. Ronson, and J.R. Morris, *A fork in the road: Where homologous recombination and stalled replication fork protection part ways.* Semin Cell Dev Biol, 2021. **113**: p. 14-26.

134. Yoshida, K. and Y. Miki, *Role of BRCA1 and BRCA2 as regulators of DNA repair, transcription, and cell cycle in response to DNA damage.* Cancer Sci, 2004. **95**(11): p. 866-71.

135. Mersch, J., et al., *Cancers associated with BRCA1 and BRCA2 mutations other than breast and ovarian.* Cancer, 2015. **121**(2): p. 269-75.

136. Famorca-Tran, J. and G. Roux, *The Consequences of a BRCA Mutation in Women.* J Adv Pract Oncol, 2015. **6**(3): p. 194-210.

137. Lord, C.J. and A. Ashworth, *PARP inhibitors: Synthetic lethality in the clinic.* Science, 2017. **355**(6330): p. 1152-1158.

138. Citarelli, M., S. Teotia, and R.S. Lamb, *Evolutionary history of the poly(ADP-ribose) polymerase gene family in eukaryotes.* BMC Evol Biol, 2010. **10**: p. 308.

139. Murata, M.M., et al., *NAD+ consumption by PARP1 in response to DNA damage triggers metabolic shift critical for damaged cell survival.* Mol Biol Cell, 2019. **30**(20): p. 2584-2597.

140. Gagné, J.-P., et al., *Proteome-wide identification of poly(ADP-ribose) binding proteins and poly(ADP-ribose)-associated protein complexes.* Nucleic Acids Research, 2008. **36**(22): p. 6959-6976.

141. Rajman, L., K. Chwalek, and D.A. Sinclair, *Therapeutic Potential of NAD-Boosting Molecules: The In Vivo Evidence.* Cell Metabolism, 2018. **27**(3): p. 529-547.

142. Kang, M., et al., *A Double-Edged Sword: The Two Faces of PARylation.* International Journal of Molecular Sciences, 2022. **23**(17): p. 9826.

143. Bryant, H.E., et al., *Specific killing of BRCA2-deficient tumours with inhibitors of poly(ADP-ribose) polymerase.* Nature, 2005. **434**(7035): p. 913-917.

144. Rose, M., et al., *PARP Inhibitors: Clinical Relevance, Mechanisms of Action and Tumor Resistance.* Front Cell Dev Biol, 2020. **8**: p. 564601.

145. Pommier, Y., M.J. O'Connor, and J. de Bono, *Laying a trap to kill cancer cells: PARP inhibitors and their mechanisms of action.* Sci Transl Med, 2016. **8**(362): p. 362ps17.

146. Murai, J., et al., *Trapping of PARP1 and PARP2 by Clinical PARP Inhibitors.* Cancer Res, 2012. **72**(21): p. 5588-99.

147. Shen, Y., et al., *BMN 673, a Novel and Highly Potent PARP1/2 Inhibitor for the Treatment of Human Cancers with DNA Repair Deficiency.* Clinical Cancer Research, 2013. **19**(18): p. 5003-5015.

148. Hopkins, T.A., et al., *Mechanistic Dissection of PARP1 Trapping and the Impact on In Vivo Tolerability and Efficacy of PARP Inhibitors.* Molecular Cancer Research, 2015. **13**(11): p. 1465-1477.

149. Pettitt, S.J., et al., *A genetic screen using the PiggyBac transposon in haploid cells identifies Parp1 as a mediator of olaparib toxicity.* PLoS One, 2013. **8**(4): p. e61520.

150. Murai, J., et al., *Stereospecific PARP trapping by BMN 673 and comparison with olaparib and rucaparib.* Mol Cancer Ther, 2014. **13**(2): p. 433-43.

151. Pettitt, S.J., et al., *Genome-wide and high-density CRISPR-Cas9 screens identify point mutations in PARP1 causing PARP inhibitor resistance.* Nat Commun, 2018. **9**(1): p. 1849.

152. Maya-Mendoza, A., et al., *High speed of fork progression induces DNA replication stress and genomic instability.* Nature, 2018. **559**(7713): p. 279-284.

153. Kunkel, T.A., *DNA replication fidelity.* J Biol Chem, 2004. **279**(17): p. 16895-8.

154. Kim, D.S., C.V. Camacho, and W.L. Kraus, *Alternate therapeutic pathways for PARP inhibitors and potential mechanisms of resistance.* Exp Mol Med, 2021. **53**(1): p. 42-51.

155. Ter Brugge, P., et al., *Mechanisms of Therapy Resistance in Patient-Derived Xenograft Models of BRCA1-Deficient Breast Cancer.* J Natl Cancer Inst, 2016. **108**(11).

156. Xu, G., et al., *REV7 counteracts DNA double-strand break resection and affects PARP inhibition.* Nature, 2015. **521**(7553): p. 541-544.

157. Noordermeer, S.M., et al., *The shieldin complex mediates 53BP1-dependent DNA repair.* Nature, 2018. **560**(7716): p. 117-121.

158. Zimmermann, M., et al., *53BP1 regulates DSB repair using Rif1 to control 5' end resection.* Science, 2013. **339**(6120): p. 700-4.

159. Schlacher, K., et al., *Double-strand break repair-independent role for BRCA2 in blocking stalled replication fork degradation by MRE11.* Cell, 2011. **145**(4): p. 529-42.

160. Rondinelli, B., et al., *EZH2 promotes degradation of stalled replication forks by recruiting MUS81 through histone H3 trimethylation.* Nat Cell Biol, 2017. **19**(11): p. 1371-1378.

161. Taglialatela, A., et al., *Restoration of Replication Fork Stability in BRCA1- and BRCA2-Deficient Cells by Inactivation of SNF2-Family Fork Remodelers.* Mol Cell, 2017. **68**(2): p. 414-430 e8.

162. Yasuhisa, K., et al., *Mechanism of multidrug recognition by MDR1/ABCB1.* Cancer Science, 2007. **98**(9): p. 1303-1310.

163. Gogola, E., et al., *Selective Loss of PARG Restores PARylation and Counteracts PARP Inhibitor-Mediated Synthetic Lethality.* Cancer Cell, 2019. **35**(6): p. 950-952.

164. Bhin, J., et al., *Multi-omics analysis reveals distinct non-reversion mechanisms of PARPi resistance in BRCA1- versus BRCA2-deficient mammary tumors.* Cell Rep, 2023. **42**(5): p. 112538.

165. Harrision, D., et al., *Poly(ADP-Ribose) Glycohydrolase (PARG) vs. Poly(ADP-Ribose) Polymerase (PARP) - Function in Genome Maintenance and Relevance of Inhibitors for Anti-cancer Therapy.* Front Mol Biosci, 2020. **7**: p. 191.

166. Noordermeer, S.M. and H. van Attikum, *PARP Inhibitor Resistance: A Tug-of-War in BRCA-Mutated Cells.* Trends Cell Biol, 2019. **29**(10): p. 820-834.

167. Min, A. and S.A. Im, *PARP Inhibitors as Therapeutics: Beyond Modulation of PARylation.* Cancers (Basel), 2020. **12**(2).

168. Mackenzie, K.J., et al., *cGAS surveillance of micronuclei links genome instability to innate immunity.* Nature, 2017. **548**(7668): p. 461-465.

169. Heijink, A.M., et al., *BRCA2 deficiency instigates cGAS-mediated inflammatory signaling and confers sensitivity to tumor necrosis factor-alpha-mediated cytotoxicity.* Nat Commun, 2019. **10**(1): p. 100.

170. Reislander, T., et al., *BRCA2 abrogation triggers innate immune responses potentiated by treatment with PARP inhibitors.* Nat Commun, 2019. **10**(1): p. 3143.

171. Parkes, E.E., et al., *Activation of a cGAS-STING-mediated immune response predicts response to neoadjuvant chemotherapy in early breast cancer.* Br J Cancer, 2022. **126**(2): p. 247-258.

172. Coquel, F., et al., *SAMHD1 acts at stalled replication forks to prevent interferon induction.* Nature, 2018. **557**(7703): p. 57-61.

173. Erdal, E., et al., *A prosurvival DNA damage-induced cytoplasmic interferon response is mediated by end resection factors and is limited by Trex1.* Genes Dev, 2017. **31**(4): p. 353-369.

174. Ho, S.S., et al., *The DNA Structure-Specific Endonuclease MUS81 Mediates DNA Sensor STING-Dependent Host Rejection of Prostate Cancer Cells.* Immunity, 2016. **44**(5): p. 1177-89.

175. MacDonald, K.M., et al., *Antecedent chromatin organization determines cGAS recruitment to ruptured micronuclei.* Nat Commun, 2023. **14**(1): p. 556.

176. Ishikawa, H., Z. Ma, and G.N. Barber, *STING regulates intracellular DNA-mediated, type I interferon-dependent innate immunity.* Nature, 2009. **461**(7265): p. 788-92.

177. Ablasser, A., et al., *cGAS produces a 2'-5'-linked cyclic dinucleotide second messenger that activates STING.* Nature, 2013. **498**(7454): p. 380-4.

178. Sun, L., et al., *Cyclic GMP-AMP synthase is a cytosolic DNA sensor that activates the type I interferon pathway.* Science, 2013. **339**(6121): p. 786-91.

179. Zhang, X., et al., *Cyclic GMP-AMP containing mixed phosphodiester linkages is an endogenous high-affinity ligand for STING.* Mol Cell, 2013. **51**(2): p. 226-35.

180. Gao, P., et al., *Cyclic [G(2',5')pA(3',5')p] is the metazoan second messenger produced by DNA-activated cyclic GMP-AMP synthase.* Cell, 2013. **153**(5): p. 1094-107.

181. Li, T. and Z.J. Chen, *The cGAS-cGAMP-STING pathway connects DNA damage to inflammation, senescence, and cancer.* J Exp Med, 2018. **215**(5): p. 1287-1299.

182. Dunn, G.P., C.M. Koebel, and R.D. Schreiber, *Interferons, immunity and cancer immunoediting.* Nat Rev Immunol, 2006. **6**(11): p. 836-48.

183. Fuertes, M.B., et al., *Type I interferon response and innate immune sensing of cancer.* Trends Immunol, 2013. **34**(2): p. 67-73.

184. Ivashkiv, L.B. and L.T. Donlin, *Regulation of type I interferon responses.* Nat Rev Immunol, 2014. **14**(1): p. 36-49.

185. Lopez de Padilla, C.M. and T.B. Niewold, *The type I interferons: Basic concepts and clinical relevance in immune-mediated inflammatory diseases.* Gene, 2016. **576**(1 Pt 1): p. 14-21.

186. Martinez-Lostao, L., A. Anel, and J. Pardo, *How Do Cytotoxic Lymphocytes Kill Cancer Cells?* Clin Cancer Res, 2015. **21**(22): p. 5047-56.

187. Boukhaled, G.M., S. Harding, and D.G. Brooks, *Opposing Roles of Type I Interferons in Cancer Immunity.* Annu Rev Pathol, 2021. **16**: p. 167-198.

188. Arico, E., et al., *Type I Interferons and Cancer: An Evolving Story Demanding Novel Clinical Applications.* Cancers (Basel), 2019. **11**(12).

189. Borden, E.C., *Interferons alpha and beta in cancer: therapeutic opportunities from new insights.* Nat Rev Drug Discov, 2019. **18**(3): p. 219-234.

190. Wenzel, J., et al., *Transcriptional profiling identifies an interferon-associated host immune response in invasive squamous cell carcinoma of the skin.* Int J Cancer, 2008. **123**(11): p. 2605-15.

191. Pidugu, V.K., et al., *IFIT1 and IFIT3 promote oral squamous cell carcinoma metastasis and contribute to the anti-tumor effect of gefitinib via enhancing p-EGFR recycling.* Oncogene, 2019. **38**(17): p. 3232-3247.

192. De Cecco, M., et al., *L1 drives IFN in senescent cells and promotes age-associated inflammation.* Nature, 2019. **566**(7742): p. 73-78.

193. Lee, M.S., et al., *OASL1 inhibits translation of the type I interferon-regulating transcription factor IRF7.* Nat Immunol, 2013. **14**(4): p. 346-55.

194. Tobelaim, W.S., et al., *Tumour-promoting role of SOCS1 in colorectal cancer cells.* Sci Rep, 2015. **5**: p. 14301.

195. Dzimianski, J.V., et al., *ISG15: It's Complicated.* J Mol Biol, 2019. **431**(21): p. 4203-4216.

196. Kamitani, T., et al., *Characterization of NEDD8, a developmentally down-regulated ubiquitin-like protein.* J Biol Chem, 1997. **272**(45): p. 28557-62.

197. Bates, E.E., et al., *Identification and analysis of a novel member of the ubiquitin family expressed in dendritic cells and mature B cells.* Eur J Immunol, 1997. **27**(10): p. 2471-7.

198. Liu, Y.C., et al., *A MHC-encoded ubiquitin-like protein (FAT10) binds noncovalently to the spindle assembly checkpoint protein MAD2.* Proc Natl Acad Sci U S A, 1999. **96**(8): p. 4313-8.

199. Dastur, A., et al., *Herc5, an interferon-induced HECT E3 enzyme, is required for conjugation of ISG15 in human cells.* J Biol Chem, 2006. **281**(7): p. 4334-8.

200. Okumura, F., W. Zou, and D.E. Zhang, *ISG15 modification of the eIF4E cognate 4EHP enhances cap structure-binding activity of 4EHP.* Genes Dev, 2007. **21**(3): p. 255-60.

201. Yuan, Y., et al., *The Functional Roles of ISG15/ISGylation in Cancer.* Molecules, 2023. **28**(3).

202. Malakhov, M.P., et al., *UBP43 (USP18) specifically removes ISG15 from conjugated proteins.* J Biol Chem, 2002. **277**(12): p. 9976-81.

203. Passmore, L.A. and D. Barford, *Getting into position: the catalytic mechanisms of protein ubiquitylation.* Biochem J, 2004. **379**(Pt 3): p. 513-25.

204. Freitas, B.T., et al., *How ISG15 combats viral infection.* Virus Res, 2020. **286**: p. 198036.

205. Takeuchi, T., S. Inoue, and H. Yokosawa, *Identification and Herc5-mediated ISGylation of novel target proteins.* Biochem Biophys Res Commun, 2006. **348**(2): p. 473-7.

206. Okumura, A., P.M. Pitha, and R.N. Harty, *ISG15 inhibits Ebola VP40 VLP budding in an L-domain-dependent manner by blocking Nedd4 ligase activity.* Proc Natl Acad Sci U S A, 2008. **105**(10): p. 3974-9.

207. Durfee, L.A., et al., *The ISG15 conjugation system broadly targets newly synthesized proteins: implications for the antiviral function of ISG15.* Mol Cell, 2010. **38**(5): p. 722-32.

208. Tang, Y., et al., *Herc5 attenuates influenza A virus by catalyzing ISGylation of viral NS1 protein.* J Immunol, 2010. **184**(10): p. 5777-90.

209. Lin, C., et al., *Regulation of STING activity in DNA sensing by ISG15 modification.* Cell Rep, 2023. **42**(11): p. 113277.

210. Kim, M.J., et al., *Negative feedback regulation of RIG-I-mediated antiviral signaling by interferon-induced ISG15 conjugation.* J Virol, 2008. **82**(3): p. 1474-83.

211. Du, Y., et al., *LRRC25 inhibits type I IFN signaling by targeting ISG15-associated RIG-I for autophagic degradation.* EMBO J, 2018. **37**(3): p. 351-366.

212. Dos Santos, P.F. and D.S. Mansur, *Beyond ISGlylation: Functions of Free Intracellular and Extracellular ISG15.* J Interferon Cytokine Res, 2017. **37**(6): p. 246-253.

213. Wardlaw, C.P. and J.H.J. Petrini, *ISG15: A link between innate immune signaling, DNA replication, and genome stability.* Bioessays, 2023. **45**(7): p. e2300042.

214. Okumura, F., et al., *Activation of double-stranded RNA-activated protein kinase (PKR) by interferon-stimulated gene 15 (ISG15) modification down-regulates protein translation.* J Biol Chem, 2013. **288**(4): p. 2839-47.

215. Holthaus, D., et al., *Direct Antiviral Activity of IFN-Stimulated Genes Is Responsible for Resistance to Paramyxoviruses in ISG15-Deficient Cells.* J Immunol, 2020. **205**(1): p. 261-271.

216. Wang, J.M., et al., *ISG15 suppresses translation of ABCC2 via ISGylation of hnRNPA2B1 and enhances drug sensitivity in cisplatin resistant ovarian cancer cells.* Biochim Biophys Acta Mol Cell Res, 2020. **1867**(4): p. 118647.

217. Rempel, L.A., et al., *Ubp43 gene expression is required for normal Isg15 expression and fetal development.* Reprod Biol Endocrinol, 2007. **5**: p. 13.

218. Henkes, L.E., et al., *Embryo mortality in Isg15-/- mice is exacerbated by environmental stress.* Biol Reprod, 2015. **92**(2): p. 36.

219. Huang, Y.F., et al., *Isg15 controls p53 stability and functions.* Cell Cycle, 2014. **13**(14): p. 2200-10.

220. Jeon, Y.J., et al., *Chemosensitivity is controlled by p63 modification with ubiquitin-like protein ISG15.* J Clin Invest, 2012. **122**(7): p. 2622-36.

221. Luo, Y., F.T. Lin, and W.C. Lin, *ATM-mediated stabilization of hMutL DNA mismatch repair proteins augments p53 activation during DNA damage.* Mol Cell Biol, 2004. **24**(14): p. 6430-44.

222. Turenne, G.A., et al., *Activation of p53 transcriptional activity requires ATM's kinase domain and multiple N-terminal serine residues of p53.* Oncogene, 2001. **20**(37): p. 5100-10.

223. Park, J.H., et al., *Positive feedback regulation of p53 transactivity by DNA damage-induced ISG15 modification.* Nat Commun, 2016. **7**: p. 12513.

224. Bergink, S. and S. Jentsch, *Principles of ubiquitin and SUMO modifications in DNA repair.* Nature, 2009. **458**(7237): p. 461-7.

225. Jackson, S.P. and D. Durocher, *Regulation of DNA damage responses by ubiquitin and SUMO.* Mol Cell, 2013. **49**(5): p. 795-807.

226. Mailand, N., I. Gibbs-Seymour, and S. Bekker-Jensen, *Regulation of PCNA-protein interactions for genome stability.* Nat Rev Mol Cell Biol, 2013. **14**(5): p. 269-82.

227. Ulrich, H.D. and H. Walden, *Ubiquitin signalling in DNA replication and repair.* Nat Rev Mol Cell Biol, 2010. **11**(7): p. 479-89.

228. Bienko, M., et al., *Ubiquitin-binding domains in Y-family polymerases regulate translesion synthesis.* Science, 2005. **310**(5755): p. 1821-4.

229. Lehmann, A.R., et al., *Translesion synthesis: Y-family polymerases and the polymerase switch.* DNA Repair (Amst), 2007. **6**(7): p. 891-9.

230. Park, J.M., et al., *Modification of PCNA by ISG15 plays a crucial role in termination of error-prone translesion DNA synthesis.* Mol Cell, 2014. **54**(4): p. 626-38.

231. Raso, M.C., et al., *Interferon-stimulated gene 15 accelerates replication fork progression inducing chromosomal breakage.* J Cell Biol, 2020. **219**(8).

232. Pinto-Fernandez, A., et al., *Deletion of the deISGylating enzyme USP18 enhances tumour cell antigenicity and radiosensitivity.* Br J Cancer, 2021. **124**(4): p. 817-830.

233. Harding, S.M., et al., *Mitotic progression following DNA damage enables pattern recognition within micronuclei.* Nature, 2017. **548**(7668): p. 466-470.

234. O'Brien, D.P., et al., *Structural Premise of Selective Deubiquitinase USP30 Inhibition by Small-Molecule Benzosulfonamides.* Mol Cell Proteomics, 2023. **22**(8): p. 100609.

235. Muntel, J., et al., *Comparison of Protein Quantification in a Complex Background by DIA and TMT Workflows with Fixed Instrument Time.* J Proteome Res, 2019. **18**(3): p. 1340-1351.

236. Perez-Riverol, Y. and P. Moreno, *Scalable Data Analysis in Proteomics and Metabolomics Using BioContainers and Workflows Engines.* Proteomics, 2020. **20**(9): p. e1900147.

237. Wolf, C., et al., *RPA and Rad51 constitute a cell intrinsic mechanism to protect the cytosol from self DNA.* Nat Commun, 2016. **7**: p. 11752.

238. Dias, M.P., et al., *Understanding and overcoming resistance to PARP inhibitors in cancer therapy.* Nat Rev Clin Oncol, 2021. **18**(12): p. 773-791.

239. Arimoto, K.I., et al., *STAT2 is an essential adaptor in USP18-mediated suppression of type I interferon signaling.* Nat Struct Mol Biol, 2017. **24**(3): p. 279-289.

240. Vuillier, F., et al., *USP18 and ISG15 coordinately impact on SKP2 and cell cycle progression.* Sci Rep, 2019. **9**(1): p. 4066.

241. Kastan, M.B. and J. Bartek, *Cell-cycle checkpoints and cancer.* Nature, 2004. **432**(7015): p. 316-23.

242. Clarke, D.J. and J.F. Gimenez-Abian, *Checkpoints controlling mitosis.* Bioessays, 2000. **22**(4): p. 351-63.

243. Murai, J., *Targeting DNA repair and replication stress in the treatment of ovarian cancer.* Int J Clin Oncol, 2017. **22**(4): p. 619-628.

244. Bolado-Carrancio, A., et al., *ISGylation drives basal breast tumour progression by promoting EGFR recycling and Akt signalling.* Oncogene, 2021. **40**(44): p. 6235-6247.

245. Lowe, J., et al., *Immunohistochemical localization of ubiquitin cross-reactive protein in human tissues.* J Pathol, 1995. **177**(2): p. 163-9.

246. Bogunovic, D., et al., *Mycobacterial disease and impaired IFN-gamma immunity in humans with inherited ISG15 deficiency.* Science, 2012. **337**(6102): p. 1684-8.

247. Tecalco Cruz, A.C. and K. Mejia-Barreto, *Cell type-dependent regulation of free ISG15 levels and ISGylation.* J Cell Commun Signal, 2017. **11**(2): p. 127-135.

248. Fan, J.B., et al., *Identification and characterization of a novel ISG15-ubiquitin mixed chain and its role in regulating protein homeostasis.* Sci Rep, 2015. **5**: p. 12704.

249. Moro, R.N., et al., *Interferon restores replication fork stability and cell viability in BRCA-defective cells via ISG15.* Nat Commun, 2023. **14**(1): p. 6140.

250. Wardlaw, C.P. and J.H.J. Petrini, *ISG15 conjugation to proteins on nascent DNA mitigates DNA replication stress.* Nat Commun, 2022. **13**(1): p. 5971.

251. Lai, X., et al., *MUS81 nuclease activity is essential for replication stress tolerance and chromosome segregation in BRCA2-deficient cells.* Nat Commun, 2017. **8**: p. 15983.

252. Cong, K., et al., *Replication gaps are a key determinant of PARP inhibitor synthetic lethality with BRCA deficiency.* Mol Cell, 2021. **81**(15): p. 3227.

253. Panzarino, N.J., et al., *Replication Gaps Underlie BRCA Deficiency and Therapy Response.* Cancer Res, 2021. **81**(5): p. 1388-1397.

254. Zardoni, L., et al., *Elongating RNA polymerase II and RNA:DNA hybrids hinder fork progression and gene expression at sites of head-on replication-transcription collisions.* Nucleic Acids Res, 2021. **49**(22): p. 12769-12784.

255. Shyian, M. and D. Shore, *Approaching Protein Barriers: Emerging Mechanisms of Replication Pausing in Eukaryotes.* Front Cell Dev Biol, 2021. **9**: p. 672510.

256. Mazurek, A., et al., *DDX5 regulates DNA replication and is required for cell proliferation in a subset of breast cancer cells.* Cancer Discov, 2012. **2**(9): p. 812-25.

257. Lang, K.S. and H. Merrikh, *Topological stress is responsible for the detrimental outcomes of head-on replication-transcription conflicts.* Cell Rep, 2021. **34**(9): p. 108797.

258. Sarni, D., et al., *Topoisomerase 1-dependent R-loop deficiency drives accelerated replication and genomic instability.* Cell Rep, 2022. **40**(13): p. 111397.

259. Bouwman, P., et al., *53BP1 loss rescues BRCA1 deficiency and is associated with triple-negative and BRCA-mutated breast cancers.* Nat Struct Mol Biol, 2010. **17**(6): p. 688-95.

260. Bermejo, R., et al., *Top1- and Top2-mediated topological transitions at replication forks ensure fork progression and stability and prevent DNA damage checkpoint activation.* Genes Dev, 2007. **21**(15): p. 1921-36.

261. Sekiguchi, J. and S. Shuman, *Site-specific ribonuclease activity of eukaryotic DNA topoisomerase I.* Mol Cell, 1997. **1**(1): p. 89-97.

262. Manzo, S.G., et al., *DNA Topoisomerase I differentially modulates R-loops across the human genome.* Genome Biol, 2018. **19**(1): p. 100.

263. El Hage, A., et al., *Loss of Topoisomerase I leads to R-loop-mediated transcriptional blocks during ribosomal RNA synthesis.* Genes Dev, 2010. **24**(14): p. 1546-58.

264. Brickner, J.R., J.L. Garzon, and K.A. Cimprich, *Walking a tightrope: The complex balancing act of R-loops in genome stability.* Mol Cell, 2022. **82**(12): p. 2267-2297.

265. Gatti, V., et al., *Senataxin and R-loops homeostasis: multifaced implications in carcinogenesis.* Cell Death Discov, 2023. **9**(1): p. 145.

266. Jurga, M., et al., *USP11 controls R-loops by regulating senataxin proteostasis.* Nat Commun, 2021. **12**(1): p. 5156.

267. Sollier, J., et al., *Transcription-coupled nucleotide excision repair factors promote R-loop-induced genome instability.* Mol Cell, 2014. **56**(6): p. 777-85.

268. Kang, J.A., Y.J. Kim, and Y.J. Jeon, *The diverse repertoire of ISG15: more intricate than initially thought.* Exp Mol Med, 2022. **54**(11): p. 1779-1792.

269. Desai, S.D., *ISG15: A double edged sword in cancer.* Oncoimmunology, 2015. **4**(12): p. e1052935.

270. Liu, Y., A. Beyer, and R. Aebersold, *On the Dependency of Cellular Protein Levels on mRNA Abundance.* Cell, 2016. **165**(3): p. 535-50.

271. Xue, X., et al., *YAP ISGylation increases its stability and promotes its positive regulation on PPP by stimulating 6PGL transcription.* Cell Death Discov, 2022. **8**(1): p. 59.

272. Weichselbaum, R.R., et al., *An interferon-related gene signature for DNA damage resistance is a predictive marker for chemotherapy and radiation for breast cancer.* Proc Natl Acad Sci U S A, 2008. **105**(47): p. 18490-5.

273. Berkovich, E., R.J. Monnat, Jr., and M.B. Kastan, *Roles of ATM and NBS1 in chromatin structure modulation and DNA double-strand break repair.* Nat Cell Biol, 2007. **9**(6): p. 683-90.

274. Zhang, Y., et al., *The in vivo ISGylome links ISG15 to metabolic pathways and autophagy upon Listeria monocytogenes infection.* Nat Commun, 2019. **10**(1): p. 5383.

275. Roux, K.J., et al., *BioID: A Screen for Protein-Protein Interactions.* Curr Protoc Protein Sci, 2018. **91**: p. 19 23 1-19 23 15.

276. Li, M., et al., *RECQ5-dependent SUMOylation of DNA topoisomerase I prevents transcription-associated genome instability.* Nat Commun, 2015. **6**: p. 6720.

277. Malakhova, O.A. and D.E. Zhang, *ISG15 inhibits Nedd4 ubiquitin E3 activity and enhances the innate antiviral response.* J Biol Chem, 2008. **283**(14): p. 8783-7.